BRNO UNIVERSITY OF TECHNOLOGY

Faculty of Chemistry

MASTER´S THESIS

Brno, 2018 Bc. Petr Hrubý

VYSOKÉ UČENÍ TECHNICKÉ V BRNĚ
BRNO UNIVERSITY OF TECHNOLOGY

FAKULTA CHEMICKÁ
FACULTY OF CHEMISTRY

ÚSTAV CHEMIE MATERIÁLŮ
INSTITUTE OF MATERIALS SCIENCE

VYUŽITÍ ČEDIČOVÝCH VLÁKEN V ALKALICKY AKTIVOVANÝCH MATERIÁLECH
UTILIZATION OF BASALT FIBERS IN ALKALI ACTIVATED MATERIALS

DIPLOMOVÁ PRÁCE
MASTER'S THESIS

AUTOR PRÁCE — **Bc. Petr Hrubý**
AUTHOR

VEDOUCÍ PRÁCE — **Ing. Lukáš Kalina, Ph.D.**
SUPERVISOR

BRNO 2018

VYSOKÉ UČENÍ TECHNICKÉ V BRNĚ
FAKULTA CHEMICKÁ

Zadání diplomové práce

Číslo práce:	FCH-DIP1176/2017
Ústav:	Ústav chemie materiálů
Student:	**Bc. Petr Hrubý**
Studijní program:	Chemie, technologie a vlastnosti materiálů
Studijní obor:	Chemie, technologie a vlastnosti materiálů
Vedoucí práce:	**Ing. Lukáš Kalina, Ph.D.**
Akademický rok:	2017/18

Název diplomové práce:

Využití čedičových vláken v alkalicky aktivovaných materiálech

Zadání diplomové práce:

vypracování literární rešerše
příprava testovacích vzorků s čedičovými vlákny
testování mechanických vlastností
charakterizace mezivrstvy matrice x vlákna
testování trvanlivosti čedičových vláken v alkalicky aktivovaném systému

Termín odevzdání diplomové práce: 7.5.2018

Diplomová práce se odevzdává v děkanem stanoveném počtu exemplářů na sekretariát ústavu. Toto zadání je součástí diplomové práce.

Bc. Petr Hrubý student(ka)	Ing. Lukáš Kalina, Ph.D. vedoucí práce	prof. RNDr. Josef Jančář, CSc. vedoucí ústavu

prof. Ing. Martin Weiter, Ph.D.
děkan

V Brně dne 31.1.2018

ABSTRACT

Alkali activated materials (AAMs) represent construction materials with a huge potential especially because of environmental and economic aspects but sufficient mechanical properties as well. A fibre or fabric reinforcement of the AAMs could support more widespread application potential due to the mechanical properties, fracture toughness or composite durability improvement. Various alkaline activators were used for a blast furnace slag (BFS) activation to produce a suitable matrix for basalt fibres (BF) implementation in this thesis. The BFs represent applicable reinforcing material because of its favourable mechanical and thermal properties. Still, the utilization of BFs in the AAMs is quite limited due to the fibres low chemical stability under the alkaline conditions. Accelerated leaching tests with a determination of basalt fibres chemical composition same as tensile strength change using various analytical techniques (XRD, XPS, SEM-EDX, ICP-OES) have confirmed these assumptions. An influence of basalt fabric reinforcement in one or more layers on the mechanical properties was determined with the meaning of the compressive and flexural strengths. The fibre/matrix adhesion and transition zone properties were studied using SEM-EDX and pull-out tests as well because they are crucial parameters for the composite material reinforcement efficiency.

KEY WORDS

Alkali activated materials, blast furnace slag, basalt fibres, durability of basalt fibres, textile reinforced composite.

ABSTRAKT

Alkalicky aktivované materiály (AAM) jsou konstrukčními materiály s velkým potenciálem, a to zejména pro jejich cenovou dostupnost, přívětivost k životnímu prostředí, ale i díky jejich mechanickým vlastnostem. Přídavek vhodných vláken či textilií vedoucích k vyztužení AAM by mohlo napomoci širšímu uplatnění, neboť by mělo být doprovázeno zlepšením mechanických vlastností, lomové houževnatosti či celkové odolnosti kompozitu. V této práci bylo pro přípravu alkalicky aktivovaných systémů na bázi vysokopecní strusky použito hned několik alkalických aktivátorů s cílem připravit matrici vhodnou pro implementaci čedičových vláken. Čedičová vlákna jsou jedním z vhodných materiálů pro vyztužení AAM díky jejich mechanickým a tepelným vlastnostem. Avšak nízká odolnost čedičových vláken v alkalickém prostředí je pro uplatnění v těchto systémech značně omezující. Odolnost čedičových vláken byla v této práci zkoumána prostřednictvím zrychlených ponorových zkoušek. Následné změny chemického složení a mechanických vlastností vláken byly studovány s využitím řady experimentálních technik (např. měření pevnosti vláken v tahu, XRD, XPS, SEM-EDX nebo ICP-OES). Výsledky těchto testů tento teoretický předpoklad potvrdily. Jako další byl zkoumán vliv přídavku jedné či více vrstev čedičové textilie na mechanické vlastnosti (pevnost při namáhání v tlaku a za ohybu). Adheze mezi vlákny a matricí, stejně tak jako vlastnosti tranzitní zóny, jež jsou klíčovými parametry pro účinnost vyztužení kompozitních materiálu, byly studovány s využitím SEM-EDX a testu vytahování vláken z matrice.

KLÍČOVÁ SLOVA

Alkalicky aktivované materiály, vysokopecní struska, čedičová vlákna, odolnost čedičových vláken, textilní kompozit.

HRUBÝ, P. *Využití čedičových vláken v alkalicky aktivovaných materiálech*. Brno: Brno University of Technology, Faculty of Chemistry, Institute of Material Science, 2018. 80 s. Supervised by Ing. Lukáš Kalina, Ph.D.

ACKNOWLEDGEMENT

I would like to express my full appreciation and gratitude to my supervisor Ing. Lukáš Kalina, Ph.D. for his guidance, patience, pleasantness, and valuable advices which he was willing to provide all the time. Also, I would like to thank other employees of the Material Research Centre at BUT for their willingness and cooperation on some measurements same as pleasant work environment formation.

DECLARATION

I declare that I have written my master's thesis on the theme of "Utilization of basalt fibres in alkali activated materials" independently, under the guidance of the master's thesis supervisor and using the technical literature and other sources of information which are all quoted in the thesis and detailed in the list of literature at the end of the thesis.

As the author of the master's thesis I furthermore declare that, as regards the creation of this master's thesis, I have not infringed any copyright. In particular, I have not unlawfully encroached on anyone's personal and/or ownership rights and I am fully aware of the consequences in the case of breaking Regulation § 11 and the following of the Copyright Act No 121/2000 Sb., and of the rights related to intellectual property right and changes in some Acts (Intellectual Property Act) and formulated in later regulations, inclusive of the possible consequences resulting from the provisions of Criminal Act No 40/2009 Sb., Section 2, Head VI, Part 4.

Brno _____ _____

(author's signature)

1 INTRODUCTION

The interest in the development of alternative building materials has been supported by the growth of the building industry as well as by the constantly increasing performance requirements but without additional cost increases. Nowadays, there has been added another very important parameter marked as an environmental friendliness of the material. It is known that a concrete production forms about 7 % account for worlds´ total greenhouse gas emissions.

Alkali activated materials (AAM) have become a point of researchers´ interests especially because of the environmental and economic aspects. In contrary to the ordinary Portland cement (OPC) the carbon dioxide emissions (about 1 tone of CO_2 per tone of the OPC) can be approximately from 50 to 100 % lower. The industrial by-products (secondary raw materials) utilization allow a lower price same as the lower carbon dioxide emission. The amount of the reduction depends on the AAMs contribution. Beside these facts the AAMs exhibit a wide variety of favourable properties like a high resistance to the aggressive environments, possibility of heavy metals immobilization, a superior durability, good high temperatures performances, earlier and higher mechanical strengths development or a lower hydration heat when compared to the OPC. However, these materials exhibit some disadvantages like a high shrinkage accompanied with a formation of microcracks and higher formation of salt efflorescenses or fast setting times as well.

These properties make them a suitable option for potential different industrial applications, but the pre-casting applications seems to be the best because of the possibility of a safety handling with the highly alkaline reagents same as a curing process control.

To more widespread applications potential, the AAMs could be supported by a fibre or fabric reinforcements, which improve the mechanical properties (tensile, compressive, and flexural strengths), fracture toughness, ductility as well as a durability of the final composite material. Basalt fibres (BF) represent a suitable reinforcing material because of its favourable mechanical and thermal properties. Still, the BFs utilization in the AAMs is quite limited due to their low chemical stability under the alkaline conditions. On the other hand, the chemical reaction between fibres and matrix can lead to a better adhesion which should result to the final composite mechanical properties improvement. This fibre/matrix interaction can also be influenced by modification of surface of the fibres by a proper coatings application as well as by the matrix composition modification. Thus, the quality of the fibre/matrix interface is a key for the fibre/fabric reinforcement in alkali activated materials to be effective and allows their production.

This paper deals with possibilities of the basalt fibres (fabric) utilization in the blast furnace slag systems activated with various alkaline activators. Hence, it focuses on an optimal matrix composition finding considering the BFs stability under the alkaline conditions. Therefore, a stability of the basalt fibres under these conditions was studied using chemical analysis (ICP-OES, XRD, XPS, SEM-EDX) but also mechanical properties determination using e.g. tensile strength measurement. The efficiency of the AAMs reinforcement by the BFs was evaluated based on mechanical properties testing. The fibre/matrix interface was characterized using the SEM-EDX and fibre pull-out tests.

2 THEORETICAL BACKGROUND

2.1 Alkali activated materials

The alkali activated materials are inorganic materials formed by the reaction between alumina-silicate precursors with an alkaline solution [1]. This reaction is named an "alkali activation" (AA). The polycondensation reactions take place as this reaction continues. So, Si and Al atoms are bonded through the shared oxygen atoms (Si-O-Al). It results to the three-dimensional (3D) structure, usually consisting of randomly situated SiO_4 and AlO_4 tetrahedrals. This 3D structure has cavities where solvated alkali ions (Na, K) are situated. The alkali ions compensate the negative charge of Al tetrahedrals. The AA products are usually amorphous or semi crystalline, regarding to a character of raw materials and conditions of the reaction. [2, 3]

2.1.1 Historical background

The first patent describing an idea of the alkali activation reaction came from Germany where Kühl (1908) [4] developed a solid material comparable to the hardened Portland cement by mixing of a vitreous slag with alkali sulphates and carbonates.

The Belgium scientist Purdon (1940) has done a noticeable progress in this problematic. He did the first extensive laboratory studies of alkali activation on different types of slag with diverse activators (sodium and calcium hydroxide) and found out that the final strength properties had been comparable to those of Portland cement. He also noticed that a precise admixture preparation was quite complicated. So, he came up with an idea of AAMs use for the precast applications. [5]

Not only the Western Europe states were active in the AAMs development. The former Soviet Union scientist Glukhovsky studied the alkali activation of aluminosilicates with the low calcium content in the 1957 [6]. He also introduced a theoretical model for the AA reaction. [3]

An extensive research and development of AAMs have been done since Glukhovskys work. The French scientist Davidovits should be mentioned. He formed binders by mixing alkalis with burnt mixture of kaolinite, limestone, and dolomite in 1981. Then he established a term "geopolymer" which was used ever since (very often incorrectly) and remarked that AAMs analogues had been used by Romans and Egyptians already. [3, 6, 7]

The AAMs research and development have been taking place all over the world since 1990s because there are many reasons to do so. The most important one is a high carbon dioxide emission associated with a cement production. [1]

As mentioned above Davidovits term "geopolymer" was determined for a specific range of AAMs. He established two criteria that geopolymers should fulfill. The first one – exhibit a ^{27}Al peak in NMR spectra only about 55 ppm and the second one – Al might be presented in the product structure exclusively in coordination 4. These criteria are fulfilled only for the AAMs based on pure metakaolin. Thus, "geopolymer" term should not be used for alkali activated materials in general. [2, 3]

2.1.2 Components of alkali activated systems

2.1.2.1 Raw materials (precursors) for alkali activation

As the definition of the AAMs says suitable precursors for alkali activation must contain silicates or aluminosilicates in an amorphous phase. Next, they should be economical favourable

and environmental friendly. The most common and the most explored precursors are blast furnace slag (BFS), fly ash and metakaolin, historically. [8]

However, there are also many others which have a good potential, but they are waiting for to be more deeply researched. It is worth to reference other types of slags like phosphorous or silico-manganese slag and a red mud as a by-product of Bayer's process alumina production. Furthermore, one can continue with different types of ashes like a coal bottom ash or a rice husk ash and products of sludges incineration or waste glass or ceramic as well. Natural minerals and so on should not be forgotten too. [9]

Alkali activation process is quite complicated for these materials because of a huge variety in a chemical composition and their properties. Hence, the AA reaction mechanism as well as hydration products differ almost for each precursor. This makes the AA process a very complex discipline.

Alkali activation of BFS based systems with different alkaline activators will only be discussed considering the experimental part of this paper.

2.1.2.2 Alkaline activators

Alkaline activators are another necessary constituent of the alkali activated systems. Glukhovsky classified the alkaline activators into the six basic groups according to their chemical composition [6]. These groups are described in Tab. 1.

Tab. 1: The alkali activator classification by Glukhovsky [6].

Group	Formula
Alkali hydroxides	MOH
Non-silicate weak acid salts	M_2CO_3; M_2SO_3; M_3PO_4; MF; etc.
Silicates	$M_2O{\cdot}nSiO_2$
Aluminates	$M_2O{\cdot}nAl_2O_3$
Aluminosilicates	$M_2O{\cdot}Al_2O_3{\cdot}(2–6)SiO_2$
Non-silicate strong acids salts	M_2SO_4

Note: M represents the alkali metal ion.

Sodium hydroxide, sodium silicate and sodium carbonate are the most economical and available of these alkali activators. Their potassium analogues were also tested but they are not used so much due to a higher cost. The choice of alkaline activator is one of the most important factors when alkali activated systems are prepared. The reaction rate, hydration products or mechanical properties development are influenced through the activator choice. [5]

The crucial requirements of substance for its using in alkali activation of the BFS according to Fernandez-Jimenez and Puertas [10] are:

- Acceleration of the solubility of the aluminosilicates (increasing pH value)
- Promotion of stable hydrates formation
- Formation of a network structure of hydrates

2.2 Alkaline activators used for the AA process

2.2.1 Water glass

The water glass is a term which represents colloidal solution of alkali metal silicate compounds defined with a general formula $M_2O{\cdot}nSiO_2$. Variability in *n* coefficient causes differences in properties as well as industrial use of the water glass. [6]

A silicate modulus (M_s) is used for the water glass composition classification. It specifies the molar ratio of Na_2O to SiO_2 in case of sodium silicate or K_2O to SiO_2 when potassium silicate is characterized. The M_s of commonly used water glasses usually ranges from 1.6 to 4.1. The water glass liquids outside this range have limited stability and they are not practical for the industrial using. [11]

Density, viscosity, and the pH value are other important characterization parameters. The density gives us the information about solution concentration and glass batch composition. The water glass is a non-newtons liquid. Its viscosity depends on the concentration and silicate modulus (the viscosity increases with higher silicate modulus or decreasing temperature). The last parameter – pH is a function of the chemical composition and concentration of the water glass. The water glass is a typical alkaline salt, because it is formed by the reaction of a strong base with a weak acid. [6, 11, 12] In compliance with publication [6] the stability of alkali silicate solutions increases steadily as their pH value increase.

There are many different types of use for sodium or potassium silicate water glass beside the preparation of AAMs, starting from application as an accelerator for concrete or binder for sand moulds production in a foundry industry. There are also many others, but they are not important regarding focus of this paper. [11, 12]

2.3 Blast furnace slag

Nowadays a blast furnace slag (BFS) is a highly valued secondary material which is produced as a by-product of the blast furnace reactions when iron is made.

2.3.1 Blast furnace slag manufacturing

The blast furnace slag is formed when iron ore or iron pellets, coke and a flux (limestone, dolomite, etc.) are melted together under the reducing conditions in the blast furnace. The flux undergoes many chemical changes when a metallurgical smelting process takes place. It helps to eliminate undesirable impurities from the molten iron and helps to prevent oxidation of the molten iron.

There was a limestone as a flux at the beginning. The limestone is decomposed into the CaO and CO_2 as it passes through the blast furnace. Carbon dioxide is also produced by reactions of coke with a hot air and iron ore reduction reactions. Calcium oxide is reliable for elimination of the molten iron impurities. The higher the CaO/SiO_2 ratio of the slag is, the more effective is the desulphurization. The BFS flows on the molten iron due to a lower density. The BFS is tapped (approximate temperature of a liquid slag is 1500 °C) in defined periods of time and undergoes cooling. Thus, based on a cooling mode, several types of slag are produced. The overall scheme of the production of the BFS is given in Fig. 1. [13–15]

The composition of slug making materials vary according to the composition of raw materials and the required final parameters of BFS – low melting point, rheological behaviour, chemical composition, etc. [6]

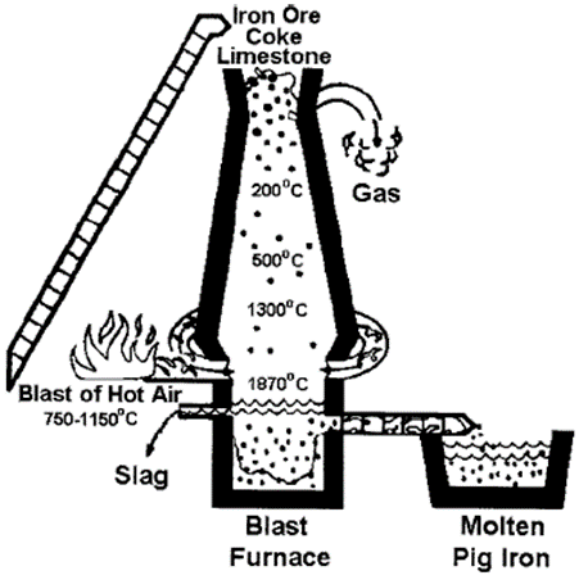

Fig. 1:Scheme of the blast furnace and the BFS production. [11]

2.3.1.1 Blast furnace slag types

The BFS is tapped from the blast furnace as a liquid which contains a lot of gases held in the solution. The BFS cooling conditions influence not only a crystallization process (amount of vitreous or crystalline phase), but also a quantity and size of gas bubbles (because it allows them to escape from the liquid before it undergoes solidification). To sum up, cooling conditions determine an internal structure, density, and porosity of the slag. [14]

Air-cooled BFS (ABFS) is produced when the solidification takes place at atmospheric conditions usually at some pit near to the furnace or somewhere at the landfill. A subsequent cooling by water is allowed with the reference to the ASTM C 125. The product of the slow cooling is mainly crystalline with vesicular structure caused by bubbles of gases dissolved in the molten slag. A particle size is modified by crushing and then it is sorted out after cooling. The ABFSs are commercially used as construction aggregates. [13, 14, 16]

Granulated BFS (GBFS) is formed when a liquid slag is rapidly cooled by large amounts of water. It results in an amorphous granular or sand-like product with a very low content of the mineral crystallization products. Then GBFS undergoes drying and grinding which leads to increase of reactivity (grounded granulated blast furnace slag – GGBFS). It exhibits cementitious properties, so it can be used as a hydraulic binder for cements, concretes but also AAMs. The GGBFS is commercially used as an additive into the OPC. [14, 17]

Pelletized or expanded BFS – an expanding process produces an aggregate with a lower density for applications such as lightweight concrete blocks (with improved fire resistance, sound attenuation, etc.) and masonry. It can be used as an additive to the Portland cement too. The production is based on mixing of the molten slag with water. The mixture flows into receptacle, no more water is added to prevent vitrifying. There is a vane rotor on the receptacle which ejects the mixture of water and slag into the air where another cooling takes place. The expanded BFS is cooled more quickly than the ABFS, which means it contains more vitreous phase, but still less than GBFS. On the other hand, the expanded BFS has more vesicular structure then the ABFS. Lower water consumption, lower drying as well as grinding energy against GBFS are the main advantages of this type of slag. The innovative slag pelletizing

process allows producers to choose between production of the lightweight aggregates or a highly amorphous slag for a binder production. The pelletizing process can be summary described as follows. A molten slag flows down a vibrating feed plate over a large spinning drum, while quenching with water. This specific combination of water and sudden air cooling turn the slag into hard-vitrified pellets with internal micro-cellular structure. [14, 16]

2.3.2 Chemistry of blast furnace slag

As discussed above, a chemical composition of the BFS varies according to the raw materials composition changes, a different fuel type used, furnace operations efficiency and so on. Still, it can be usually described by a CaO-SiO_2-Al_2O_3-MgO quaternary diagram with additional components including manganese, sulphur, or titanium.

The optimal slag composition was determined according to Osborn et al. [6]. However, the range of the BFS chemical composition in an industrial production is quite wide. It varies from one manufacturing facility to another in a small range, especially for MgO and Al_2O_3 content. The typical chemical composition of the blast furnace slag is described in Tab. 2. [14]

Tab. 2: Typical chemical composition of BFS. [14]

Chemical composition in wt. %						
CaO	SiO_2	Al_2O_3	MgO	S	Fe_2O_3	MnO
32–45	32–42	7–16	5–15	1–2	0.1–1.5	0.2–1.0

The determination of a slag hydraulic activity is necessary, therefore there are many standards. It can be ASTM C 1073 regarding the AAMs for instance. It specifies the hydraulic activity of the slag by a strength measuring of the hardened NaOH activated slag mortars. Thus, problems arise when another alkali activator is used. [6] Many factors influence the hydraulic activity of the BFS. Including chemical composition, glass content and grind fineness. The most important ones´ description follows.

A chemical composition of the BFS is determined by an internal structure which is related to a cooling speed and a slag composition. A rapidly cooled slag is more amorphous and hydraulically active, whereas a slowly cooled slag has no hydraulic activity because of a high crystalline content. For neutral and basic slags Ca-Al-Mg silicates, especially gehlenite (C_2AS), akermanite (C_2MS_2), melilite – a solid solution of gehlenite and akermanite and in case of acid slags anorthite (CAS_2) or diopside (CMS_2) are the most common minerals. The rapidly cooled slags contain from 90 to 95 % of vitreous phase. [6, 15]

It is known that a grinding prolonging increases not only the surface area of material, but also the number of imperfections or active centres due to the atomic structure modifications. Thus, the higher fineness is, the higher reactivity of slag will be. On the other hand, there are noticeable cost increases mainly due to the high economical demand of grinding. [6]

The strength development and final microstructure of the AAMs are influenced by the slag fineness beside the hydraulic activity or setting time. The increased fineness provides higher development of compressive strengths but also reduces the setting times according to Provis et al. [5]. A storage time of the BFSs affects the setting times too due to the humidity sorption. The optimal fineness range for AAMs production was established by Wang et al. [18] and Puertas [19] and it ranges between 400–550 $m^2 \cdot kg^{-1}$.

The hydraulic activity of the BFS can be expressed and measured through some parameters, which consider the main oxides content. Speaking of the basicity (M_b) and the quality (Q) coefficients defined in Equations (1) and (2). [5]

$$M_b = \frac{CaO + MgO}{SiO_2 + Al_2O_3} \quad (1)$$

$$Q = \frac{CaO + MgO + Al_2O_3}{SiO_2 + TiO_2} \quad (2)$$

However, there is not always a good correlation between these parameters and final mechanical properties of the AAMs. In the AA process the BFS with $M_b > 1$ (basic slags) are usually used. The slag reactivity can also be characterized by a degree of depolymerization (DP) which is defined as a molar ration between reactive Ca and Si contained in the slag. The DP of the BFS usually ranges from 1.3 to 1.5. A higher value represents more depolymerized, thus more reactive system.

As summarized in publications [5] and [6], the BFSs with a vitreous phase ratio of CaO/SiO_2 between 0.5–2.0 and of Al_2O_3/SiO_2 0.1–0.6 are considered as a suitable for an alkali activation.

2.4 Alkali activation of blast furnace slag

2.4.1 Alkali activated BFS – hydration process

The alkali activation of the BFS is a complex process where the reaction between precursors and alkali solution with high pH value take place. It is a highly heterogeneous process consisting of four main steps. Beginning with the dissolution of the reactive precursor particles (original structure of precursor is broken down), followed by a nucleation and growth of the initial solid phases. The mutual interactions and mechanical binding at newly formed phase boundaries takes place too, as well as diffusion of the reactive species through the already formed hydration products. [5, 20]

The hydration products and AAMs final mechanical properties character depends on many factors as presented in several studies [21, 22]. For the instance, type of aluminosilicate precursor and type of alkali activator should be mentioned as basic ones, followed by concentration and dosage of the alkali activator, water/binder ratio, curing conditions/time, etc.

The AA efficiency depends on the pH value of the activating solution, because it influences a precursor dissolution reaction rate as well as following polycondensation reactions. The favoured pH value is 12 or higher, lower value causes dissolution process to delay, although it still occurs according to Fernandez-Jimenez and Puertas [21]. The anion type of the alkaline activator solution is the main factor influencing setting time and mechanical strength development when the pH is higher than 12. This anion can react with ions dissolved from the precursor (mainly Ca^{2+}) to generate stable hydration products. So, in the presence of silicate ions an initial calcium-silicate-hydrate is formed. It leads to a higher consumption of Ca^{2+} which helps other dissolution of Ca^{2+} from the precursor. Therefore, the setting time and strength development are accelerated. The opposite effect has been found for carbonate ions, mainly due to the activator solution lower pH and the initial formation of sodium-calcium-carbonate.

Higher short time mechanical strength is reached when NaOH as an activator is used as mentioned in paper [22]. However, at later ages higher strengths are reached for sodium

carbonate or sodium silicate activated materials. The mixtures of Na_2SiO_3 and NaOH lead to the highest long-time strength values. The same results are presented in study [23] where authors explain lower strengths of NaOH activated materials due to a denser C-S-H gel formation with increased coarse porosity in later ages. So, it leads to not well distribution of the hydration products throughout the matrix. A curing temperature also influences the product formation and strength development. Curing of NaOH as well as sodium silicate activated slags at elevated temperatures greatly accelerates product formation and the strength development as presented in paper [24].

Shi and Li [6] found out that hydration of the BFS could be described by three models due to the variation of alkaline activator type. The differences between them can be explained by a different shape of calorimetric curves (for a better illustration three typical shapes are shown in Fig. 2).

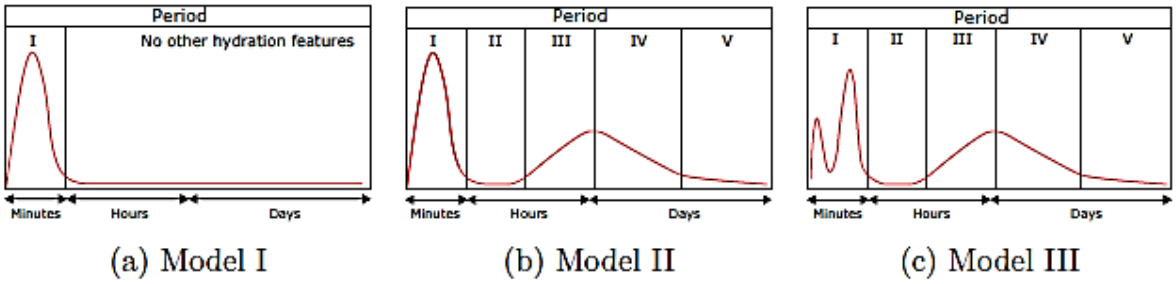

Fig. 2: The typical shapes of calorimetric curves for AA process. [6]

The first one is defined for systems without alkali activator, e.g. systems consisting of the BFS and water/Na_2HPO_4 at 25 or 50 °C. Only a small initial heat evolution peak is visible (it belongs to slag particles dissolution), no other peaks are detected in this case. Thus, the product usually does not undergo setting and hardening. The reaction of BFS particles with water leads to the Si-O, Al-O, Mg-O, and Ca-O surface bonds breaking due to the polarization effect of $(OH)^-$. These dissolved species are responsible for $(H_2SiO_4)^{2-}$, $(H_3SiO_4)^-$, $(H_4AlO_4)^-$ and Ca^{2+} formation in a water solution. The concentration of Ca^{2+} in water is much higher than others because of weaker Ca-O than Si-O and Al-O bonds. So, rich layers of Si-Al are formed on the surface of the slag particles quickly. The Si-Al layer may adsorb H^+ in the water thus concentration of OH^- increases (as well as the pH of the solution). Still, the pH value is not high enough for Si-O and Al-O bonds breaking reaction to take place in amount necessary for the formation of hydration products (C-S-H, C-A-H, or C-A-S-H) in a significant amount. [6, 25]

The second one is typical for the BFS alkali activation with NaOH at 25 or 50 °C. The calorimetric curve observes two peaks same as the curves of the ordinary Portland cement (OPC). There is a noticeable initial peak before the induction period (it belongs to wetting and dissolution of the slag particles) and one accelerated hydration peak after the induction period. The position and magnitude of these peaks are influenced by a dosage of activator and hydration temperature. The hydroxide ions concentration allows to break Si-O and Al-O bonds same as Ca-O bonds when the slag is mixed up with this high pH activator solution. This leads to a quick precipitation of thin C-S-H, C-A-H, and C-A-S-H layers through the solution. Calcium hydroxide cannot precipitate from the solution because of the higher solubility than other phases mentioned before in contrary to the OPC. [6, 20]

The last one type of curves contains two peaks before the induction period and one accelerated hydration peak after the induction period. The intensity of initial and the additional

initial peaks are dependent on the dosage/type of activator and hydration temperature. So, due to their close-range position, sometimes they can merge into the one peak. The type III is commonly used when Na_2CO_3, Na_2SiO_3 at 25 °C, Na_3PO_4 at 50 °C and NaF at 25 or 50 °C activation takes place. The initial peak belongs to wetting and dissolution of slag particles. Then, the additional initial peak formation is explained by the reaction between Ca^{2+} and anion/s group/s from the activator according to Shi et al. [6]. The solution has a high concentration of $(SiO_4)^{2-}$ which reacts with Ca^{2+} to form products like C-S-H gel in case of Na_2SiO_3 activation. The sodium carbonate activation provides $CaCO_3$ as a reaction product of Ca^{2+} and $(CO_3)^{2-}$ interaction but it is only a transitional product. This can be reason for shorter induction period of sodium carbonate than sodium silicate alkali activation. [6, 25]

The heat of hydration should also be discussed. A total amount of heat generated depends mainly on the alkaline activator type. But there are also other influencing factors like the dosage of the activator, pH value at the beginning of the reaction, water to binder ratio (w/b) or temperature during hydration. These parameters influence each other [6]. In general, as the activator dosage increases the heat of hydration increases too. For the activation using water glass, it also depends on its silica modulus. The higher water glass dosage as well as its silica modulus is, the higher cumulative heat of hydration will be. [26] An influence of the solution pH varies with type of activator. With the constant content of Na_2O the highest pH shows NaOH solution. Thus, it shows the shortest induction period and the highest hydration peak. On the other hand, Na_2CO_3 has lower pH than sodium water glass but still has a shorter induction period. The hydration of the BFS rely more on the activator anion type than the generated pH value as already discussed. Concerning the temperature during hydration, for a constant Na_2O dosage, the accelerated hydration peak appears earlier, and it is more intensive with an increasing hydration temperature. Same results are gained when activator dosage is increased at constant hydration temperature. [6]

2.4.2 Alkali activated BFS – hydration products

The main hydration product of alkali activated BFS is an amorphous or semi crystalline aluminium substituted C-S-H gel, marked as C-A-S-H gel. Its structure is usually derived from a disordered tobermorite. It has been found out that Na^+ ions can particularly substitute Ca^{2+} which leads to the formation of inner C-(N)-A-S-H gel next to the outer C-A-S-H phase. [5, 23]

A type of alkaline activator creates a variety of hydration products. The minor phases like C_4AH_{13} (for the BFSs with high CaO and low Al_2O_3 content activated with sodium silicate), $3CaO{\cdot}Al_2O_3{\cdot}CaCO_3{\cdot}12H_2O$ (for the BFSs activated with sodium carbonate) or C_4AH_{13}/C_2ASH_8 for the BFSs activated with NaOH can coexist next to the major C-A-S-H gel as mentioned in publication [6].

Some by-product phases can be formed during the AA of the BFS beside the C-A-S-H and C-S-H as result of the BFS chemical composition difference. To give an example, strätlingite phase (C_2ASH_8) or zeolites such as gismondine and garronite are formed when slags with high Al_2O_3 and low MgO (< 5 %) content are used. The use of slags with high MgO content leads to formation of hydrotalcite because of limited Mg substitution to C-A-S-H. The ferrous oxide content in the BFSs helps to formation of a low crystalline phase like hydrogranates with approximate composition $C_6AFS_2H_8$. The BFSs containing sulphate ions are responsible for ettringite formation at later hydration progress. [5, 27, 28]

The C-A-S-H gel has disordered tobermorite like structure as discussed before. It can be compared to the gel structure formed during the OPC hydration but with lower Ca content and

more Al substitution in tethraedrals. So, the C-A-S-H has more crosslinks in the tobermorite structure due to the connection of linear units through the Al contained. However, there is a limit of Al content in C-A-S-H when another crosslinking does not take place any more (approximately 6–10 chain sites). The C-S-H gel (Q and Q^1) of alkali activated BFS forms Q^3 units in contrary to the OPC. The number of Q^3 units is lower for NaOH activated systems than sodium water glass activated systems. [28]

The suitable cross-linked substituted tobermorite model (CSTM) for C-(N)-A-S-H is presented in [29] and it is shown in Fig. 3.

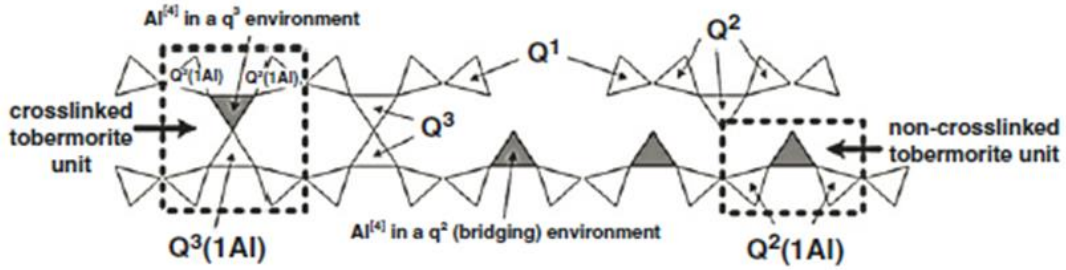

Fig. 3: Scheme of crosslinked and non-crosslinked tobermorite units representing the generalized structure of C-(N)-A-S-H type gel. [5]

2.5 Basalt

Basalt is an inorganic material firstly discovered by an American scientist in 1923. The basalt was classified as a material mainly for military and aeronautical researches in those days. Its development extensively continued during the World War II and continues ever since. [30]

The utilization of basalt fibres (BF) has attracted attention of scientists because of its high modulus, strength or strain to failure, good chemical and high temperature resistance, acoustic and vibration isolation properties and extended operating temperature range as well as easy handling. An environmental aspect of the basalt fibres utilization should also be considered due to the strict regulations. The BFs are non-reactive to water and do not cause an air pollution. The fumes released by fire exposure are less poisonous than fibres of carbon. The basalt is ecologically pure substance with three times better insulating capability in contrary to the asbestos. Likewise, there are no health hazards when the BFs are spun with a diameter higher than 6 μm. Thus, it represents a suitable replacement for asbestos. It is also 100 % recyclable. Last but not least, advantage is a low cost of the BFs given its properties. The BFs have the most preferable ratio of quality and the price parameter when compared with other types of fibres like carbon, glass, alkali resistant glass, etc. [30–33]

2.5.1 Physical and mechanical properties of basalt fibres

The basalt fibres have many favourable properties as noticed in previous lines. The Tab. 3 and Tab. 4 not only summarizes and quantifies the most important ones but there is also a comparison with other types of fibres. The basalt is a hard material with hardness value between 5 and 9 on the Mohr´s scale. Next, the BFs have density from 2.8 to 2.9 $g \cdot cm^{-3}$ which makes them suitable for concrete reinforcement (a concrete density about 2.4–2.8 $g \cdot cm^{-3}$) and preventing them from floating or diving. Given the properties of basalt and other types of fibres the price comparison gives us the interesting information too. Basalt fibres cost approximately half of the AR-glass fibres and about ten times less then carbon fibres. [31, 32, 34]

Tab. 3: Physical and mechanical properties of the BFs. [31, 32, 34]

Properties	Basalt fibre	E-glass fibre	S-glass fibre	Carbon fibre
Tensile Strength (MPa)	3.00–4.84	3.10–3.80	4.02–4.65	3.50–6.00
Modulus of Elasticity (GPa)	79.3–93.1	72.5–75.5	83–86	230–600
Elongation at Break (%)	3.1	4.7	5.3	1.5–2.0
Fibre Diameter (μm)	6–21	6–21	6–21	5–15
Linear Density (tex)	60–4 200	40–4 200	40–4 200	60–2 400
Temperature Withstand (°C)	−260/+700	−50/+380	−50/+300	−50/+700
Average market price (€/kg)	2	0,9	1,2	24

Tab. 4: The thermal stability properties of the BFs. [31]

Properties	Basalt	E-glass
Maximum operating temperatures (°C)	980	650
Sustained operating temperatures (°C)	700	48
Minimum operating temperatures (°C)	−260	−60
Thermal conductivity ($W \cdot m^{-1} \cdot K^{-1}$)	0.031–0.038	0.034–0.04
Melting temperature	1 280	1 120
Thermal expansion coefficient (ppm/°C)	8.0	5.4

It is worthy to notice an excellent thermal property of the BFs. They can withstand exposure to temperatures of 1 100–1 200 °C for hours without any psychical damage. Moreover, unstressed fibres keep their integrity up to 1 250 °C. Meanwhile, basalt can be used even at temperatures about −260 °C as well. [31]

The thermal stability of the BFs has been more studied in paper [32]. Authors studied the BFs tensile strength changes when exposed to increased temperature for two hours. They found out that up to 200 °C there had not been significant strength decrease. But with temperature over 200 °C, tensile strength started to decrease with increasing temperature. On the other hand, the BFs preserved 90 % of the original tensile strength up to 600 °C. The fibres maintained their shape and seemed to have not lost the mechanic integrity even after two hours of exposure at 1 200 °C. Still, the recommended sustained operating temperatures are under 700 °C [33].

2.5.2 Chemistry of basalt

The Basalts term is commonly used for a variety of volcanic rocks with dark colour (grey, black), formed by solidification of the molten lava on the open air. The largest deposits have been found in Russia and East Asian countries. The basalt is abundant and comprises up to 33 % of the earth´s crust. A chemical composition of basalts differs due to the geographical distribution. The crystal structure of the igneous rocks is influenced by the molten lava cooling rate on the earth´s surface.

A chemical composition of basalt is rich with SiO_2, Al_2O_3, Fe_2O_3, CaO, MgO in general, Na_2O, K_2O or titanium oxide, etc. can also be contained as minor components. [30, 31] For the igneous rock classification as the basalt it must contain from 45 to 52 % of SiO_2 and less than five percent of total alkalis as mentioned in publication [36]. An average chemical composition of basalt reached by 3 594 analyses of the basaltic rocks is presented in Tab. 5.

Tab. 5: Average chemical composition of the basaltic rocks. [36]

Chemical composition in wt. %										
SiO_2	Al_2O_3	CaO	FeO	MgO	Fe_2O_3	Na_2O	TiO_2	K_2O	P_2O_5	MnO
50.0	16.0	9.6	7.2	6.8	3.8	3.0	1.9	1.1	0.4	0.2

The main components of BFs are plagioclase, pyroxene, clinopyroxene and olivine but there are also some minor components [31]. The basalt tetrahedron (Fig. 4) is used for a better understanding of a basalt classification [37]. It describes the mineral distribution within basalt concerning the chemical nature and geological events taken place during the basalt formation. The basalt rich in silica and poor with alkalis is categorized as a tholeiitic basalt. While the alkali basalt is rich in alkalis and deficient in silica. Between these two types, there is the intermediate basalt with alumina concentration more than 17 %. [30]

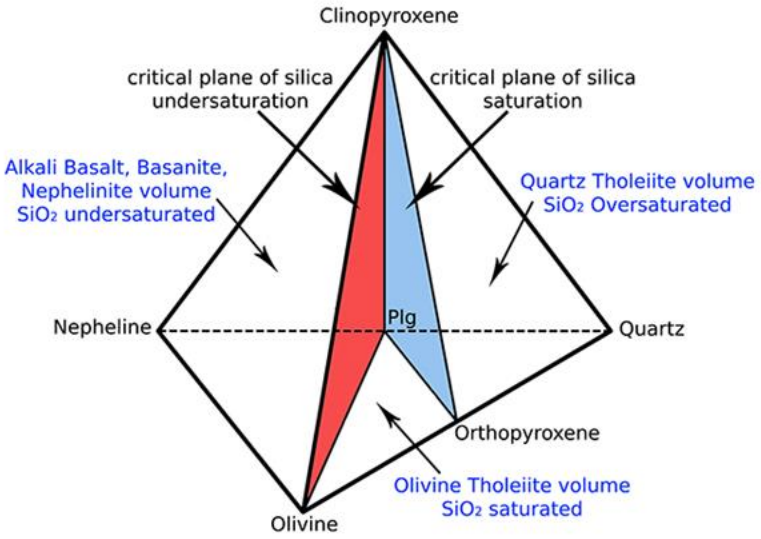

Fig. 4: Scheme of the basalt tetrahedron. [37]

2.5.2.1 Chemical resistance of basalt fibres

The chemical resistance of basalt fibres has been studied in several publications. The fibres stability under different conditions is usually expressed by change of defined properties. The most common ones are:

- Loss of mass of the fibres
- Loss of tensile strength of the fibres
- Fibres chemical composition modification and formation of the reaction products at the fibres surface

Many parameters such as temperature, an aging time, an immersion solution composition/concentration/volume, a fibres composition, a type of fibre coating, a fibre diameter or an exposed surface area of the fibre influence the corrosion rate. [38]

Let's start with the stability under the acid conditions where more widespread agreement across the publications [33, 38, 39] can be found. Wei et al. [38] studied the BFs stability during exposure to the boiling 2M HCl from 0.5 to 3 hours. As a result three times better chemical resistance of the basalt fibres compared to the glass fibres under acid conditions is presented. Still, there is a noticeable drop of tensile strength after thirty minutes exposure. But self-healing

effect of the BFs was noticed (explained by cracks filling with some reaction products) which partially compensate the tensile strength loss. The surface of the fibres is enriched with SiO_2 layer leading to a higher acid resistance at the same time. The BFs weight loss about 2.2 % after three hours of treatment is presented in paper [33].

More complicated situation arises in case of the BFs stability under the alkali conditions. There is a discrepancy regarding the stability in highly alkaline environment. So, there are some studies which present stability of the basalt fibres under alkaline conditions [31, 33, 40], while other studies report their low resistance when exposed to the alkaline solutions [30, 32, 38, 39, 41–43]. With regards to the planed applications of the BFs into the alkali activated systems with high pH value of their pore solution, stability of basalt fibres under these alkaline conditions is necessary for their implementation into this type of matrix.

Welter et al. presented that the removal of fibre size has only been noted and none fibre degradation was noticed due to the 12.5M NaOH exposure for 150 h at 40 °C in study [40]. Hence, there are no obstacles for the BFs utilization in the highly alkaline matrix based on this publication. But more authors present the opposite results. For instance, Wei et al. [38] reported loss of mass about 7 % when the BFs had been exposed to the boiling 2M NaOH for three hours, while Funke et al. [44] reported the 15 % BFs mass loss after 28 days in 1M NaOH. Next, Lee et al. present about 20 % BFs mass loss after 28 days in 10 % NaOH in paper [43]. The mass loss about 40 % is even reported after 90 days. Lee et al. also compared effect of different alkalis – 10% KOH, 10% NaOH and saturated $Ca(OH)_2$. The potassium hydroxide exposure has shown lower mass loss (about 10 % after 28 days and about 24 % after 90 days) compared to NaOH. The leaching in saturated $Ca(OH)_2$ solution did not show a significant mass loss (only about 3 % after 90 days) opposed to NaOH and KOH.

The basalt fibres mass loss is accompanied with the decrease of the rapid tensile strength. As Lee et al. presented in paper [43] a massive strength loss takes place at early stages of immersion under alkaline conditions. The tensile strength of immersed basalt fibres was lower than 7 % of their initial values after 90 days treatment in NaOH or KOH solutions. According to the results presented for the $Ca(OH)_2$ immersion, where a noticeable drop of the tensile strength is also visible, they had made a conclusion that the fibres were easily interacting even with the week OH^- medium. They compared the change of BFs properties change during leaching in 0.4% NaOH and 10% NaOH to support this statement. While the mass loss in 0.4% solution was quite stable compared to the 10% solution (approximately 3 % vs. 40 % mass loss after 90 days of treatment), the tensile strength decrease was the same in both solutions regardless to the solution concentration. Wei et al. reported even worse results in paper [38]. The tensile strength of the BFs was below 20 % of initial values after thirty minutes treatment in a boiling 2M NaOH. The tensile strength continues to decrease with increasing immersion time, until none can be measured. Sim et al. [32] also reported that basalt fibres had lost about 80 % of their tensile strength due to the immersion in 1M NaOH for 28 days.

The BFs contain large amount of SiO_2 and Al_2O_3 which causes problems when fibres are exposed to the alkali conditions. The Si-O-Si bonds as well as Al-O-Al bonds are broken down by the hydroxyl anions in the alkaline solution. Thus, the aluminosilicate network of the fibre starts to dissolve through the pores and microcracks in the surface layer and causes the decomposing of the fibre. A schematic illustration of this process is shown in Fig. 5 and the real SEM images of the fibres dissolution in NaOH solution are shown in Fig. 6. [42, 43]

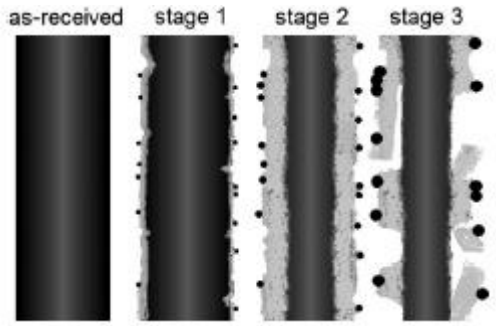

Fig. 5: Schematic illustration of the fibre dissolution process. [41]

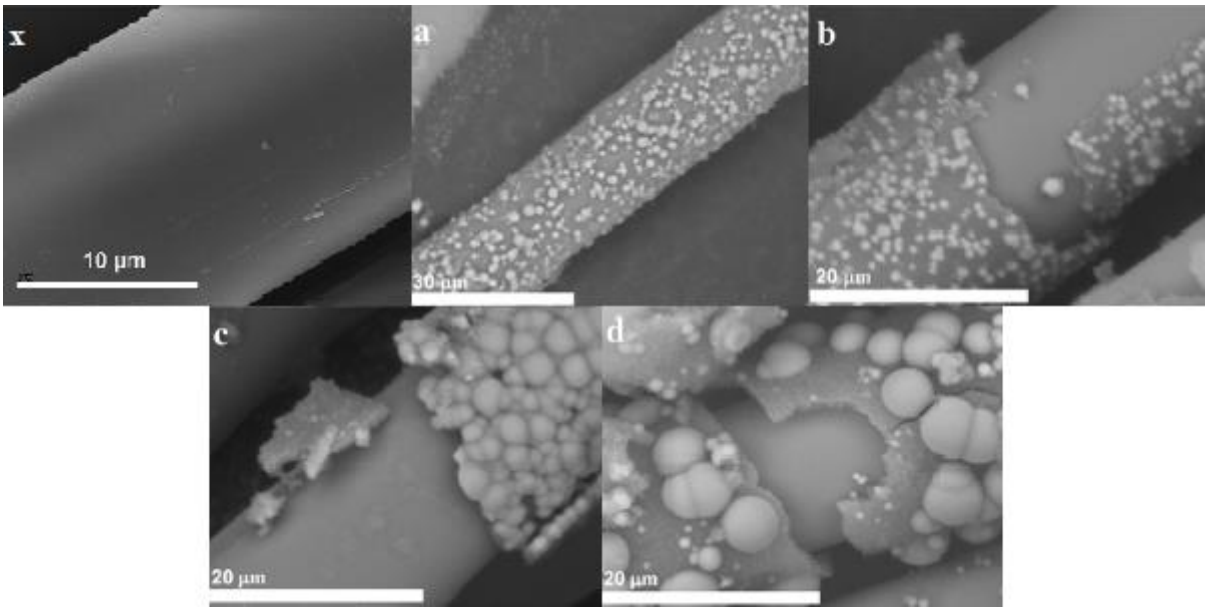

Fig. 6: SEM images of the BFs under 2M NaOH solution for different time: x – without immersing, a – 8 days, b – 16 days, c – 32 days and d – 64 days. [41]

This process can be reduced by the application of proper coating on the surface of the fibres as reported in publications [41, 42]. There is mentioned that the zirconia coating presence slows down the corrosion rate of the BFs under the alkaline conditions. The mechanism of alkali resistance improvement is based on the formation of the thin stable hydrated, zirconium rich layer on the fibre surface, which is responsible for retarding of hydroxide ions diffusion rate. Lipatov et al. [42] reported that the chemical composition in the centre of the fibre remained the same after three hours of leaching in boiling 1M and 0.5M NaOH while the surface layer underwent significant changes.

Sodium and potassium ions are firstly removed from the surface of the fibres due to their weak bonds with glass network, followed by silicon and aluminium dissolution. So, only the poorly soluble compounds as magnesium, titanium, iron, and zirconium remains on the fibre surface and form a surface shell which slows down the corrosion rate. Without the zirconia presence, the alkali resistance of the BFs is realized through the insoluble compounds of Fe^{3+}, Ti^{4+} and Mg^{2+}. Hence, formation of these compounds is a key to the alkali resistance improvement.

These assumptions are supported by results of Lipatov et al. [42] experimental research. They reported that weight loss of zirconia coated basalt fibres with optimal ZrO_2 content had

been approximately about 40 % lower than in case of the uncoated fibres when immersed in mixture of 1M NaOH and 0.5M Na_2CO_3 for 3 h at 98 °C. They also found out that amount of ZrO_2 had influenced the tensile strength of the fibre. The first small amount of Zr^{4+} leads to the strength improvement, because it behaves as a network former. Another addition of Zr^{4+} is not responsible for a network forming but Zr^{4+} only fulfil the vacant positions in the glass network. Thus, the tensile strength does not change. On the other hand, the zirconium surplus leads to the glass structure deformation, so the final tensile strength falls. They established that the optimal zirconia coating application on BFs surface leads to the better alkali resistance. The tensile strength of the zirconia coated BFs was about 50 % higher compared to the uncoated BFs after 3 h exposure to alkaline mixture defined above. It should be mentioned that the initial tensile strength of the zirconia coated BFs was about 22 % higher than uncoated ones. Hence, these reached properties are comparable to AR glass but with lower cost.

2.5.3 Basalt fibres production process

Nowadays, there are several methods used for the BFs manufacturing but their basic principles, respectively key operations are the same:

- Raw material preparation
- Rocks melting
- Homogenization of melt, delivery to the bushings
- Melt drawing through the bushing units
- Drawing of elementary filaments
- Application of sizing agents etc.

The differences between producers are made by another furnace and feeder designs same as cooling or winding conditions and so on.

The whole process starts with the raw material preparation. So, the basalt rock is crushed to get a fraction from 5 to 12 mm. Then it undergoes magnetic separation to eliminate metals and magnetic impurities. The process continues with a screening, washing, and drying. The prepared raw material is continuously loaded into the hopper of the loader above the furnace. A melting of rocks takes place in the furnace. A recuperative bath heated by gas burners is the most common one furnace type but there are also others. Either way the main requirements for the melting process are to get a required temperature about $1\,500 \pm 50$ °C necessary for the basalt rock melting in the whole bath as homogeneously as possible. That is why the two-stage heating system is usually used. They are independent on each other. The first one controls temperature in the initial heating zone, so it can be less precious than the second one which is responsible for the temperature regulation of the furnace outlet zone where extrusion bushings feeding is realized. The homogenization of melt takes place during melting and transporting processes. The homogeneous molten basalt flows to the feeder and through the electrically heated feeding tubes right into the electrically heated Platinum-Rhodium bushings. The fibres are drawn from the melt under the hydrostatic pressure and undergo cooling to form hardened filaments. The surface of the continuous fibres is covered with the sizing agent during the drawing process. It helps to prevent formation of micro-cracks on the surface as well as it reduces friction between the fibres and makes their association into the yarns easier. The fibres properties such as fibre/matrix (F/M) adhesion can be influenced by the composition of sizing agents. The filament yarn passes through the gathering shoe and it is winded to the spool. The spool with fibres is removed from the holder and replaced with the empty one and the manufacturing continues when the winding is done. A schematic illustration of the whole BFs

manufacturing process is shown in Fig. 7. The moisture of fibres at the end of the process does not overlap 1 %. [31, 33]

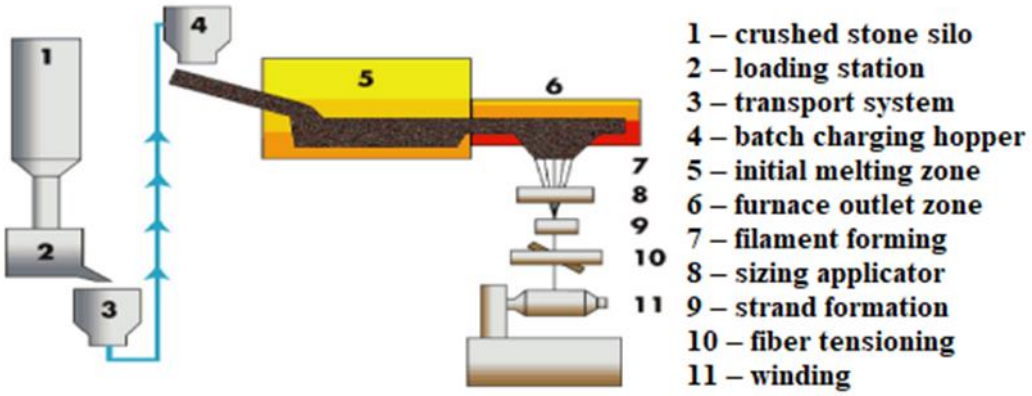

Fig. 7: Scheme of the continuous BFs production. [31]

The BFs production is a complex process and many factors influence the fibres final quality. Let´s start with a proper raw materials choice and optimal technological parameters selection. Other important parameter of the continuous fibres is a diameter of a monofilament. The elasticity increases as it reduces. The diameter depends on the melt temperature in the feeder and drawing speed (increasing the temperature same as the drawing speed increase allows to produce the fibres with a lower diameter). The melt viscosity must be optimal too. Neither high or low melt viscosity is good. A high viscosity causes fibres resistance to stretch. A low viscosity leads to preferring formation of glass drops instead of the continuous fibres. Another problem is caused by a gradual crystallization of various structural components because of the differences in their crystallization temperatures (they vary from 720 to 1 010 °C). The fresh BFs are mainly amorphous due to the rapid quenching but they have ability of partial crystallization. The BFs with higher crystalline content are produced by a slow cooling. [31, 33]

2.5.4 Application

The BFs are environmentally friendly, recyclable, fire resistant, sound proving and relatively cheap replacement for other fibres types with current maintenance or improvement of their mechanical and thermal properties likewise chemical resistance, etc. as already discussed. These facts as well as a high compatibility of BFs with other materials like concrete, metals, polymers, resins, glues, etc. predestine a broad spectrum of an industrial use. There are many variations of the basalt fibres types which also allow different uses (continuous fibres, chopped fibres, fabrics, tapes, reinforcing meshes, non-woven textiles, etc.).

To be more specific, it is mainly used for a material reinforcement to form a composite material with distinct types of matrix and production techniques. So, the automotive industry (reinforcement for brake blocks, clutch discs, interior composite materials, bumpers, car mufflers etc.), chemical and petrochemical industry (chemically resistant hard pipes for transportation of abrasive and corrosive chemicals, hot gas filters, etc.), electro insulating materials, thermal insulation and fire protection materials, laminates and prepreg production, road surfaces reinforcement or construction and production of building materials are just some of the possible uses. [30, 31, 33]

The utilization of the basalt fibres utilization as the AAMs reinforcement will be discussed more in a separated chapter considering the topic of this thesis.

2.6 Textile reinforced concrete (TRC)

The TRC has been used all around the world for different purposes as a replacement or at least partially replacement of the steel reinforced concrete (SRC) in recent years. The SRC has been used mainly because of its low cost. On the other hand, a high susceptibility to corrosion of the steel reinforcement was noticed under the conditions where it was not passivated.

The TRC exhibits a several benefits like a high durability, a high strength, a high corrosion resistance or a light weight against the traditional building materials. Given these properties the TRCs are used not only for new structures building but repairing and strengthening of the old ones as well. [45, 46]

A closer definition of the TRC term should be mentioned, before we continue. The TRC represents a material based on a combination of a fine-grained matrix reinforced with non-corrosive fibre grids. Moreover, it can be characterized as a three-phase material composed of a matrix (cementitious, AAMs, etc.), fibre/yarn structure and fibre/matrix interface. Since the matrix is cementitious or AAMs in both cases it produces a highly alkaline environment for the fibres. Thus, the fibre choice must consider these conditions as well as the temperature and humidity changes, carbonation, etc. The AR glass fibres, carbon fibres or basalt fibres can be considered as a suitable choice according to these facts. A degradation of the fibre sizing/coating and the fibre/matrix interface quality are the most critical aspects for a long-time durability of the TRC. [45, 47]

The main purposes of fibre/yarn reinforcement of the matrix are to provide a control of the cracking and to increase the fracture toughness of the brittle matrix through the stress transfer during both micro and macrocracking. The local stress transfer is realized by the de-bonding, sliding and pulling-out of the fibres. The stress is transferred to the fibres in the beginning of the macrocracking, so it helps to prevent and control the opening and growth of the cracks. Hence, the energy necessary for the crack propagation increases. The ability of the stress transfer depends on the volumetric fibre fraction, fibres orientation and distribution as well as a matrix/interface adhesion. [46] There are some techniques for anti-cracking capacity improvement such as a textile pre-stress which was studied by Du et al. [45] using a basalt textile and a cementitious matrix. The number of textile layers influence to the tensile behaviour was also studied in their publication. They reported that the specimens with one or two layers did not exhibit reinforcement efficiency. But the TRCs with three to five layers showed strain-hardening behaviour and enhancement of the tensile properties behaviour. The pre-stress application led to the first crack stress improvement, but the ultimate tensile strength was influenced just slightly. The decreasing strain capacity with increasing pre-stress level was observed.

The reinforcement of the AAMs using a basalt fabric was researched in the experimental part of this paper that is the reason the basic principles of the TRC were discussed. There are no many publications specifically focused on the utilization of basalt fabrics in the AAMs matrix. Thus, a complex point of view on the basalt fibres utilization in the AAMs will be discussed in the next chapter.

2.7 Basalt fibres utilization in the alkali activated systems

The basalt fibres utilization in the AAMs is conditioned by the fibres stability in highly alkaline pH same as a good matrix/fibre interface formation and it has been already studied in some publications. The compressive, flexural, and tensile strengths, but also the toughness or other

fracture parameters changes because of the addition of the BFs into the AAMs were the mostly researched.

Timakul et al. [48] reported that 10 wt. % addition of the chopped BFs (to the system based on the fly ash activated with mixture of Na_2SiO_3 and NaOH) had led to improvement of the compressive strength from 35 to 48 MPa (37 %) after 28 days. The compressive strength starts to decrease with addition of the BFs higher than 15 wt. % probably because of lower precursor dissolution which results to lower C-S-H content. They also suggested the formation of calcium silicate compounds at the F/M interface. On the other hand, Dias [46] reported about 6.5 % lower compressive strength with 1 wt. % addition of the short BFs.

The study [49] focuses on the flexural strength changes due to the chopped BFs addition into the matrix based on metakaolin activated with KOH. Authors reported that the fibres addition in 10 wt. % dosage had led to the flexural strength improvement from 1.9 to 19.5 MPa. There is also mentioned that removing of the silane coating from the fibres caused the strength reduction because of the fibres agglomeration. Ribero and Kriven [50] studied the similar admixture but they used the chopped fibres as well as woven basalt. Their addition led to the flexural and tensile strength improvement in both cases. More preciously, the 42 wt. % addition of chopped fibres resulted to the flexural strength rise from 4.5 to 31.7 MPa, respectively from 1.2 to 19.7 MPa in case of the tensile strength. Therefore, the mixture with 47 wt. % of the woven fibres reached values of 45.2 and 37.7 MPa for the flexural and the tensile strengths. Masi et al. [51] also investigated a flexural strength behaviour at increased temperatures. They reported the flexural strength increase between 600 and 1 000 °C due to improved F/M bonding after the sintering as result.

Same authors [51] noted that between the AAMs matrix and the BFs had been found just a minimal chemical interaction at laboratory temperatures. Because of Al_2O_3 and SiO_2 layer formation at the fibre surface which improves the alkaline resistance and leads only to a physical bondage between F/M instead of the chemical one. Thus, at laboratory temperatures the BFs addition did not significantly improved the mechanical properties. So, for a better F/M interaction they recommended the PVA fibres instead of the BFs.

The effect of the BFs addition on the fracture parameters like a fracture toughness (K_c) and a crack tip opening displacement ($CTOD_c$) in the metakaolin based AA system was studied in paper [46]. Dias and Thamaturgo reported the beneficial effect of the BFs on the tensile and splitting tensile strength. They evaluated the toughening factor of the BFs as a ratio between K_c of the composite with and without fibres. They found out that the fracture toughness had been doubled even with 1 wt. % BFs addition compared to the pure AAM. Moreover, the $CTOD_c$ was more than three times higher when compared to the pure AAM. There is also mentioned that the reinforced AAMs exhibited higher strengths than the reinforced OPC concrete.

Li and Xu [52, 53] investigated the impact properties of the BFs reinforced AAMs including the deformation and energy absorption capacity and dynamic compressive strength. The conclusion of their work is following: the addition of the BFs can significantly improve the deformation and energy absorption capacity of the AAMs but there is no significant improvement in the dynamic compressive strength. The optimum fibres fraction volume (0.3 wt. %) was established by the energy absorption capacity measuring. This amount of the BFs led to the increase of the AAMs specific energy absorption from 8.9 % (at 40 s^{-1}) to 13.2 % (at 100 s^{-1}).

A high temperature behaviour is influenced by the BFs addition too as noted in studies [49] and [50]. The pure AAM treatment at 400–500 °C results in a dehydration cracking of the

material because of a pressure gradient formed by capillary forces. But the reinforcement addition reduces the severity of the dehydration cracking by bridging actions.

Welter and Mackenzie provided a quite different point of view in their report [40] focused on the evolution of F/M interactions (in composite system based on basalt fibres in matrix of the dehydroxylated halloysite activated with mixture of NaOH and sodium water glass) after heating. They have pointed out that the AAM reinforced with BFs systems should be suitable to withstand temperatures even up to 800 °C. So, it can be possible cheaper replacement of the ceramic based composites at midrange temperatures application. They reported that no significant degradation or microstructural interaction of the BFs with the AAMs matrix have not taken place up to 600 °C. Above this temperature the crystallization and melting of the fibres had been noticed. Same as many diffusion processes within the fibres itself but between the fibres and the matrix are realized as well. Beside Fe diffusion and formation of Fe_3O_4 crystallites around the fibre, the diffusion of sodium from the matrix to the F/M interface as well as the diffusion of calcium from the fibre into the matrix are realized. So, the BFs interaction with the AAMs matrix facilitated by the inter-diffusion of the alkali ions lead to formation of albite at temperatures about 1 000 °C. It indicates different behaviour of the BFs when they are alone (softening and some degree of sintering take place at 1 000 °C) than if they are in contact with the matrix. Alkali ions defunded from the matrix act like a flux and causes softening and partial melting of the reinforcing BFs at lower temperatures. It results to the brittle failure of the fibre as well as the whole composite. Hence, the BFs/AAM composites are suitable for uses up to 600 °C.

To sum up, the AAMs reinforcement with the BFs is a suitable option, especially not only because of environmental and economic aspects but also the mechanical properties improvement as well as high temperature resistance of this composite type. On the other hand, a quality of fibre/matrix interaction is a key for successful application. The F/M interaction is quite complicated due to the high pH value of the pore solution in the AAMs which leads to high requirements for the BFs stability. The application of coating on the BFs is one of the possible ways how to improve the interface but it increases the cost at the same time. Another option considers the pore solution pH lowering by modification of the AAMs composition. Hence, there are many researches that must be done before the industrial applications.

3 GOALS AND OBJECTIVES OF THE THESIS

This thesis is focused on the possibility of the BFs utilization as the reinforcement for the alkali activated systems, including the optimal matrix composition finding as well as a final composite characterization. To achieve the aim of the thesis it is essential to accomplish the following partial goals:

- A preparation of the testing samples utilizing the BFs
- The mechanical properties testing of these samples
- The fibre/matrix interface characterization
- A testing of the BFs durability in the alkali activated systems

4 MATERIALS AND METHODS

This chapter provides information about the materials used as well as on the testing samples preparation. Different samples testing, and measurement methods are also described. Thus, the first part deals with specification of used materials, the second one focuses on the various testing samples preparation and the last one describes more complicated instrumental methods.

4.1 Materials

4.1.1 Blast furnace slag

Blast furnace slag was obtained by Kotouč Štramberk, Ltd. having a specific surface of 400 $m^2 \cdot kg^{-1}$ according to the information on the package. The chemical composition specified by the X-ray fluorescence spectroscopy (XRF) is shown in Tab. 6. The crystalline and amorphous content of the slag was determined by X-ray diffraction analysis (XRD). It has been showed that the BFS is 84 % amorphous and the rest of its contribution (16 %) belongs to the following crystalline phases: akermanite (9.5 %), calcite (3.7 %), merwinite (2.3 %) and quartz (0.5 %). The relevant diffractogram is given as Attachment 1.

Tab. 6: Chemical composition of the BFS determined by XRF analysis.

Chemical composition in wt. %									
CaO	SiO_2	MgO	Al_2O_3	SO_3	TiO_2	K_2O	MnO	Na_2O	Fe_2O_3
41.1	34.7	10.5	9.1	1.4	1.0	0.9	0.6	0.4	0.3

4.1.2 Alkaline activators

A list of alkaline activators used follows:

- Liquid sodium water glass (composition was determined by acid-base titration with conductivity simultaneous measurement – *conductometric analysis of water glass*)
    - Produced by Vodní sklo, Inc.
    - Silicate modulus – 2.24
    - Na_2O content – 15.53 %
    - SiO_2 content – 33.72 %
- Sodium hydroxide – was delivered by PENTA Ltd. in technical quality for mortars and pastes preparation while pure analysis quality was used for immersion solutions preparation
- Sodium carbonate (calcinated) – INCHEMA Ltd.

4.1.3 Basalt fibres/fabric

Basalt textile constituted of filament yarns connected into the square net and was provided by the Institute for textile technique at RWTH Aachen University. Basalt fibres have been used in form of biaxial warp knitted textile but also as unique filament yarns in some cases (specified when necessary). Filament yarns have different tex (length density of yarns – defined as weight of 1 km of yarn) in longitudinal and transverse directions. The longitudinal yarns (direction with

white threads as can be seen in Fig. 8) have tex approximately 2.6 while transverse yarns have tex about 1.3. Tab. 7 gives us information about the chemical composition of basalt fibres from Kammeney Vek determined by XRF. The phase composition was studied using XRD analysis (Attachment 2). It has been found out that basalt fibres used for the experiments have been amorphous. A total appearance of the fabric same as appearance of fibre yarns created from this fabric as they were used for different purposes can be seen in Fig. 8.

Tab. 7: Chemical composition of the BFs from Kammeney Vek determined by XRF analysis.

Chemical composition in wt. %								
SiO_2	Al_2O_3	Fe_2O_3	CaO	MgO	Na_2O	K_2O	TiO_2	Other
55.69	15.44	10.80	7.43	4.06	2.40	1.51	1.23	1.44

Fig. 8: Photos of basalt fabric and filament yarn created from the fabric as were used in experimental procedures.

4.1.4 Other materials

4.1.4.1 Water

The demineralized water produced at the Faculty of Chemistry was used for samples preparation.

4.1.4.2 Shrinkage reducing admixture

STACHEMENT AC 600 produced by Stachema Kolín Ltd. was used as a shrinkage reducing admixture.

4.1.4.3 Aggregates

Standard siliceous sand according to ČSN EN 196-1 was used for the mortar preparation. More precisely an equal distribution of three fractions has been used – fine sand PG I, medium sand PG II and coarse sand PG III. The sand to binder weight ratio in mortars was 3 : 1.

4.2 Testing samples preparation

This part deals with describing of testing samples preparation procedures for different purposes.

4.2.1 Mortar/paste preparation

Mortars or pastes preparation have been done according to ČSN EN 196-1. The whole mixing process took three minutes. Individual steps can be described as follows:

- In advance prepared activator solution including water was poured into the mixing bowl same as the slag. Then a low speed rate stirring started while tracking time.

- A defined amount of standard sand (equally distributed to fraction from 0 to 2 mm) was added after one minute in case of mortars while stirring. Then the stirring speed was increased.
- A stirring was stopped after 30 s and the mixture adhered to the bowl walls was wiped out with a plastic spatula during another thirty seconds.
- High speed stirring was realized until the time of three minutes was reached.

This procedure was followed by other actions depending on the intended testing use. Single testing procedures will be discussed more closely in following paragraphs. Water to binder ratio was 0.49 for mortars and 0.36 for pastes preparation in all cases. An amount of shrinkage reducing admixture added was also the same in all cases (0.75 % by slag weight). Following alkaline activators compositions were used for the blast furnace slag AA during different experimental procedures related to this paper (note: percentage of Na_2O by weight of BFS):

- Sodium water glass + sodium carbonate (WG/SC) – M_s = 0.5; with different wt. % of Na_2O (6; 8; 10 and 12 %).
- Sodium water glass + sodium hydroxide (WG/SH) – M_s = 0.5; with different wt. % of Na_2O (6; 8; 10 and 12 %).
- Sodium water glass (WG) – M_s = 2.24; with different wt. % of Na_2O (8 and 10 %).
- Sodium hydroxide (SH); with different wt. % of Na_2O (8 and 10 %).

4.2.2 AAMs reinforced with basalt fibres

It should be mentioned that mortars or pastes have been used mainly as matrices for reinforcing material (fabric/fibre) implementation to form a AAM reinforced with BFs. But they also served as a reference to the comparison between properties of reinforced and non-reinforced samples. The reinforcing material (fibre/fabric) has been placed to the defined positions and orientation in the moulds manually.

A testing sample preparation process basically consisted of matrix casting to the specific mould, continued with compacting, emplacement of reinforcing material in correct place with proper orientation and mould completion with matrix followed by another compacting for 15 s on the compacting table. The prepared moulds were placed into the plastic bag and stored under wet air conditions for 23 hours (until samples were pulled out from the mould). The samples were then wrapped with a plastic film and stored until the next testing took place at laboratory temperature in wet repository.

4.2.3 Compressive and flexural strength

Compressive and flexural strengths determination was chosen as a basic parameter for the mechanical properties testing. Specimens with dimension 40 × 40 × 160 mm served for the flexural strength test (three-point bend arrangement), while the compressive strength tests were performed on the broken parts of the specimens after the flexural strength tests. These tests were carried out at the age of 24 hours, 7 and 28 days after the specimen preparation according to the ČSN EN 196-1. Long-time mechanical properties development was studied as well in several cases. Thus, testing intervals were prolonged to 56; 84 and 112 days. The flexural strength has been tested on two specimens, so there have been four specimens for compressive strength

testing at each time interval for each sample. The mechanical properties testing was done using the Desttest 4310 Compact A (Beton System, Ltd.).

These tests were realized on mortars (reference) and mortars reinforced with the basalt fabric. Commonly one layer of the fabric was added to the middle of the specimen, but influence of number of fabric layers was studied too (fabric layers were distributed equally, so the same amount of mortar was between the layers always).

4.2.4 Single fibre yarn pull-out test

It is a method used for a direct estimation of fibre/matrix interfacial bond properties based on pulling out of a single fibre yarn of its surrounding matrix. The knowledge of F/M interfacial properties is important due to the control and prediction of composite macroscopic behaviour. Principally, better the interfacial shear bond strength better the composite is. Increase of the interfacial bond strength leads to the composite strength and toughness increasement. On the other hand, beyond certain bond strength, composite toughness starts to decrease because of the fibre rupture. Hence, pull-out of the fibres rather than their rupture ensures a larger ductility to the fibre reinforced composite (FRC). A fibre debonding as same as pull-out at the interface also influence the energy absorption during the crack propagation. The contributions of frictional and chemical bonds characterize the interfacial bond strength. [54–56]

The typical single fibre pull-out curve given in Fig. 9 can be described as follows. The load resistance increases up to P_a while the fibre embedded length does not change – displacement corresponds only to the elastic stretching of the de-bonded fibre segment and the fibre free length (this part belongs to debonding). It is followed by the load decrease from P_a to P_b. A character of this drop is important for prediction of the dominant bond type. If the drop is significant it indicates that the chemical bond between F/M has broken down. In contrary if the P_a is close or equal to P_b it indicates nonchemical F/M bonds. Hence, reaching of load P_b means that fibres are de-bonded and slippage regime starts. The fibre load resistance is realized by frictional forces. The frictional forces are usually more significant to the total interfacial bond strength than contribution of chemical bonds during the pull-out process. [54]

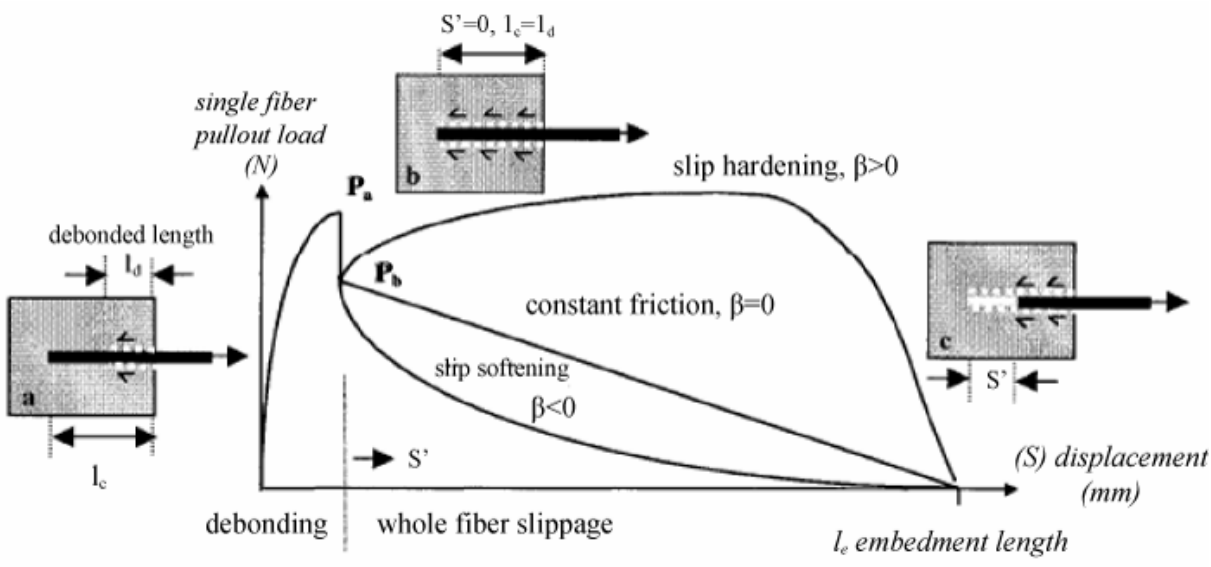

Fig. 9: Scheme of general single-fibre pull-out curve. [54]

The F/M interface properties are experimentally determined using a load-displacement relation of the fibre which is pulled-out from the surrounding matrix. Interfacial shear strength bond can be determined using following equation as defined in study [56]:

$$\tau_0 = \frac{P_b}{\pi d_f L_e} \quad (3)$$

Where τ_0 belongs to the interfacial shear bond strength; P_b represents the load after the sudden drop following the peak of pull-out load (70 % P_a); L_e is the fibre embedment length; and d_f is the diameter of the fibre.

The testing samples were prepared into a special mould – illustration of preparation of testing samples can be seen in Attachment 3. Varying mortars have been prepared as defined in 4.2.1. and have been filled into the open mould to its half, then a fibre yarn was placed into the specific spot in the mould and the mould was closed after that. A fibre embedment length was measured using meter and modified if required. The moulds were fulfilled with mortar and compacted for 15 s after that. Storage conditions were the same as described in 4.2.2. The different embedment lengths same as curing time were tested. The embedment length of 0.5 cm and curing time of 72 hours proved to be the most appropriate for intended experiments. Testing samples had shape of cubes with dimension 40 × 40 × 40 mm and were reinforced with fibre yarn right in the middle. Fifteen samples were prepared, tested, and evaluated for each matrix type (WG/SC and WG/SH activator mixtures with activator dosages 6–12 % Na_2O).

The pull-out tests have been measured using Universal mechanical testing machine Instron 5985 (testing set-up can be seen in Fig. 10) with following parameters: testing speed 2 mm/min; fibre length between matrix and jaw – 10 cm. A maximal force (F_m) has been measured before the fibre broke down or was pulled out along with deformation.

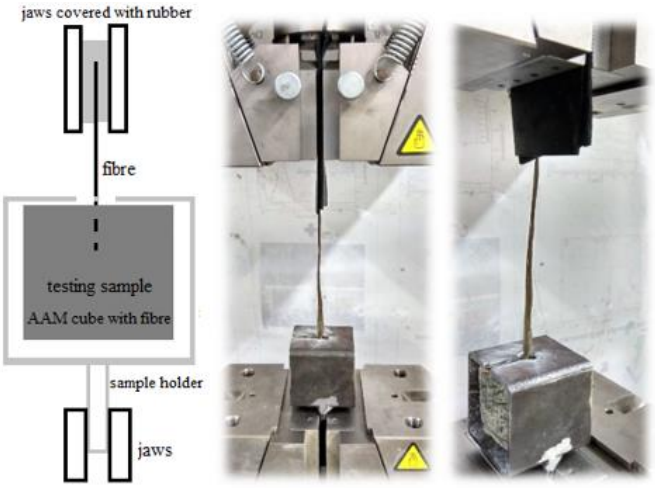

Fig. 10: Schematic drawing and photos of pull-out testing set-up.

4.3 Basalt fibres testing

The testing of the BFs has been done with a goal to figure out the influence of immersion under alkaline environment like conditions in the AAMs to their properties. Changes of these specific properties have been studied for this purpose during alkaline immersion of the fibres.

4.3.1 Accelerated leaching tests

The accelerated leaching tests according to paper [47] have been done due to an effort to predict the behaviour of BFs from a long-time point of view. This test can be specified as an immersion of prepared fragments of the BFs in solutions with a specific composition at increased temperature (60 °C) for defined time.

The leaching solutions were designed based on a mixture composition at the begging of the mortar/paste mixing process (water, alkaline activator) with a goal to overproportionate real pore solution conditions. Since the concentration of alkalis in alkaline activator mixture with water are the highest at the beginning of mixing process and their concentration in pore solution decreases with increasing hydration time of the AAMs. Thus, the leaching of BFs in this initial solution gives us the information about the behaviour under the worst scenario conditions. The studied solutions were mixtures with following constitution:

- WG/SC – M_s = 0.5; activator dosage 6; 8; 10 and 12 % Na_2O; w/b = 0.49.
- WG/SH – M_s = 0.5; activator dosage 6; 8; 10 and 12 % Na_2O; w/b = 0.49.

4.3.1.1 Loss of mass of the fibres

The loss of mass of the fibres can be easily specified by a weight change of the samples. Thus, the BFs samples (the basalt fabric cut to fragments about 2 × 2 cm) have been weighted using analytical balance and placed into a suitable container. The container was filled with defined amount of solution and placed into the drying machine heated up to 60 °C thereafter. This process has been repeated with various solutions. Two fragments had been taken out in defined time intervals (1; 7; 14; 21 and 28 days); washed in distilled water for 24 h and then dried at 60 °C until the constant sample weight was reached. Finally, the weight of the sample was measured and the loss of mass (weight change) of the fibres was determined.

4.3.1.2 Loss of tensile strength of the fibres

Same as the loss of mass the loss of tensile strength of the fibres due to the immersion under alkaline conditions can be determined. The leaching, washing, and drying experimental procedures were quite the same but with different sample size (the BFs fabric was cut into the bundle of filaments with length about 35 cm). The prepared samples (immersed for 1; 7; 14; 21 and 28 days in various solutions) underwent tensile strength testing using Universal testing machine Zwick Z010. A testing procedure was based on the ASTM D2256 but with different deformation rate (5 mm/min). The gauge length between jaws was also changed (100–150 mm) during measuring due to the different disintegration of immersed testing samples. The maximal strength before break and deformation were measured and then evaluated. Because of the fibres immersion under alkaline conditions these parameters development have been noticed. Results are expressed as a percentage change against the reference (fibres kept at 60 °C for the same time as the samples but without immersion), hence as a tensile strength maintenance. Two samples of each solution type were tested in each testing interval.

4.3.1.3 Fibres chemical composition changes

An influence of the leaching of the fibres to their chemical composition changes and the reaction products formation have been studied on the fragments remained from the loss of mass tests. These samples were tested with instrumental techniques XRD and XPS which will be discussed later.

4.4 Instrumental techniques

4.4.1 Inductively coupled plasma optical atomic emission spectroscopy

The inductively coupled plasma optical atomic emission spectroscopy (ICP–OES) is a precious analytical technique which provides a multi-elemental analysis of the sample. As a result, it gives us the information about the elemental composition of the sample. A content of each element in that sample can be determined as well. The detection limits of the ICP-OES allow to even trace elements determination.

Sample ionization takes place at the torch with the inductively coupled plasma (argon plasma generated by an alternating high frequency field is the most common plasma source) at the beginning of the measuring. The sample injection into the plasma leads to the sample drying, evaporation and atomization. The revealed atoms are ionized and excited due to the high energy of the plasma. These excited states are highly unstable, thus a deexcitation takes place. The emission rays are released when the excited atoms return to the basic (stable) energetic levels as a result. The corresponding wavelengths of photons are measured at the detector. A line spectrum is a result of the measurement. A peak position allows to identification of the element while a peak height is equal to a signal intensity respectively it allows the concentration of element to be determined.

The samples were prepared by immersion of the fragments of the basalt fabric with defined weight in defined amount of various solutions (specified in 4.3.1) for defined time (1; 7; 14; 21; 28; 56; 84 days) at 60 °C. The required amount of samples solutions was taken out, filtered through the 0,45 μm syringe filter and then pipetted and 500times diluted with distilled water at each interval. Such prepared samples have been measured using Horiba scientific Ultima 2 with a goal to determine solutions composition change due to the fibres dissolution. Measured elements were Si, Al, Fe, Ca and Mg regarding to the composition of BFs same as the AAMs characteristics. [57]

4.4.2 X-ray Fluorescence spectroscopy (XRF)

The XRF is non-destructive analytical technique which allows to determine elementary composition of the sample. Detection limits depends on the element type and usually ranges between $10–10^{-4}$ %.

It is an X-ray technique thus, it is based on the X-ray interaction with electrons in sample and the secondary (fluorescence) radiation emission. When an inner orbital electron is ejected from an atom, an electron from higher energy level will be transferred to its place while a characteristic photon is emitted (characteristic X-ray of the element) and its energy is equal to the energy difference between two orbitals where electron transition was realized. Hence, the energy determination of photon emitted allows to specify an identity of the element. An amount of the analyte in the sample can be characterized by the peak intensity (number of photons with specific energy emitted per unit time). There are two commonly used XRF types. The first one is energy dispersive (ED-XRF) which detects the secondary radiation based on different released photon energy and the second one is wavelength-dispersive (WD-XRF) which contain a crystal responsible for radiation decomposition by wavelengths. [57]

The purpose of XRF analysis use in this thesis consisted in characterization of raw materials and it was done using XENEMETRIX EX-6 600 SSD.

4.4.3 X-ray Diffraction analysis (XRD)

The XRD analytical technique is commonly used for the structure determination of the solid crystalline substances. Each crystalline substance forms a unique diffractogram. It is based on the diffraction principles and interactions between the X-ray and particles in the lattice planes. So, the radiation scattering take place at the lattice and it is followed by radiation interference leading to the diffraction maximums formation due to the regular arrangement of atoms in crystalline phases. The position, intensity and shape of these diffraction maximums depend on the atom types and their configuration.

Thus, the basic principle can be described as follows. The X-ray impacts to the analysed substance where a smaller part of radiation is reflected and scattered, the rest enter the substance where the scattering process is repeated on the individual lattice planes. An interference of scattered radiation takes place and the characteristic diffraction maximum is formed when a characteristic X-ray impact angle (*Bragg´s angle*) is reached.

The knowledge of this specific angle same as knowledge of the *Bragg´s* equation (4) allow us to determine the lattice planes distance as well as the lattice parameters which characterise the crystalline structures. [58, 59]

$$2d \cdot \sin\theta = n \cdot \lambda \tag{4}$$

Where n – positive integer, λ – wavelength of the incident wave, d – lattice planes distance, θ – *Bragg´s angle.*

The scheme of the X-ray diffraction on the crystalline lattice same as simplified scheme of the XRD arrangement is shown in Fig. 11. The XRD results presented in this thesis have been measured using the Empyrean device made by Panalytical. This technique was used for the raw materials characterization and residual reaction products from basalt fibres leaching determination.

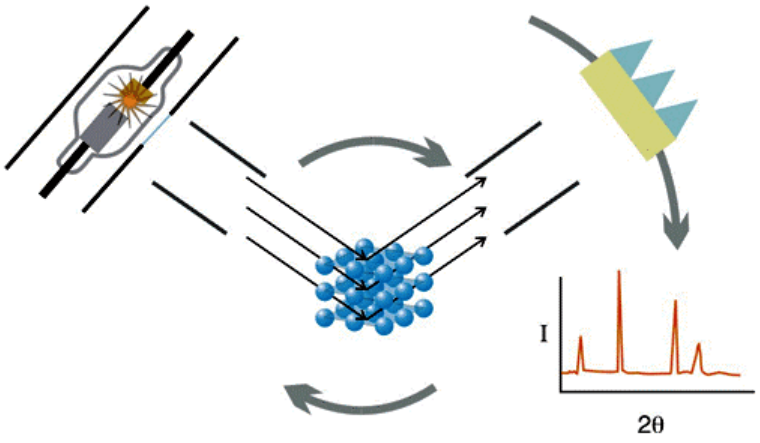

Fig. 11: Simplified scheme of the X-ray diffraction on the crystalline lattice. [58]

4.4.4 X-ray Photoelectron Spectroscopy (XPS)

The X-ray photoelectron spectroscopy is the semi-quantitative technique based on a photoelectric effect which is commonly used for surface analysis (1–10 nm) and composition determination. The photoemission process from a solid sample takes place when a high energetic photon interacts with matter to cause electron removal from an atomic orbital and reaching the vacuum level. This process usually consists of these steps – absorption and

ionization; atom response and photoelectron formation and finally electron transport to the surface and its escape to the vacuum. A simplified scheme of photoelectron emission principle and Auger relaxation effect is shown in Fig. 12.

The sample is irradiated with mono energetic X-rays to cause photoelectrons emission from the surface of the sample. The kinetic energy of these photoelectrons is characteristic for the element from it originated. Each chemical element has unique electronic structure; hence the electrons are emitted with specific kinetic energies. They are separated by their kinetic energy and frequency in analyser (e. g. hemispherical electron energy analyser) and detected. Thus, the peaks intensity and their position in an energy spectrum provide required information about a chemical state and quantity. It should be noticed that the binding energy is calculated according to following equation:

$$E_{\text{binding}} = E_{\text{photon}} - (E_{\text{kinetic}} + \phi) \tag{5}$$

Where E_{binding} is the binding energy of the electron; E_{photon} is the energy of the X-ray photons being used, E_{kinetic} represents the kinetic energy of electrons measured by the analyser and the ϕ belongs to work function of the spectrometer.

According to the basic principles of XPS it allows to detect all elements with atomic number three and above. The detection limits are about from parts per thousand to parts per million depending on experimental conditions and the element type. [57, 60]

The XPS analyses were carried out with Axis Ultra DLD spectrometer using a monochromatic Al Kα (hν = 1486.7 eV) X-ray source operating at 75 W (5 mA, 15 kV). The spectra were obtained using an analysis area of 300 × 700 μm approximately. The Kratos charge neutralizer system was used for all analyses. The high-resolution spectrum was measured with the step size 0.1 eV and a pass energy of 20 eV. Instrument base pressure was $2 \cdot 10^{-8}$ Pa. The spectra were analysed using CasaXPS software and have been charge corrected to the main line of the carbon C 1s spectral component (C\C; C\H) set to 284.80 eV. A standard Shirley background was used for all sample spectra. The XPS measurements were done with a goal to characterize the changes of BFs surface layer due to the immersion under the alkali conditions. Measurements were realized on the samples remaining from the loss of mass testing described above.

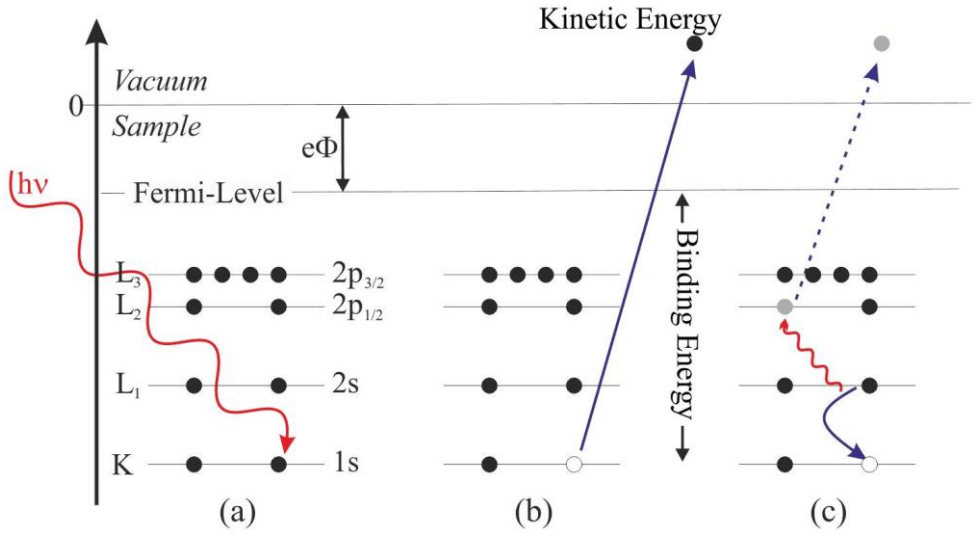

Fig. 12: Scheme of photoelectron emission principle (a, b) and Auger relaxation effect (c). [60]

4.4.5 Scanning Electron Microscopy (SEM)

The basic principle of SEM is based on interaction of the primary electrons (released from cathode and fastened by the affecting electric field) which are scanning the surface of the sample and a small space underneath (1–3 μm). Varying responses are formed (secondary electrons – SE, backscattered electrons – BSE, Augers electrons – AE, characteristic X-ray, braking X-ray, or fluorescence) because of this interaction. A scheme of these interactions and responses is shown in Fig. 13.

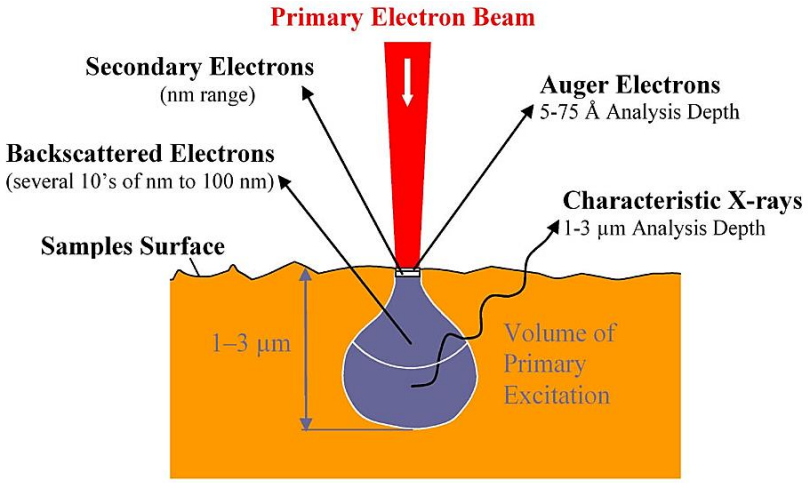

Fig. 13: Scheme of electron-surface interaction during SEM analysis. [61]

The main source of information for the SEM analysis is SE that determine the sample relief and the BSE which provide us information about the element composition or the sample crystallography. The X-ray signal or AE as minor sources are relevant to morphology or character of chemical bonds. The final image produced by electron scanning of sample surface is based on contrasts. The contrasts are produced due to the protons number (material contrast) where heavier elements have a brighter colour and lighter elements are darker but also due to the different surface topography (relief contrast) where hollows provide lower signal intensity, thus they are darker than lighter elevations which provide a stronger signal. The electron penetration depth depends on the sample atomic weight, a proton number, material density or fastening voltage intensity. The SEM analysis is suitable only for conductive samples. So, if they are not they have to be metallized by a thin layer of electrically and heat conductive metal.

The element analysis of the sample can be done using the energy dispersive X-ray spectroscopy (EDX) or by wavelength dispersive spectroscopy (WDX). The EDX uses detection and analysis of characteristic X-ray energy to form a spectrum specifying frequency of X-ray signals in individual energetic areas. Hence, this spectrum contains characteristic peaks belonging to single elements and the height of these peaks is directly proportional to the concentration of the element in the sample. The EDX analysis has lower resolution and detection limit than WDX, but it is faster and allows to measure all elements at once.

The ZEISS EVO LS 10 scanning electron microscope with EDX analysis has been used with an accelerating voltage 10 kV for experimental purposes of this paper. The prepared samples (reached by breaking down of hardened pastes reinforced with basalt fibres and excessive fibres removal) were stuck on a carbon tape and sputter-coated with gold. The SEM tests were performed at the age of 7 and 28 days of hydration.

5 RESULTS AND DISCUSSION

5.1 Alkali activated materials reinforced with basalt fabric

The influence of basalt fabric addition into the matrix consisting of BFS activated with varying alkaline activators to the mechanical properties (compressive and flexural strength) and their development will be discussed in following paragraphs. A closer investigation of the matrices properties themselves will be done as well.

5.1.1 AAMs based on WG/SC and WG/SH alkaline activator solutions

The blast furnace slag activated with alkaline activator based on sodium water glass with lowered silicate modulus (0.5) was chosen as a basic matrix for other modifications, testing and fabric implementation. It resulted from previous research which has been done by Material Research Centre at BUT. Silicate modulus reduction to 0.5 was obtained by sodium carbonate or sodium hydroxide addition and kept the same all the time same as water to binder ratio (mortars – 0.49; pastes – 0.36). Meanwhile a dosage of alkaline activator ranged from 6 to 12 % Na_2O (by slag weight) in both WG/SC and WG/SH cases. It should be mentioned that the optimal activator dosage is not only a question of mechanical strength development but also of cost and other properties.

The flexural and compressive strengths development of BFS activated with sodium water glass and sodium carbonate as a function of alkaline activator dosage are shown in Fig. 14 and Fig. 15, respectively. The influence of basalt fabric implementation in one layer into the matrix is presented in the same figures, too. Studied variables were the same in case of BFS activated with sodium water glass and sodium hydroxide these results are presented in Fig. 16 (flexural strength) and Fig. 17 (compressive strength).

Let's focus on compressive strengths of pure matrices without fabric addition before anything else. The strength increases with rising activator dosage (6–12 % Na_2O) in both cases (WG/SC; WG/SH) after one day. But the strength development trend shape changes with prolonging curing time. This statement can be supported by results of WG/SC with dosage of 12 % Na_2O because the lowest strength gain has been noticed after 7 days and ever since. It can be also confirmed by theoretical assumptions presented in paper [18] where authors noted that after reaching a certain % Na_2O value there is no further significant strength increase, moreover a strength decrease can be noticed. The Na_2O dosages ranging from 6–10 % led to significant strength increase after 7 days. More preciously 50.1; 28.5 and 12.3times higher compressive strengths were obtained when compared to the ones after one day. It can be also seen that WG/SC mixtures with 6 and 8 % Na_2O had no other significant strength gain after 56 days. In contrary to the 10 % Na_2O WG/SC mixture where a noticeable strength increase has been noticed even after 112 days (84 vs. 112 days – improvement about 15 %). This mixture also had the highest strength gain between 7 and 28 days since the compressive strength increased about 47.5 %. With respect to these results same as the compressive strength (83.8 ± 4.2) MPa obtained after 112 days; BFS activated with 10 % Na_2O WG/SC activator mixture seems to be the most preferable. Considering the standard deviations, the results obtained fulfil the theoretical assumptions as presented in publication [62] where the compressive strength increase with Na_2O dosage from 4 to 8 % had been stated.

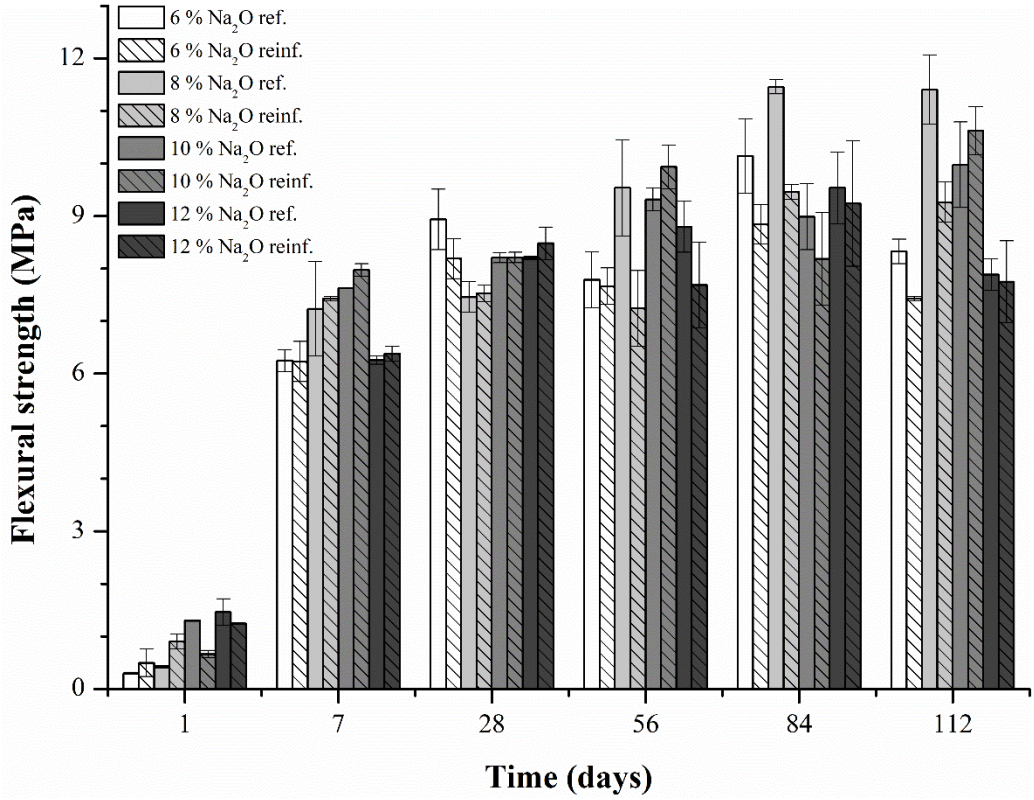

Fig. 14: Flexural strength development as a function of alkaline activator dosage (6–12 % Na_2O) and basalt fabric reinforcement for WG/SC activated systems.

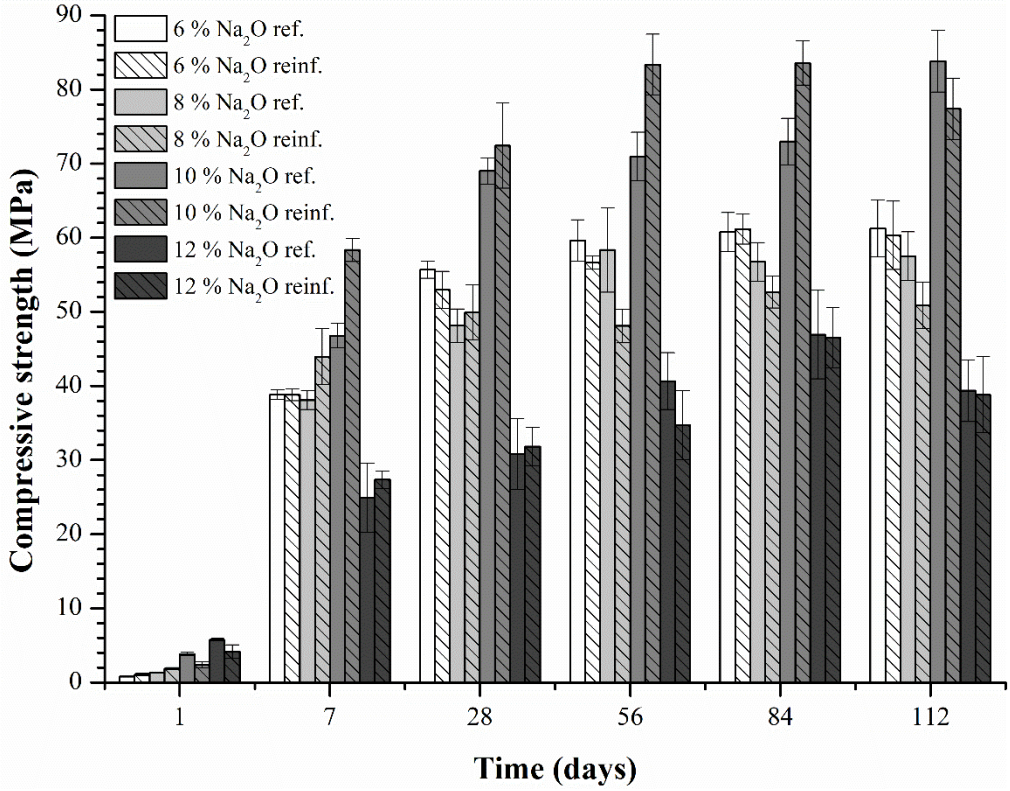

Fig. 15: Compressive strength development as a function of basalt fabric reinforcement and alkaline activator dosage (6–12 % Na_2O) for WG/SC activated systems.

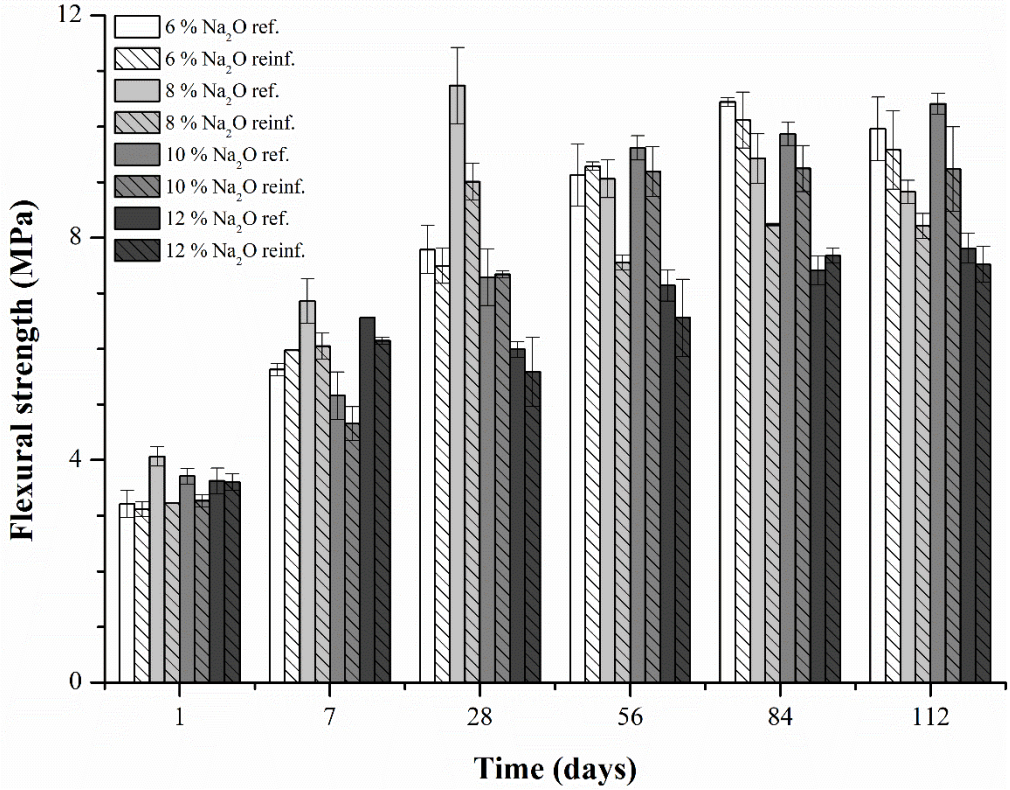

Fig. 16: Flexural strength development as a function of alkaline activator dosage (6–12 % Na_2O) and basalt fabric reinforcement for WG/SH activated systems.

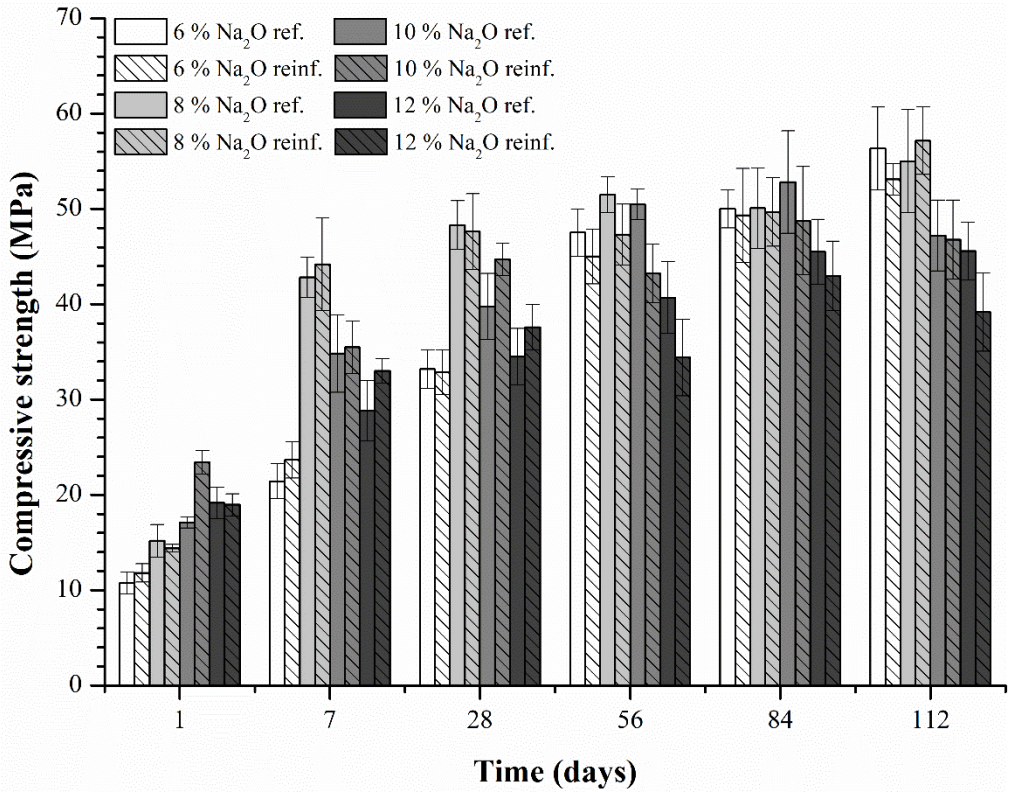

Fig. 17: Compressive strength development as a function of basalt fabric reinforcement and alkaline activator dosage (6–12 % Na_2O) for WG/SH activated systems.

The closer investigation of WG/SH activator results obtained should be done too. The most significant compressive strength gain (2.82times higher compressive strength) was observed by 8 % Na_2O dosage between one and seven days (but another strength improvement was noticed just slightly beyond this age (16 % incr. after 84 days and 28 % incr. after 112 days when compared compressive strength after 7 days). Other activator mixtures showed following strength improvement: 6 and 10 % Na_2O had 7 days compressive strength approximately 2times higher while in case of 12 % Na_2O increasement was just about 1.5 when compared to the ones after one day. On the other hand, this improvement continued more significantly for 10 and 12 % Na_2O dosages up to 84 days of curing, moreover up to 112 days for 6 % Na_2O dosage. Hence, the beneficial effect of SC replacement with SH to the initial mechanical strengths (one day) was observed. These results are in good agreement with papers [21] and [22] where the higher activator solution pH explains this fact. As opposed to the WG/SC activated systems finding the best Na_2O dosage is quite difficult for WG/SH activated systems. However, regarding the pH and cost reduction dosage of 6 or 8 % Na_2O mixture would be probably preferred.

With respect to the activator used and the results obtained for long-time compressive strength properties of WG/SC and WG/SH with 6 or 8 % Na_2O activated systems are comparable and there is no significant difference between them. Nevertheless, mechanical strength results achieved by 10 % Na_2O WG/SC activated systems seem to be over the others. The test results of flexural strength measurements are less convincing due to higher standard deviations same as lower number of testing samples (two vs. four specimens for compressive strength testing). Considering all factors general trends can be considered as like the ones described above for both activator compositions. A lower flexural strength difference between 6–12 % Na_2O mixtures is worth to mention speaking of WG/SC activated systems. Still, 8 and 10 % Na_2O mixtures seems to be preferable. There are no significant exceptions in case of WG/SH activated system. Mechanical properties dominance for BFS activated with 10 % Na_2O WG/SC mixture was reduced based on the flexural strength testing.

We should focus on basalt fabric reinforcement influence on the mechanical properties now because this knowledge is crucial in behalf the topic of this thesis. Let´s start with WG/SC mixtures. The 10 % Na_2O dosage seems to be the most beneficial when investigating compressive strengths with respect to all activator dosages used. The addition of one layer of basalt fabric led to the compressive strength improvement for up to 84 days, but beyond this age strength decrease was observed. More preciously, increase of compressive strength about 24.7; 0.5; 17.5 and 14.5 % was noticed after 7; 28; 56 and 84 days of curing. Still it ranges around the standard deviations quite often. It indicates that trend of improvement is not that simple and clear as we would hope when considering standard deviations. The basalt fabric addition in one layer had no beneficial effect for 6; 8 and 12 % Na_2O WG/SC mixtures (one day compressive strengths are not considered, because this time-period does not seem to be enough for sufficient F/M interaction formation). There was observed no improvement of flexural strengths for any WG/SC activated mixture due to the basalt fabric implementation when investigating thoroughly the entire 112 days testing interval.

WG/SH activated systems will also be described. Unfortunately, any of tested alkaline activator dosages did not led to compelling compressive or flexural strength improvement when reinforced with the one layer of basalt fabric. The difference between mechanical properties of pure matrix and the reinforced one lies in standard deviations almost all the time.

Finding of comparisons in the literature is quite complicated because there are not many publications focusing on basalt fabric addition into the AAMs based on BFS activated with

WG/SH or WG/SC mixtures exactly. For instance, authors presented compressive strength increase about 37 % after 28 days in paper [48]. However, these results should be taken with reserve because authors used 10 wt. % of chopped basalt fibres instead of fabric in AAM based on fly-ash activated with WG/SH.

It is necessary to focus on factors which can influence the efficiency of the fabric reinforcement in AAMs considering the achieved results. One of the most crucial is F/M adhesion. It seems that F/M interaction leading to a good adhesion could be realized for 10 % Na_2O WG/SC mixture based on mechanical strength results obtained. On the other hand, this assumption was partially disproved by SEM analysis of interfacial zone (it will be discussed in 5.2.1). Thus, is not surprising that low or none F/M adhesion leads to poor stress transfer same as mechanical properties improvement. Nevertheless, some sort of F/M interaction in interfacial zone for the BFS activated with 10 % Na_2O WG/SH mixture was observed using SEM and still, there was no significant or stable mechanical properties improvement when reinforced with fabric. This fact may be related to other factors like fibre/fabric orientation in matrix, fibre/fabric dimension and content or the fabric itself (bundles/fibres diameter, connection type, etc.). The impact of these factors to the mechanical properties is described in publications [63] or [64]. Some important remarks from these sources will be outlined just briefly. The orientation of reinforcement (the angle in degree between the reinforcement fabric and direction of applied stress) affects the mechanical strength because it determines the mode of material rupture. A local disorientation not only will result into the inefficient stress transfer between the F/M, but it will act like a stress concentrator. A local bending in the fibre around the crack will induce flexural stresses in the fibre and will lead to local compressive stresses in the matrix at the same time. The rupture mode gradually shifts from tensile and shear failure to the critical break in the transverse direction with an increasing angle.

The form of arrangement of the basalt fabric used in this thesis can be responsible for significant mechanical properties improvement absence as well. The longitudinal and transverse filament bundles are connected just loosely with a thread which leads to the individual bundles movement. It can result into the local bundles disorientation against the planned arrangement. Hence, another fabric type or utilization of moulds with a possibility of fabric hitch to fix their orientation could lead to mechanical properties enhancement due to the elimination of local disorientations. The distortions and local disorientations could be seen on specimens' fracture surfaces in some cases. Thus, the obtained mechanical properties results may be explained based on information gained from sources above.

The deterioration of basalt fibres mechanical properties due to the immersion in AAMs which could resulted into the reduction of fibres capability to carry the stress transferred from the matrix as one of the possible reasons for reinforcement inefficiency is necessary to mention as well. Significant BFs tensile strength drop was observed in accelerated leaching tests (5.3.2).

The BFS activated with $M_s = 0.5$; WG/SC; 10 % Na_2O mixture showed the highest strengths of all tested mortars reinforced with basalt fabric. Considering the mechanical properties testing results, it seems as the most suitable matrix for the basalt fabric implementation from all WG/SC and WG/SH mixtures with $M_s = 0.5$. Another parameter supporting this decision is the activator solution pH about 11.6 which is the lowest from all tested activator solutions beside the other WG/SC mixtures. This fact is quite important due to the stability of BFs under the alkaline conditions.

5.1.2 AAMs based on sodium water glass with M_s = 2.24

The mechanical strengths development of blast furnace slag activated with pure sodium water glass (M_s = 2.24) materials were also studied. These tests were performed with a goal to determine the silicate modulus influence on the mechanical properties development same as on the behaviour of basalt fabric reinforcement under these conditions. Unlike the WG/SC and WG/SH activated systems alkaline activator dosages of 8 and 10 % Na_2O were only studied.

The compressive strength development as a function of activator dosage and the basalt fabric addition for 112 days testing period is shown in Fig. 18. The flexural strength development was studied as well, and results are presented in Fig. 19.

The compressive strengths were comparable to the WG/SH activated systems after one day. Hence, higher strengths than in case of WG/SC activation were observed due to higher activator solution pH. The compressive strength gain continued significantly up to 56 days of curing, but beyond this age no extensive increase was observed. With an exception of 10 % Na_2O WG/SC activator mixture where compressive strength has been higher about 16.5 %; silicate modulus increasement from 0.5 to 2.24 caused reaching of higher compressive strengths after 112 days (with the same 8 % alkaline activator dosage higher M_s resulted to compressive strength increase about 27 % (WG/SC) and 33 % (WG/SH)). The results obtained also indicate that no extensive strength improvement was caused by activator dosage increase from 8 to 10 % Na_2O. These results are in a partial agreement with publications [62] or [65] where authors presented just slight compressive strength improvement with increasing activator dosage. There is also mentioned in paper [65] that influence of activator dosage decreases with increasing silicate modulus and that higher long-term compressive strengths had been reached with increasing M_s.

Similar results and trends have been observed for flexural strengths development. However, lower difference between WG (M_s = 2.24) and WG/SC or WG/SH mixtures when investigating flexural strengths was noticed after 84 days. The activator dosage of 8 % Na_2O seems to be a better choice than 10 % based on the results achieved when higher silicate modulus of activator mixture is required.

Finally, let´s evaluate the difference in mechanical strengths with reinforcement implementation. There was no relevant difference of flexural or compressive strengths when matrix was reinforced with one layer of basalt fabric. The values for non-reinforced same as reinforced ones lies within the standard deviations in the entire testing period. It indicates that there is no significant difference of mechanical strengths when activator solution composition changes rapidly. It can be explained by a predominant effect of fabric properties and local disorientations of bundles leading to the stress concentration instead of its transfer as already discussed in 5.1.1. The pure WG activator solutions with M_s = 2.24 tested had pH about 12.6 which is quite a lot considering the BFs durability under alkaline conditions.

Hence, based on these results there was no further investigation of WG (M_s = 2.24) activated systems realized in this thesis.

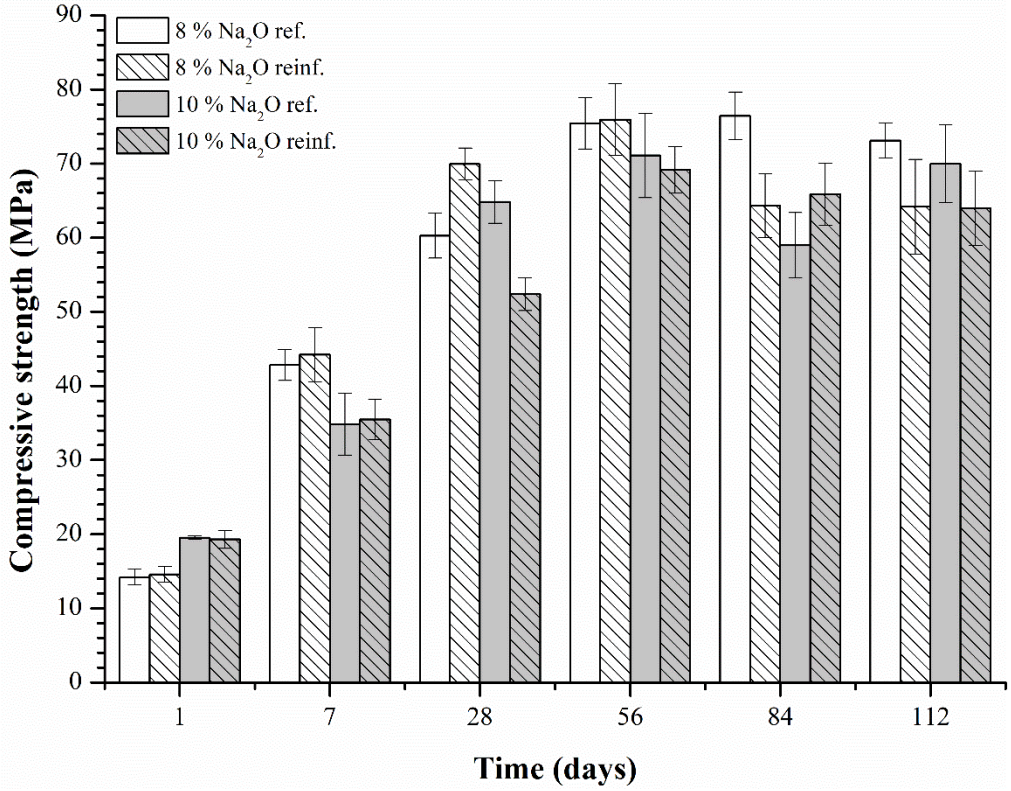

Fig. 18: Compressive strength development as a function of alkaline activator dosage (8; 10 % Na_2O) and basalt fabric reinforcement for WG (M_s = 2.24) activated systems.

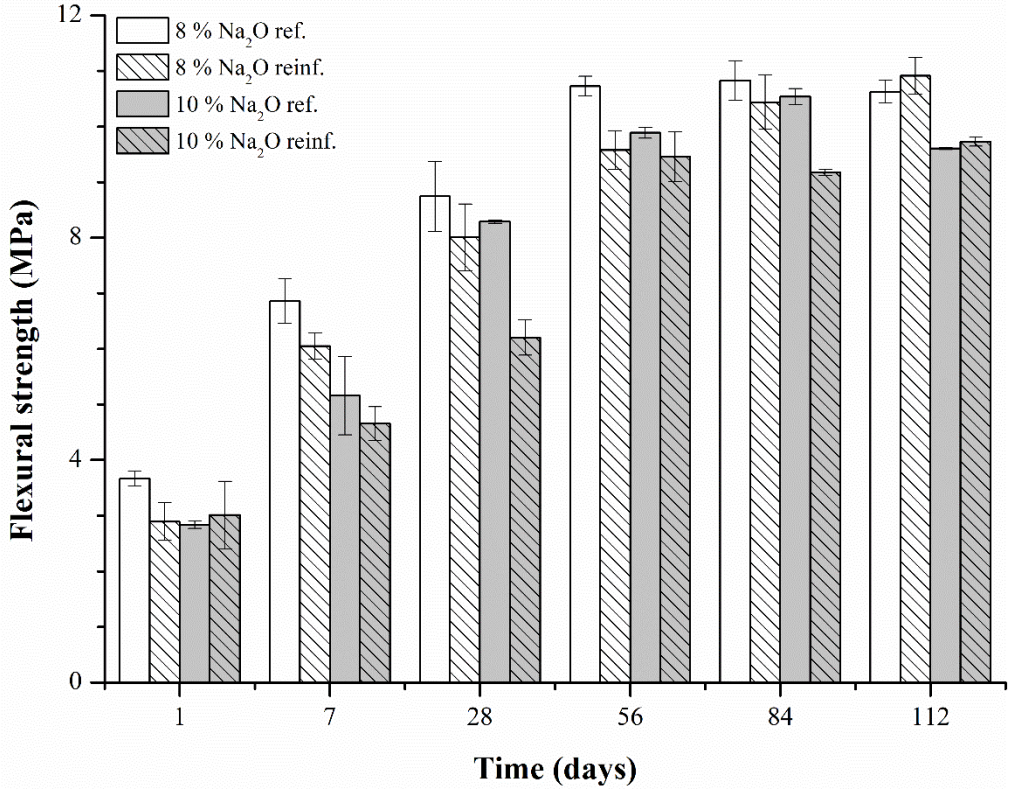

Fig. 19: Flexural strength development as a function of alkaline activator dosage (8; 10 % Na_2O) and basalt fabric reinforcement for WG (M_s = 2.24) activated systems.

5.1.3 AAMs based on sodium hydroxide

The influence of silicate modulus to the mechanical strengths development has been studied as discussed in the previous chapter. Thus, it is not surprising that AAMs based on activator with $M_s = 0$ should be also studied at least partially. The alkali activation of BFs with pure SH was investigated in 8 and 10 % Na_2O dosages. The compressive strength development of this matrix type in time same as the influence of basalt fabric implementation can be seen in Fig. 20. Same parameters were also studied for flexural strengths and they are presented in Fig. 21.

The compressive strengths for pure SH activated systems were significantly lower than in case of WG/SH or pure WG activator mixtures (2.8 and 3.4times for WG/SH or 2.6 and 3.9times for WG mixtures in 8 and 10 % Na_2O dosages, respectively) after one day. On the other hand, compressive strengths of pure SH activated systems were slightly higher than in case of WG/SC activator mixture in both tested alkaline activator dosages after one day. Nevertheless, there was no other considerable improvement when compared to all other tested activator mixtures during curing period which resulted in approximately three times lower compressive strengths after 112 days. The results obtained can be explained by the activator nature. The pH of SH activator solution is higher than for WG/SC which explains higher initial strengths. The long-term compressive strength drop against other mixtures can be clarified by the silicate ions absence resulting to lower silica gel formation as intimated in papers [18] or [21]. Still, three times lower compressive strengths seem to be too much beyond expectations. The results obtained for flexural strength testing indicate the same trend as for the compressive strengths. The drop of flexural strengths against the other mixtures is still about 40 %.

With respect to the results gathered for flexural and compressive strengths when reinforced with basalt fabric no improvement has been found during testing period. It may be related with the fabric deformation etc. as already discussed in previous cases.

To sum up, no beneficial effect of basalt fabric implementation to the mechanical properties has been observed when pure SH in dosages 8 and 10 % Na_2O was used as activator of BFS based systems. Moreover, the mechanical properties of this matrix type were evaluated as the worst of all tested matrices. The pH about 12.7 of SH alkaline activator is not very helpful to this assessment either. Thus, same as alkali activation with WG ($M_s = 2.24$) there no further investigation of AAMs based on the pure SH was done in this thesis.

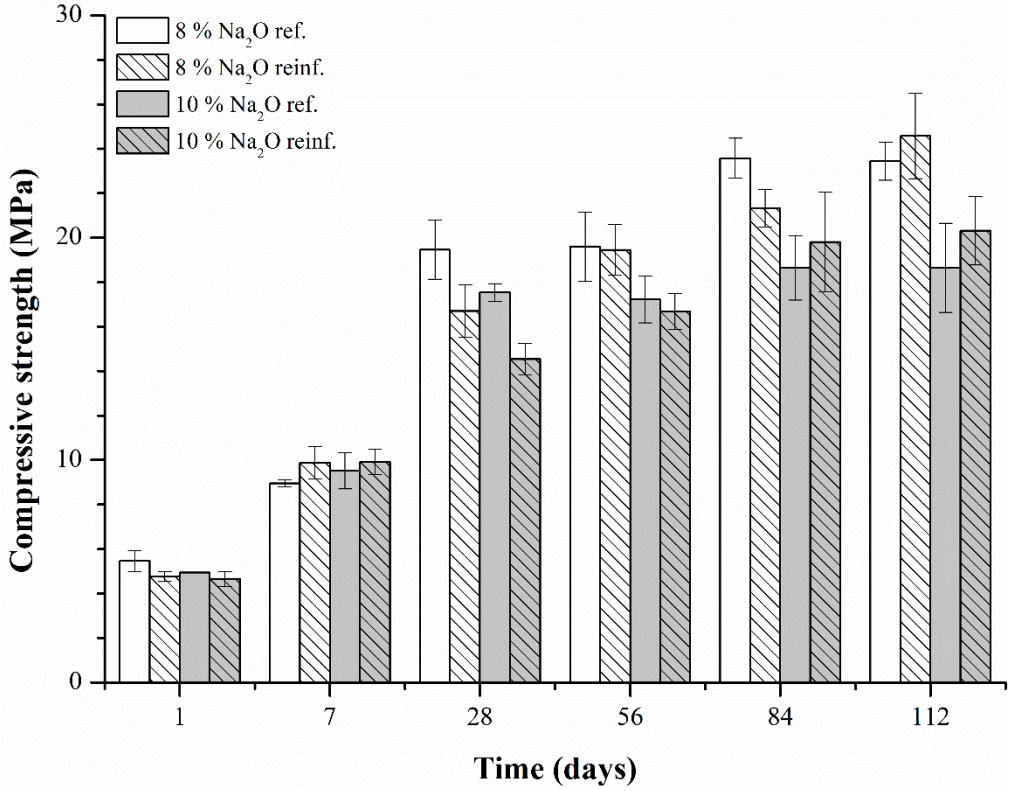

Fig. 20: Compressive strength development as a function of alkaline activator dosage (8; 10 % Na_2O) and basalt fabric reinforcement for pure SH activated systems.

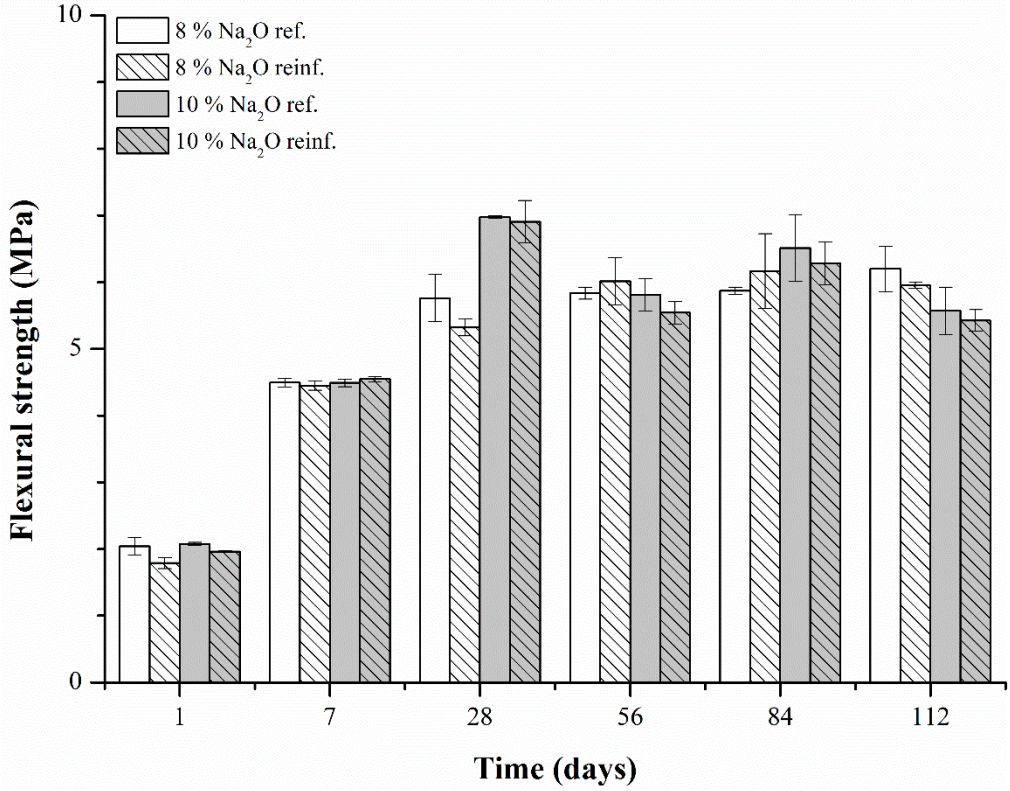

Fig. 21: Flexural strength development as a function of alkaline activator dosage (8; 10 % Na_2O) and basalt fabric reinforcement for pure SH activated systems.

5.1.4 Influence of fabric layers number to the mechanical properties

With reference to the previous results another possibility of fabric reinforced alkali activated material mechanical properties improvement consists in more fabric layers addition into the specimens. Hence, another layer(s) implementation may be related with compressive and flexural strengths improvement. This presumption was experimentally investigated using the most suitable matrix from previous experiments (activator composition: M_s = 0.5; 10 % Na_2O; WG/SC).

The flexural strength development is shown in Fig. 22. A definite trend could not be found based on these results. The matrix reinforcement with one fabric layer seems to be the most effective considering the results from the entire testing period. However, the results obtained by samples testing overlap each other within standard deviations quite often. Thus, the difference of flexural strengths of the reinforced samples when compared with the reference is not significant enough for more fabric layers addition to be considered as beneficial.

The compressive strength development as a function of fabric layers number can be seen in Fig. 23. The highest strength gain of all tested samples had the matrix reinforced with one fabric layer up to the 84 days. But the following testing showed that highest compressive strength belonged to the reference without any fabric layer after 112 days. On the other hand, the results obtained for none or one fabric layer usually overlap each other within the standard deviations. An addition of two and three fabric layers led to the compressive strength decrease when compared with reference after 28 days. The difference between two and three layers lies in standard deviations in all cases. Decrease of the compressive strength against the reference may be related to the formation of lower amount of hydration products due to the basalt fabric implementation after 112 days. The drop is more significant with increasing number of fabric layers.

The beneficial effect of two or more fabric layers addition was not observed. It indicates that possibility of local deformation and disorientation of fabric increases with increasing number of fabric layers which leads to the stress concentration and easier crack propagation. Hence, addition of one fabric layer seems to be the most efficient if the matrix reinforcement is required.

These results partially correlate with results presented in paper [45] where authors presented that in case of cement matrix reinforced with basalt fabric either one or two layers did not exhibit significant reinforcement efficiency resulting to the compressive strength improvement which is quite similar to the results obtained in this thesis. On the other hand, they reported that three or more fabric layers implementation led to the strain-hardening behaviour, but these results do not match the experimental results achieved in this paper. This difference should not be caused just by matrix type difference which also indicates the possibility of local stress concentrations existence due to the fabric local bending or fibres stress transfer capability deterioration due to the degradation.

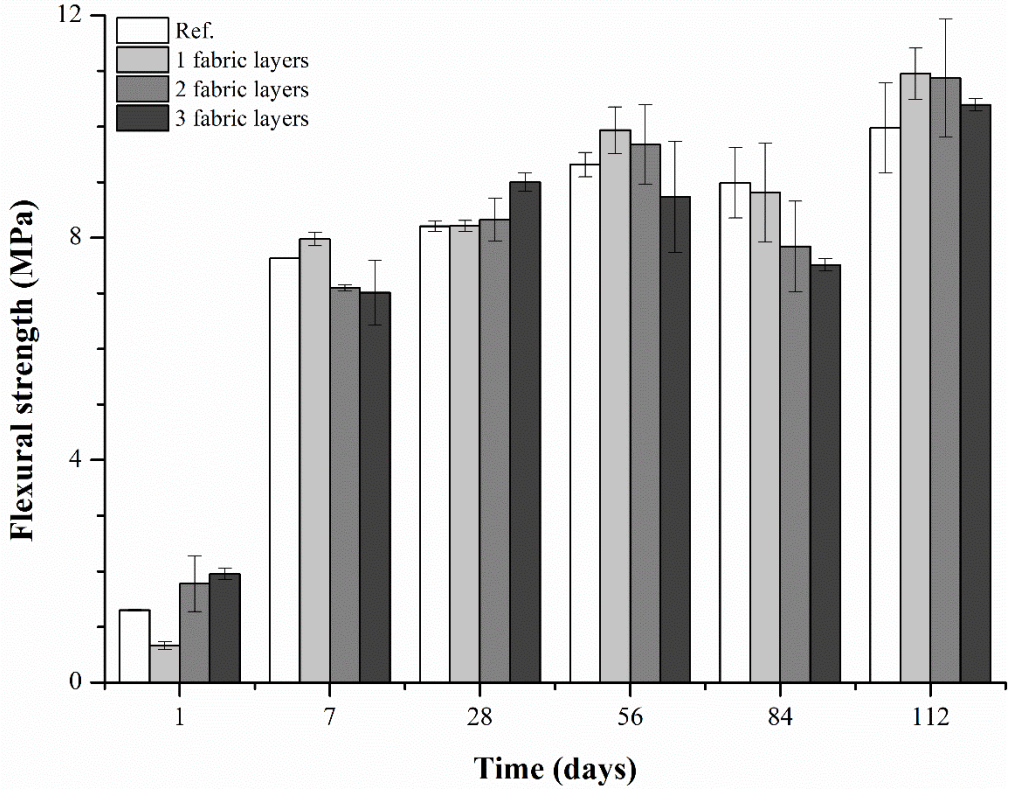

Fig. 22: Flexural strength development as function of fabric layers number for M_s = 0.5; WG/SC; 10 % Na_2O based AAM.

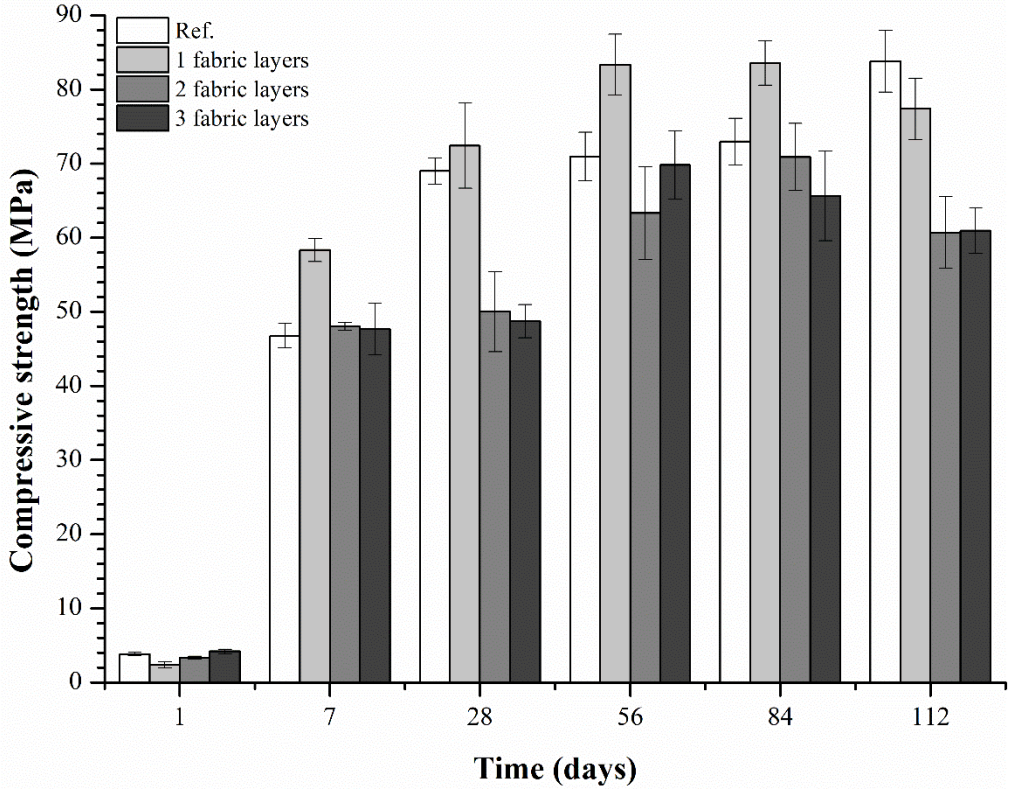

Fig. 23: Compressive strength development as a function of fabric layers number for M_s = 0.5; WG/SC; 10 % Na_2O based AAM.

5.1.5 Conclusion

Just a brief summary of results for influence of basalt fabric utilization in AA matrix on the mechanical properties will be presented in this paragraph. There was not observed any significant improvement of tested mechanical properties when the various matrices were reinforced with one or more layers of basalt fabric. This fact can be explained by poor F/M interaction which leads to poor adhesion (will be discussed in following chapter) and ineffective stress transfer or fibres stress transfer capability deterioration due to their degradation. Nevertheless, fabric local disorientations or bending same as poor constitution of fabric seem to be quite important factors as well. An indication of considerable improvement was noticed in case of AAM consisting of BFS activated with $M_s = 0.5$; 10 % Na_2O; WG/SC mixture only. Based on these results utilization of different basalt fabric/fibre type, e. g. chopped basalt fibres could be a better alternative for mechanical properties improvement as presented in following publications [49–51] (various types of AAMs were used in those papers). On the other hand, other problems like workability deterioration or reduction of hydration products formation arises when chopped basalt fibres were used according to those papers. A testing of matrices based on the alkali activated fly-ashes would be interesting and could bring useful results however the realisation of all these experiments was not possible given the extent of this thesis.

5.2 Fibre/matrix transition zone (interface) characterization

The transition zone between alkali activated paste and basalt fibres is the crucial region for the fibre reinforcement to be effective. A high-quality adhesion between F/M is necessary due to the stress transfer realization beside the other factors like volumetric fibre fraction, fibres/fabric orientation and distribution which are quite important too. The stress transfer is main principle of reinforced materials function because it helps to transfer the load from the matrix to the fibres. It can be realized through the de-bonding, sliding and pulling-out of the fibres when macro and micro cracking take place and followed by the bridging effect of the fibres across the matrix cracks in later stages of loading. The F/M interface controls many important properties of final composite; hence a closer study should be done. The interfacial zone same as the fibre/matrix interaction study in following paragraphs will be based on the chemical analysis (comparison of hydration products of pure AAM and the fibre reinforced one) using SEM-EDX but mechanical properties testing as well using the fibre pull-out test.

5.2.1 Microstructure analysis using SEM-EDX

The microstructural development of the AAMs samples activated with WG/SC and WG/SH mixtures (10 % Na_2O) reinforced with a bundle of basalt fibres were investigated with a goal to determine and characterize microstructure differences, moreover adhesion between F/M same as a transition zone presence if there is, after 7 and 28 days using SEM-EDX analysis.

Firstly, we will focus on the facts obtained from the SEM images. The chosen ones are given in Figures 24–28 while the other complementary images are provided as Attachments 4–9. The WG/SC activated systems showed up relatively smooth surfaces of the paste under the fibres (the excessive fibres were removed before analysis). The grooves in paste were clearly visible after the fibres removal. The surface of the fibres remained smooth without significant damage or degradation. There was not observed an adhered paste presence on the fibre surface neither after 7 or 28 days. These facts indicate that there is no quality adhesion between basalt fibres and AAM for WG/SC activated BFS matrix. More and larger matrix fragments should be

visible on the surface of the fibres same as some holes in the paste caused by the removal of the fibres. This can be seen in Fig. 26 which shows the microstructure of WG/SH activated system after seven days of hydration. The presence of many paste fragments ("*protrusions on the fibre*") on the surface of the fibres indicate that better F/M adhesion is realized for WG/SH than WG/SC activated systems. On the other hand, this effect was not noticed after 28 days. Hence, it could also be caused just by lower degree of hydration or more probably it could be associated with higher interaction between fibres and matrix due to the slightly etched surface of the fibre (pore solution pH decreases over time). Furthermore, the surface of the fibres remained without significant degradation throughout the entire interval. These results can be compared with the one presented in paper [51]. Authors used fly-based systems instead of the BFS like in this thesis, unfortunately. However, they also stated that no chemical interaction between the matrix and fibres was realized at laboratory temperatures.

The slight concentration of Si decrease in the fibres was observed by EDX analysis when placed in the AAM paste but it cannot be uniquely attributed to the fibres dissolution.

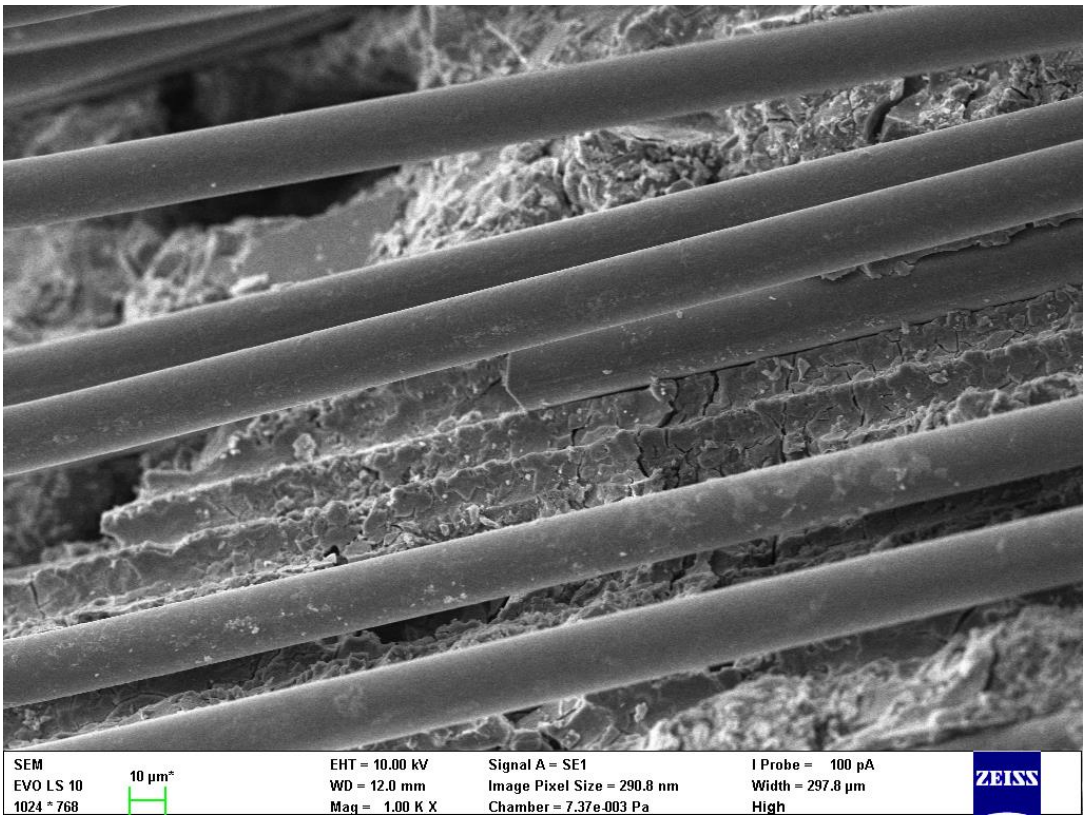

Fig. 24: SEM image showing the fibre/matrix interaction of WG/SC (10 % Na_2O) activated system after 7 days of hydration.

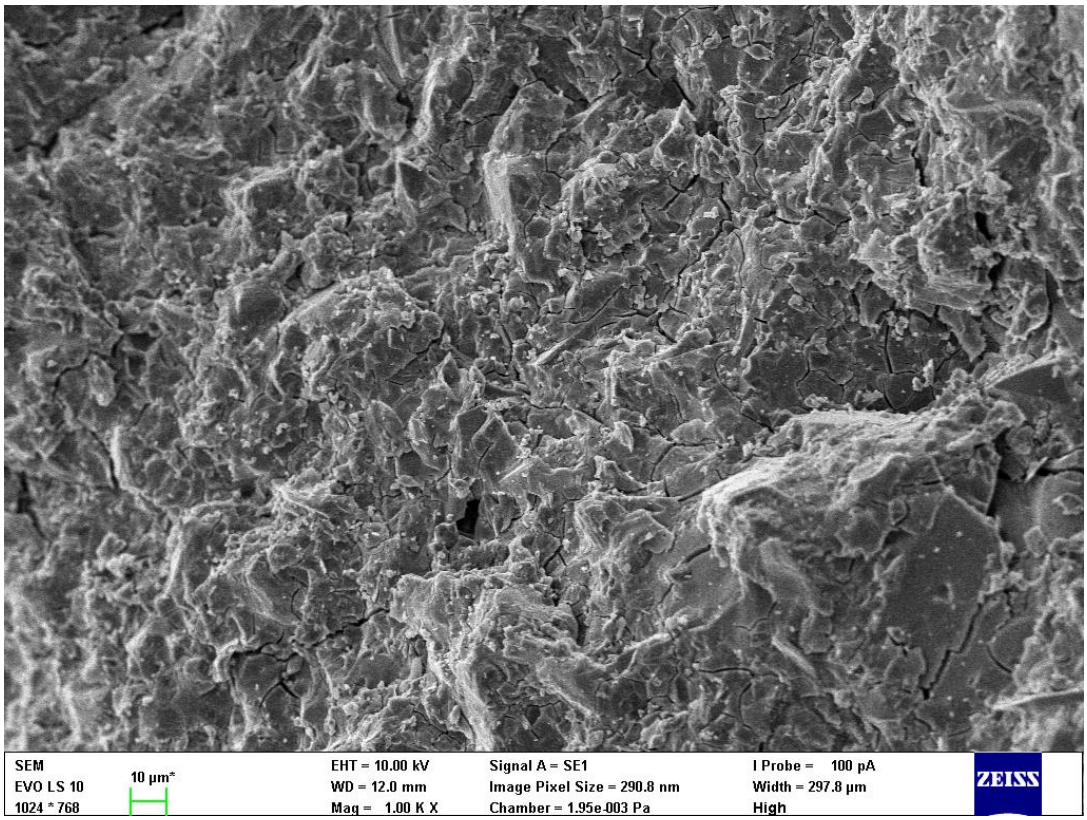

Fig. 25: SEM image showing the pure matrix of WG/SC (10 % Na_2O) activated system after 28 days of hydration.

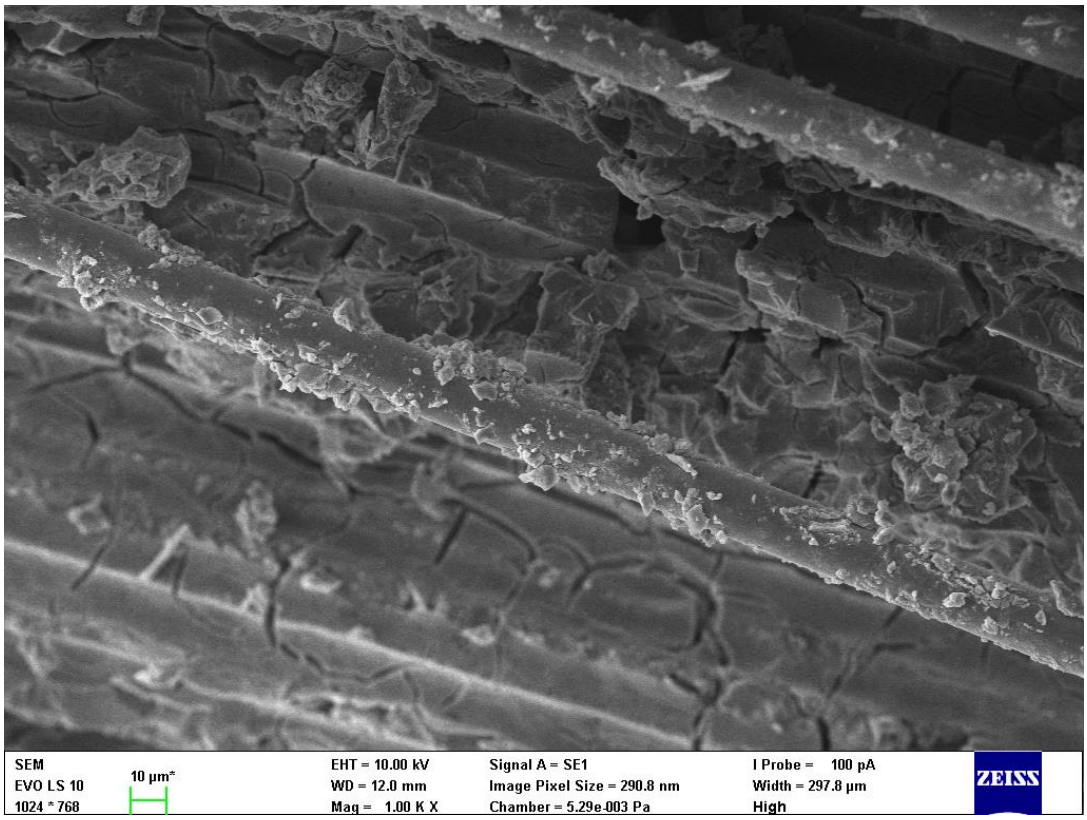

Fig. 26: SEM image showing the fibre/matrix interaction of WG/SH (10 % Na_2O) activated system after 7 days of hydration.

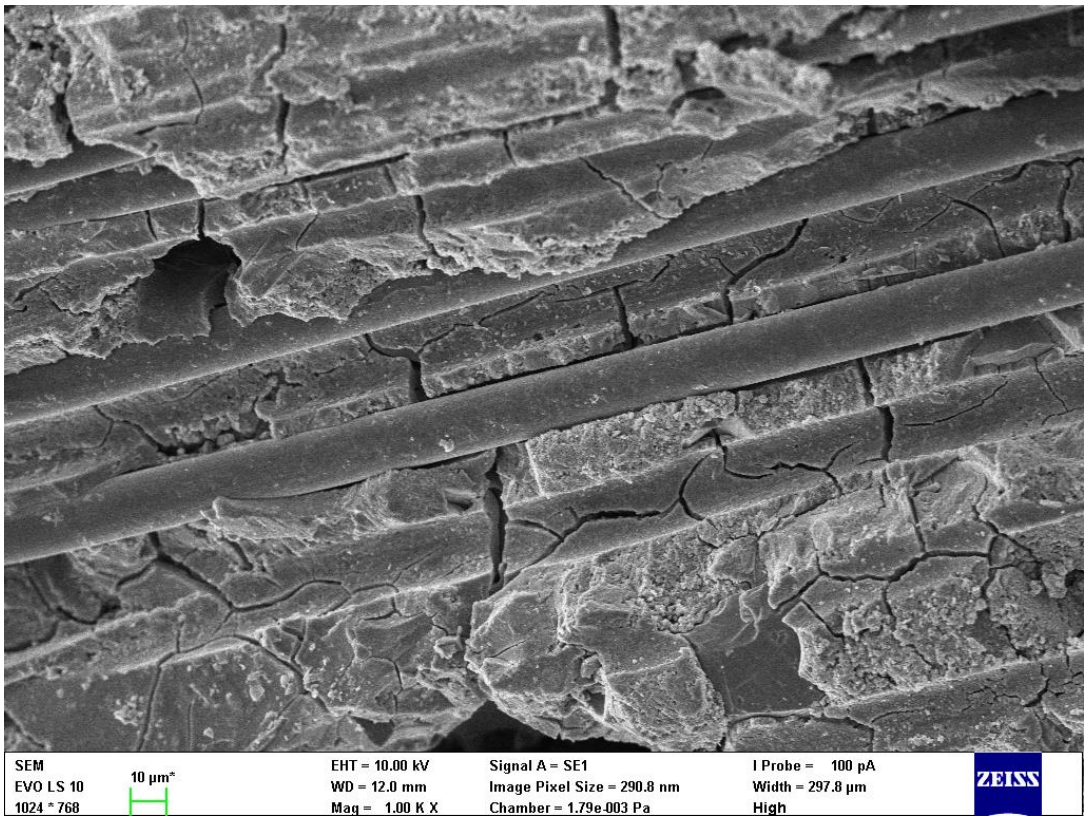

Fig. 27: SEM image showing the fibre/matrix interaction of WG/SH (10 % Na_2O) activated system after 28 days of hydration.

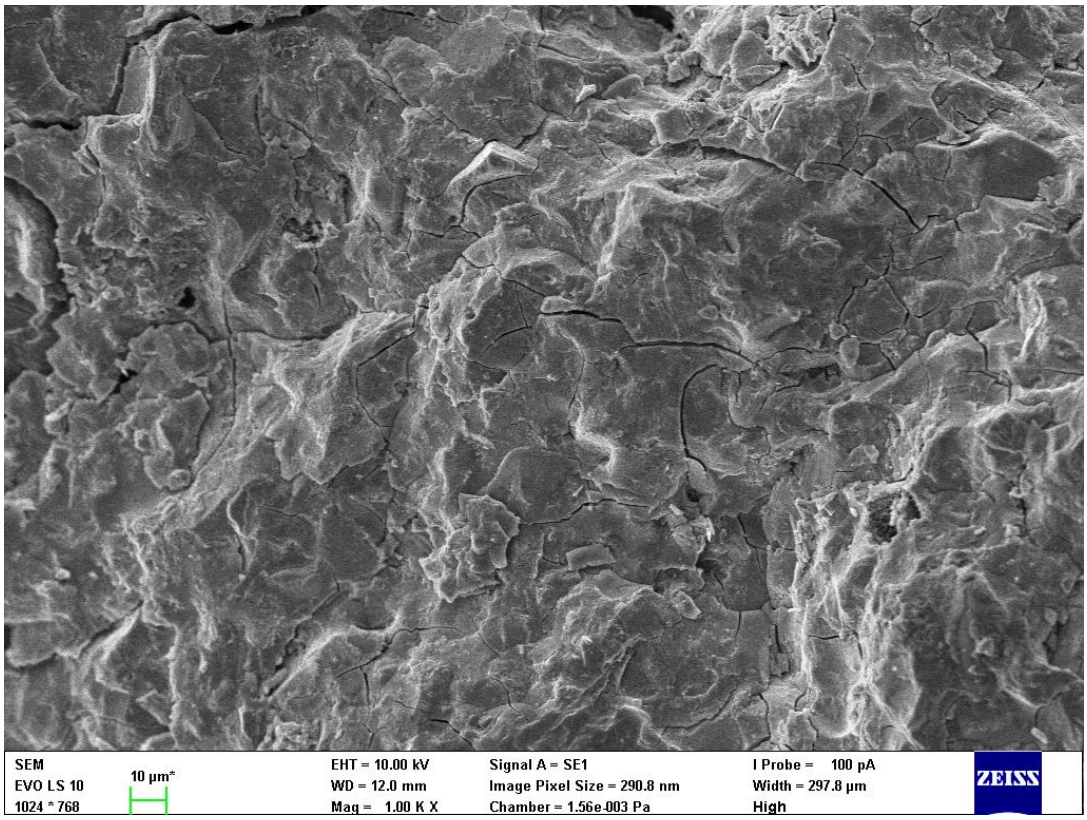

Fig. 28: SEM image showing the pure matrix of WG/SH (10 % Na_2O) activated system after 28 days of hydration.

The influence of basalt fibre reinforcement implementation to the AAMs on type of hydration products will be discussed now. A compositional analysis was normalised relative to Si. The chosen elementals ratios are summarised in Tab. 8 (for WG/SC activated system) and Tab. 9 (for WG/SH activated system). Their comparison served for the determination of composition difference if the fibres implementation caused any.

Presence of C-A-S-H as a major matrix phase for both activated systems type can be predicted based on the SEM-EDX results. These systems had Ca/Si ratio about 0.9–1 and Al/Si ratio about 0.2. Minor hydrotalcite formation can be predicted regarding the Mg/Si ratios from 0.2 to 0.3 same as partial Na substitution in C-A-S-H. Other minor phases can be formed as well considering the alkaline activator composition difference. A pure matrix represents area far from the fibres 3 mm at least. Its composition is quite stable for both activator types between 7 and 28 days. Let´s continue with an area closer to the fibres. "*Transition zone"* term on this place should be defined before anything else. It represents the area which is more distant from fibres (1–50 μm) than area "*near the fibre*" and was specified visually in both cases by different hydration progress around the fibres which is related to the paste colour change in case of AAMs. This colour difference was not observed for any of tested reinforced AAM samples after 28 days. Thus, it was not analysed beyond 7 days of hydration. A transition zone composition of WG/SC activated systems was quite the same when compared to the pure matrix investigating Ca/Si, Al/Si and Mg/Si ratios but with higher Na content. Meanwhile, WG/SH activated systems showed differences between transition zone and pure matrix in Na content as well but also for Ca/Si ratio (0.8 vs. 1.0). The transition zone existence can be assumed based on these results. Still, rather than place with different hydration products it is a place with a lower degree of hydration which can also be confirmed by the fact that this area is no longer recognizable after 28 days of hydration, same as by the presence of higher amount of unreacted slag particles. We will focus on the area "*near the fibres"* which lies around or under the fibres in distance from 0 to 1 μm as determined with the meaning of the SEM interaction volume for the AAMs, now. Ca/Si ratio higher about 0.3 against pure matrix was observed for this area in WG/SC activated system. Meanwhile, Al/Si or Mg/Si ratios were almost the same. The amount of Na was higher in the "*near the fibres"* zone but this difference diminished as hydration continued. It indicates that basalt fibres presence might slightly influence the nearby hydration products (different morphology of C-A-S-H due to positional growth inhibition). WG/SH activated system showed no difference between "*near the fibres"* and pure matrix areas for Ca/Si, Al/Si and Mg/Si ratios after 7 days. However, the difference was formed after 28 days of hydration. Ca/Si ratio was higher about 0.4 and Mg/Si ratio increased about 0.1, meanwhile Al/Si remained the same. The last studied specific area occurred only at WG/SH activated system. Some protrusions on the fibre surfaces were observed and analysed. The composition of these protrusions corresponds to the composition of the paste near the fibres with a small deviation for Ca/Si (0.2) after seven days. Hence these protrusions are most likely just adherent fragments of this nearby paste.

Closer study of the microstructure appearance due to the fibres implementation should be done as well. A grown limitation of C-A-S-H phase was observed because of fibre presence (reduction of volume available). It resulted to a less developed C-A-S-H structure near the fibres. The presence of cracks was detected for both activator mixtures throughout the entire interval. The cracks occurrence was slightly higher near the fibres. The presence of unreacted slag particles was lower for WG/SH activated system, but it was found out for both activator mixtures and it decreased over time. The microstructure of both tested AAMs seems to be dense. C-A-S-H development from a diminutive fluffy to the well-developed one was noticed for WG/SH activated system throughout time beside the areas around the fibres where C-A-S-H

phase growth was limited. No significant difference between the WG/SC activated paste microstructure appearance was noticed over time except the number of unreacted slag particles decrease. The surface of WG/SC paste seemed to coarser than the one activated with WG/SH.

Tab. 8: Chosen elemental atomic ratios observed for analysis of the AAM reinforced with basalt fibres based on BFS activated with 10 % Na_2O WG/SC mixture using SEM-EDX.

Hydration time	Zone of analysis	Atomic ratios				
		Ca/Si	Al/Si	Mg/Si	Na/Si	K/Si
7 days	basalt fibre	0.23	0.39	0.13	0.13	0.05
	near the fibre	1.36	0.19	0.21	1.35	0.01
	transition zone	1.00	0.23	0.27	0.94	0.02
	matrix	1.02	0.24	0.26	0.62	0.02
28 days	basalt fibre	0.24	0.38	0.18	0.22	0.03
	near the fibre	1.20	0.24	0.21	0.49	0.02
	matrix	0.87	0.23	0.28	0.74	–

Tab. 9: Chosen elemental atomic ratios observed for analysis of the AAM reinforced with basalt fibres based on BFS activated with 10 % Na_2O WG/SH mixture using SEM-EDX.

Hydration time	Zone of analysis	Atomic ratios				
		Ca/Si	Al/Si	Mg/Si	Na/Si	K/Si
7 days	basalt fibre	0.21	0.35	0.10	0.09	0.05
	protrusion on the fibre	0.72	0.18	0.13	1.19	0.01
	near the fibre	0.94	0.20	0.17	1.20	0.02
	transition zone	0.79	0.16	0.10	0.97	–
	matrix	0.99	0.19	0.17	0.32	0.02
28 days	basalt fibre	0.16	0.39	0.12	0.11	0.04
	protrusion on the fibre	0.47	0.19	0.09	1.16	0.02
	near the fibre	0.52	0.21	0.09	1.08	0.02
	matrix	0.92	0.21	0.22	0.79	0.02

Finally, a brief summary of the most important findings will be made. There has not been observed any significant signs of good fibre/matrix adhesion for any of AAMs tested since the adherent paste fragments for WG/SH activated system after seven days of hydration have not been sufficiently persuasive. Neither signs of rapid fibres degradation due to their implementation in paste of AAM have been found out. Following facts will be valid for both AAMs. Pure matrix is formed mainly by C-A-S-H gel with some possible minor phases. Transition zone formation can be attributed to lower hydration rate around the fibres. Minor changes of Ca/Si ratios were observed when comparing zone near the fibres and pure matrix.

5.2.2 Pull-out testing

Characterization of fibre/matrix transition zone can also be done using tests based on mechanical properties testing and interfacial shear bond strength determination. The fibre pull-out test provided interesting results which are presented in following paragraphs.

Simplified pull-out test has been done due to the limited instrumental equipment. A maximal force (F_m) before the fibre broke down or was pulled out was measured.

The measurement of the fibre embedment length change during the pull-out test realization would be useful but there was not necessary equipment. Hence, only the F_m dependence on the fibre strain was measured. The F_m values were than used for interfacial shear bond strength (F_i) determination – Equation (3). Since this has been just a simplified pull-out test, the obtained nominal F_i values must be taken with reserve. However, given the fact that all samples were tested in the same way, these results can be used to their interfacial shear bond strengths comparison. The pull-out tests were carried out for AAMs (based on the BFS activated with $M_s = 0.5$; WG/SC and/or WG/SH mixtures with activator dosages from 6 to 12 % Na_2O) reinforced with yarn of basalt fibres as described in 4.2.4.

Different fibres embedment lengths (from 0.5 to 4 cm with a step size of 0.5) same as time of curing (1; 3; 5 and 7 days) were tested. The optimal measuring parameters selection was quite complicated due to the fibre critical length (last fibre length when the stress transfer can be realized). It was necessary to find such combination of fibre embedment length and curing time, when the fibre could still be pulled out from surrounding matrix instead of its breakage (basalt fibre breakage took place at F_m about 333 N). It led to the 0.5 cm fibre embedment length and three days of curing selection as the most suitable option. The results with these parameters are given in Fig. 29 for WG/SC and WG/SH activator mixtures.

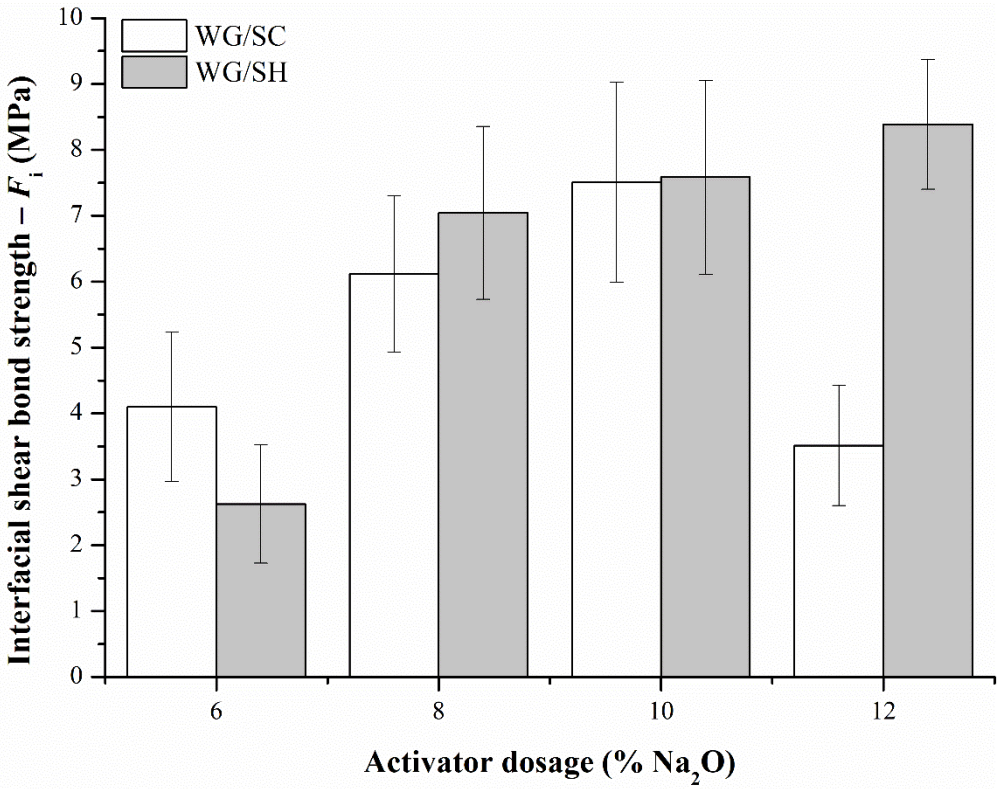

Fig. 29: Interfacial shear bond strength (Fi) development as function of the activator dosage for WG/SC and WG/SH activated systems with fibre embedded length 0.5 cm after 3 days of hydration.

Interfacial shear bond strength increases for up to 10 % Na_2O for WG/SC activator mixtures, but beyond this dosage a significant F_i drop was observed. These results are in good agreement with results obtained for compressive strength testing at early ages where the same trend has been found. It is not surprising because F_i improvement is closely connected to the compressive strength gain, respectively mechanical properties development at all. It confirms that fibre resistance against the pull-out is realized mainly due to the frictional bonds whose strength is related to the strength of the matrix itself. Hence, the chemical bondage is formed

just partially or not at all. Because if chemical bondage was formed it should result to better adhesion in some case at least and a noticeable change in the trend would be observable.

Similar finding but with some exceptions may be done in case of WG/SH activated mixtures. The interfacial shear bond strength increases with increasing alkaline activator dosage even in the 12 % Na_2O case where a rapid drop was found out for WG/SC mixture. Second difference is also related to the 12 % Na_2O dosage, because the F_i should be lower than it is based on the compressive strength results. So, it can indicate that some influence of chemical forces could be formed beside the frictional bonds resistance against the fibre pull-out. This can also be confirmed by SEM-EDX analysis from previous chapter, where some sort of interaction was found for WG/SH activated system while there was none in case of WG/SC activated systems.

To sum up, it was found out that fibre resistance against pull-out from the AAM matrix is mainly realized by frictional forces. The highest interfacial shear bonds strengths have been found for 10 % Na_2O when investigating WG/SC and 12 % Na_2O for WG/SH mixtures. The difference between them is about 11.7 %. Still, it should be born in mind that relatively large standard deviations were determined. Pull-out experiments realization in later ages than three days would be better considering the interface formation, but fibre tensile strength did not allow it.

5.3 Basalt fibres durability in the AAMs

Finally, the last partial goal of this thesis will be discussed in following paragraphs. It focuses on the mechanical properties same as chemical composition changes of the basalt fibres as a result of the accelerated immersion tests under alkaline conditions simulating the environment like exists in the AAMs. The main goal is to find out correlation between the initial alkaline activator mixture composition (WG/SC and WG/SH mixtures with various 6–12 % Na_2O dosages) and the durability of the fibres.

5.3.1 Loss of mass of the fibres

One of the simplest techniques for the investigation of BFs durability under alkaline conditions is a determination of their mass loss due to the immersion in specific solutions. The compositions of mixtures same as accelerated immersion conditions were specified more preciously in 4.3. Thus, we would limit to describing them as WG/SC or WG/SH mixtures with different activator dosages now.

The weight changes of the fibres due to the immersion can be seen in Fig. 30 and Fig. 31 for the WG/SC, respectively WG/SH activator mixtures.

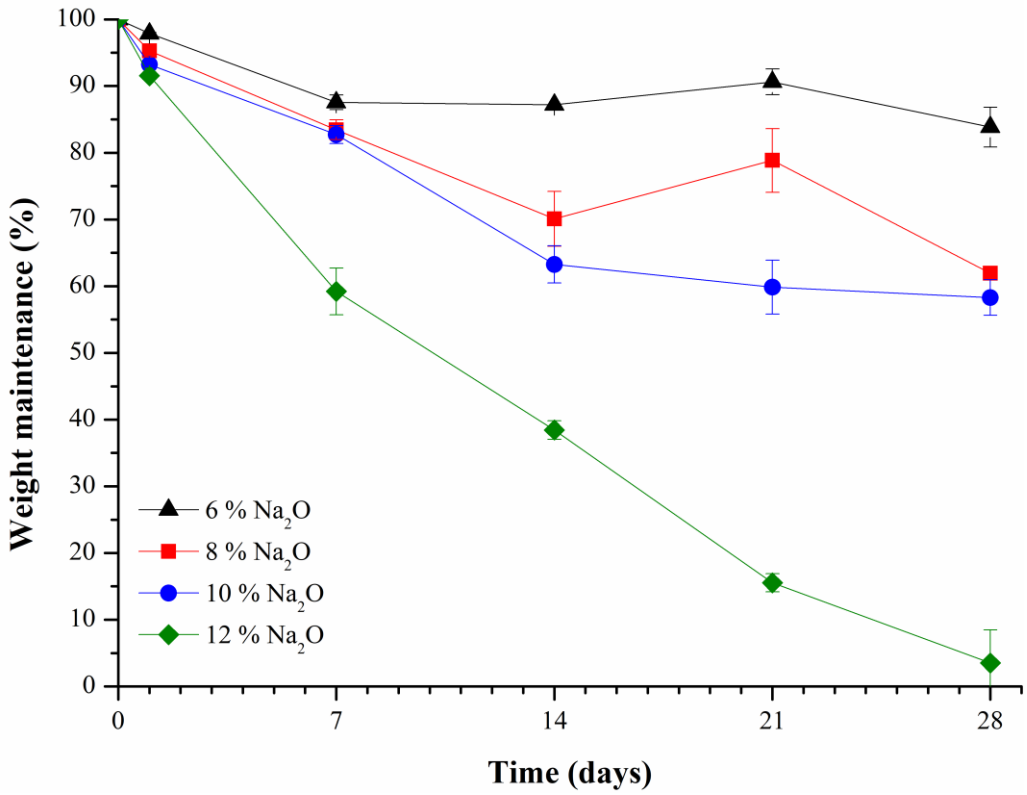

Fig. 30: Fibres weight maintenance development as a function of alkaline activator dosage ranging from 6 to 12 % Na_2O for WG/SC based immersion solutions.

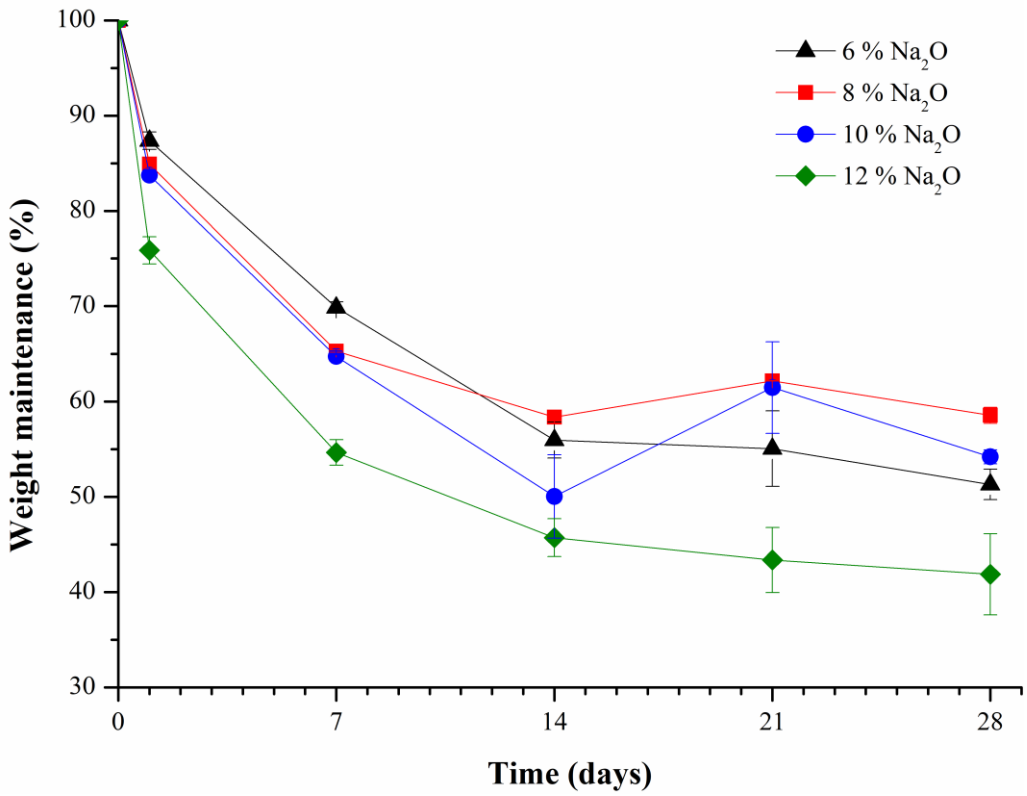

Fig. 31: Fibres weight maintenance development as a function of alkaline activator dosage ranging from 6–12 % Na_2O for WG/SH based immersion solutions.

Just a brief reminder of basalt fibres dissolution mechanism under alkaline conditions will be delivered as described in publications [39] and [43] because it explains the results obtained in this thesis well. The BFs attack by alkaline ions $(OH)^-$ is the process of –Si–O–Si– and –Al–O–Si– bonds break which is followed by the fibres dissolution through the pores and microcracks on the surface. As the dissolution of aluminosilicate network occurs the gel layer is formed on the fibre surface and its thickness increases with time. Meanwhile, the dissolution reaction moves forward to the fibre core leaving insoluble oxides, hydroxo-carbonates and hydroxides as crystalline and amorphous phases behind. These are responsible for formation of insoluble protective layer and diffusion rate of hydroxyl ions retarding. The diffusion rate through this layer is controlled by ion exchange and transformation of the protective (passivating) layer into the porous gel layer and it is lower compared to the beginning of the dissolution process. It is assumed that growing of crystalline phase deplete and destabilize the gel, so when it happens gel porosity increases and allow aqueous species to percolate rapidly through the gel and dissolution rate increases again. The overall dissolution rate of glassy structure may be also influenced by factors like aqueous transport of chemical species in the near surface region or the tendency to reprecipitate a solid if the equilibrium is approached as described in paper [66].

The weight loss was the most crucial during first 14 days of immersion and it slowed down over time in all tested mixtures with an exception of 12 % Na_2O WG/SC mixture. It is related to the presence of some insoluble or protective layer formed by compounds of Fe^{3+}; Mg^{2+} and Ti^{4+} as indicated in previous paragraph but also in study [42]. Another possible reason can be related to some ion oversaturation in the solution resulting into the dissolution rate decrease. The modification of immersion solutions composition will be discussed more preciously in 5.3.3.

The lowest weight loss has been found for fibres leached in 6 % Na_2O WG/SC mixture. There was a weight loss about 12.4 % (after 7 days) and 16.1 % at the end of the 28 days testing interval. In contrary to the 12 % Na_2O WG/SC mixture with the highest weight loss about 96.5 % after 28 days. The fibre weight losses about 38.1 and 41.7 % were obtained for 8 and 10 % Na_2O WG/SC mixtures after 28 days and are presented for replenishment There was more significant weight loss difference between the individual activator dosages for WG/SC than WG/SH mixtures. The trend of increasing loss of the mass with increasing activator dosage was also found more convincing for WG/SC mixtures. This trend suits only up to 7 days but beyond this age the results are less conclusive when investigating WG/SH mixtures. The loss of mass of the fibres in WG/SH mixtures have been in this descending order 8; 10; 6 and 12 % Na_2O after 21 days and ever since. It resulted to the mass loss about 41.5; 45.8; 48.7 and 58.1 % in the same descending order. The results obtained in this thesis are comparable to the ones presented in paper [43]. There was presented fibre weight loss about 40 % when immersed in 10% NaOH after 80 days at laboratory temperature. A lower fibre weight loss (15 %) was published in study [44] but this result had been reached after 28 days of leaching in 2M NaOH at laboratory temperatures.

In conclusion, given that it is an accelerated corrosion test, even under the worst possible alkaline conditions (corresponding with the initial AA mixtures composition with the highest pH which decreases as hydration process occurs) the weight loss results can be considered as satisfactory with an exception for 12 % Na_2O WG/SC mixture. This can also be confirmed by SEM images (mentioned in 5.2.1) where no significant degradation of the fibre or its rupture was visible after 28 days embedding in pastes of BFS activated with 10 % Na_2O WG/SC and

WG/SH mixtures. An interesting follow-up would be the study of various fibre surface treatments to increase their durability under the highly alkaline conditions as outlined in 2.5.2.1.

5.3.2 Loss of tensile strength of the fibres

The mechanical properties change of the BFs due to the immersion under alkaline conditions can be characterized using tensile strength measurement as a function of immersion time and leaching solution composition. The leaching solutions were the same as in case of other durability tests of BFs (M_s = 0.5; WG/SC or WG/SH mixtures with 6–12 % Na_2O). It should be mentioned that evaluation of tensile strength change has been done using values of maximal strength until the fibre broke down because other quantities determination like surface area after leaching, tex etc. would be quite complicated. Hence, the results obtained can serve for comparison of the samples with each-other but nominal values should be taken with reserve same as in case of already discussed pull-out tests. Based on these facts, the results are presented as related to the reference.

The graphs representing fibres tensile strength dependence on leaching solution composition and immersion time at 60 °C can be seen in Fig. 32 (WG/SC) and Fig. 33 (WG/SH).

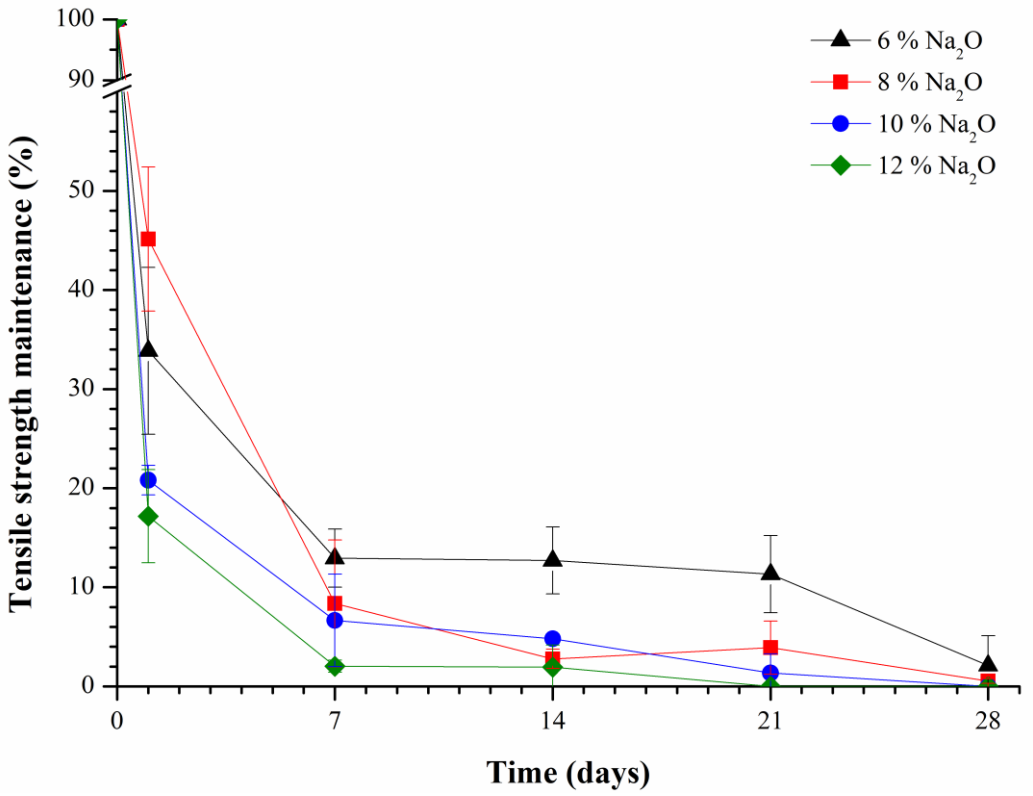

Fig. 32: Maintenance of basalt fibres tensile strength development as a function of alkaline activator dosage (6–12 % Na_2O) for WG/SC based immersion solutions.

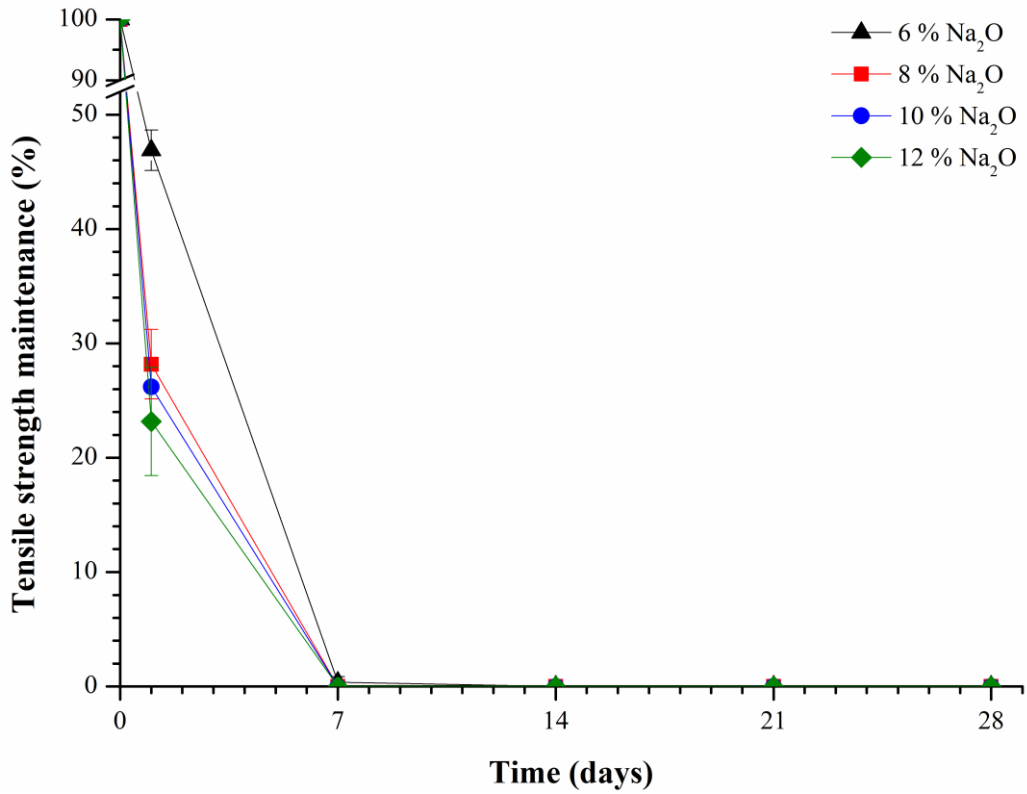

Fig. 33: Maintenance of basalt fibres tensile strength development as a function of alkaline activator dosage (6–12 % Na_2O) for WG/SH based immersion solutions.

The most significant tensile strength drop for WG/SC mixtures has been observed after one day of immersion. It resulted to the reduction of tensile strength to 33.9; 45.1; 20.8 and 17.2 % when compared with the reference for 6; 8; 10 and 12 % Na_2O dosages. The second rapid tensile strength drop was noticed after seven days. The tensile strengths of the fibres continued to fall gradually until non-strength could not been measured after that. There exists an exception for 6 and 10 % Na_2O WG/SC mixtures where the tensile strength maintenances about 2.1, respectively 0.5 % were observed after 28 days. When we look at the results for WG/SC immersion mixtures from a complex point of view a correlation between the alkaline activator dosage and tensile strength maintenance can be found. As the activator dosage increases from 6 to 12 % Na_2O, the tensile strength maintenance decreases over time, which is also in a good agreement with results of the loss of mass tests (5.3.1). It is interesting that weight loss almost stops within the standard deviations for 6–10 % Na_2O after 21 days, while the loss of tensile strength continues. It may be related to the formation of layer of some compounds at the fibre surface (their presence has been confirmed using XRD) which is ineffective for tensile strength behaviour.

The tensile strengths drop off drastically from the very early stages of immersion in WG/SH solutions. Tensile strengths were only about 46.9; 28.2; 26.2 and 23.2 % of the ones reached for the non-immersed samples for 6; 8; 10 and 12 % Na_2O dosages even after one day. The degradation of fibres has advanced so much that tensile strength of specimens immersed in these solutions could not been measured due to their cracks and pieces falling off thereafter. With increasing activator dosage of WG/SH mixtures the tensile strengths drop increases. As already noted the stability of SiO_2 (main constituent of the BFS – 55.7 wt. %) would be poor in strong $(OH)^-$ mediums. It seems that the instability of basalt fibres in WG/SH solutions originated from high dissociation constant of hydroxyl ions. This is also stated in paper [43].

On the other hand, weight loss determination of these samples had not such a catastrophic scenario as already discussed in 5.3.1. However, in study [43] there is also stated that immersion had led to the significant tensile strength drop while the weight retention had not showed a big change in some cases (NH_3 or saturated calcium hydroxide solutions). It is explained by the existence of stable degraded material layer at the surface which is inefficient to the tensile strength behaviour. A rapid tensile strength drop of basalt fibres when immersed in boiling sodium hydroxide was also observed in publications [38] or [39].

Such different behaviour for WG/SC and WG/SH mixtures may result from following factors: lower pH of the WG/SC solution, presence of protective layer on the surface of the fibres, diffusion coefficient, etc. A comparison with the literature would be advantageous, however no publications using the same mixtures composition was found. The AAMs based on WG/SC activator solutions seems to be more suitable for basalt fibres utilization regarding the tensile strength behaviour of basalt fibres under alkaline conditions and based on the results obtained overall.

5.3.3 Determination of basalt fibres chemical changes due to their leaching

5.3.3.1 Determination of change of composition of leaching solutions

A change of the immersion solution composition due to the basalt fibres leaching determination using the ICP-OES should serve as additional experiment for loss of mass investigation. So, it is not surprising that these tests were done for the same WG/SC and WG/SH mixtures. Since the dissolution of the fibres is realized it should be accompanied by the increase of concentration of released elements in the immersion solutions. A concentration change of Si, Al, Fe, Ca and Mg in immersion solutions was studied regarding the composition of the fibres same as the properties of AAMs. The results obtained were recalculated to the same immersed fibre weight (1 g) due to the possibility of various immersion solutions comparison. The concentration changes of analysed elements are presented in Fig. 34 for WG/SC solutions.

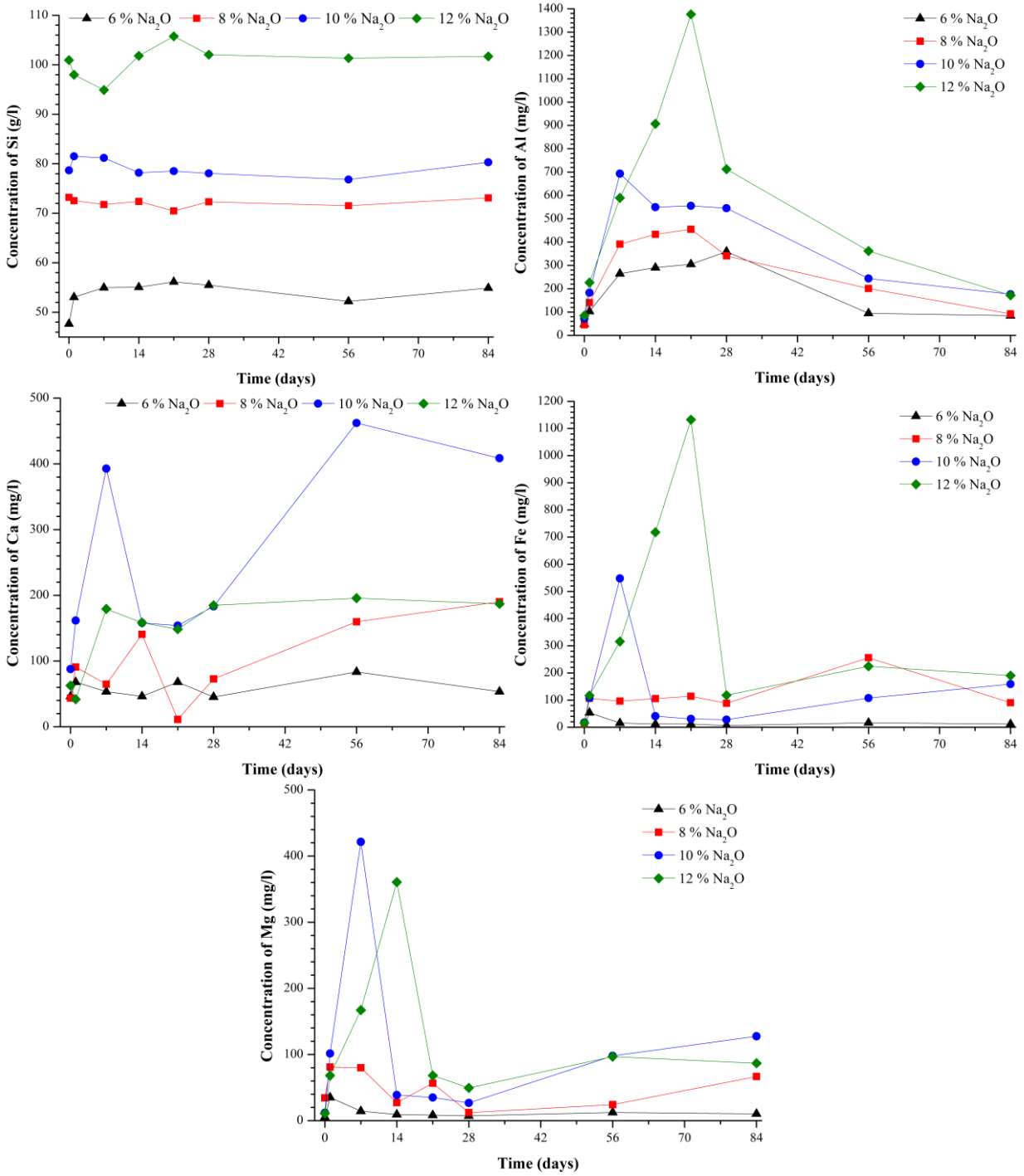

Fig. 34: Concentration development of chosen elements as a function of activator dosage due to the immersion of basalt fibres in WG/SC solutions.

It should be noticed that all analysed elements were present in beginning solutions already, before the immersion of BFs took place. The main constituent of the beginning solutions was silicon which originated from sodium water glass used for WG/SC or WG/SH mixtures preparation. Hence, it was probably present in form of silicate ions. The dissolution of fibres should lead to the silicon concentration increase regarding the fact that BFs contain about 55.7 % SiO_2. Nevertheless, it necessary to take changes in the concentration of Si with reserve, due to its high initial concentration and the relatively small contribution of the Si originating from the subsequent dissolution of the fibres. The presence of other analysed elements in the

beginning solution was not expected but it can be attributed to the quality of distilled water used or impurities presence in other chemicals used for solutions preparation. However, their concentration was quite low, so further investigation of its development regarding the fibres dissolution was easier when compared with the Si.

The element concentration development in WG/SC solutions will be discussed first because of more clear results were obtained for them. Si concentration increases with increasing Na_2O dosage (6–12 %) which is in good correlation with higher sodium water glass contribution in the initial solutions. The highest increase of Si concentration was found for 6 % Na_2O dosage (15.2 %), whereas immersion in 10 % Na_2O solution resulted in 2.1 % increasement and concentration of Si did not change at all in 8 and 12 % Na_2O solutions when comparing beginning composition of solutions and the one after 84 days of fibres immersion. In a complex view of the Si concentration changes over the entire test interval and for different WG/SC solutions, fluctuations around the mean value can be observed. The individual changes can hardly be assigned directly to the dissolution of the fibres, considering the possibility of inhomogeneity of the composition of the solution. Especially for 6 % Na_2O solution where Si concentration increase about 7.3 g/l exceeds the maximal theoretical amount of overall Si contained in the fibres (recalculated using the results of XRF analysis).

More persuasive results were obtained for concentration of Al (the second most abundant component in the BFs) determination during BFs leaching in WG/SC solutions. General trend can be described as follows. Concentration of Al increases gradually until it reaches maximum (fibres dissolution take place and continues until some sort of chemical equilibrium between fibres dissolution and solution composition is reached) but beyond this point a simultaneous decrease of concentration was observed (exceeding the solubility parameter – formation of oversaturated solution – followed by elimination/recrystallization/precipitation of the least soluble component). Al concentration achieved after 84 days was the closest to the values reached after one day of immersion. The most significant concentration of Al increase at the initial period from one to seven days (with an exception of 12 % Na_2O) confirms that dissolution of the fibres is the most critical during this period. Aluminium concentration increased 5.5; 8.6 and 9.6times for 6–10 % Na_2O WG/SC solutions at this initial interval. Meanwhile, the amount of Al leached from the fibres was not such rapid between 7 and 28 days of immersion. It is in good agreement with results of loss of mass of the fibres where a reduction in a weight loss rate was observed after 14 and more days of immersion for 6–10 % Na_2O WG/SC solutions. Moreover, the ICP-OES results showed the highest increase of Al concentration (16.3times) for 12 % Na_2O mixture (after 21 days), hence the concentration increase continued longer and more significantly than with other activator dosages which is the similar results as was obtained for the loss of mass determination (it was the only one mixture where loss of mass continued rapidly up to the 28 days). The amount of Al leached from the fibres increases with an increasing activator dosage (6–12 % Na_2O) which also confirms results presented in 5.3.1. So, these results can serve as the evidence that the fibres dissolve and release their components into the solution.

Similar results were obtained for concentration of Fe change due to the fibres leaching in WG/SC solutions. Maximum amount of Fe leached from the fibres increased with activator dosage from 6 to 12 % Na_2O. The interesting results were obtained for 6 % Na_2O solution where almost none iron concentration increase was found beside the one day of immersion. It may be related with some stable insoluble layer formation on the surface of the fibres containing Fe. The significant increases of iron concentration in solution were observed during initial immersion period and were followed by a rapid drop and iron concentration stabilization for

10 and 12 % Na_2O mixtures which was the same for concentration of Al development. The 8 % Na_2O solution show the signs of both these extremes but have more common with 6 % Na_2O solution. Leaching of Fe from the fibres into the solution depends on the oxidation number. Fe^{3+} are poorly soluble from fibres and helps prevent dissolution while Fe^{2+} passes into the solution much easier. It can be claimed that results for Fe concentration development confirms results obtained for Al and the ones for the loss of mass tests.

Calcium is along with iron the third most appearing element in basalt fibres. More divergent trends for development of Ca concentration in time due to the fibres leaching were obtained. Unlike the other discussed elements, the highest reached maximal amount of Ca concentration was detected for 10 % Na_2O after 56 days of fibres immersion. There is also second one (lower about 17.6 %) after 7 days which is in better correlation with trends and results for other analysed elements in the same solutions. Amount of Ca leached decreased according to the solution composition in following descending order 12; 8 and 10 % Na_2O. From a complex point of view Ca concentration did not underwent significant change in 6 % Na_2O solution during testing interval. Calcium carbonate presence was detected on the fibre surface using XRD analysis, hence it explains drop of Ca concentration when compared with maximums. Sporadic jumps in concentration can be attributed to the solution inhomogeneity during sampling.

Last analysed element was Mg, which can also be responsible for insoluble layer formation as mentioned in paper [42]. Trends of concentration of Mg changes were like the ones obtained for Al or Si. Thus, concentration of Mg increased rapidly up to 14 days for 10 and 12 % Na_2O WG/SC solutions and it is followed by a significant drop. On the other hand, slight concentration of Al increase between 28 and 84 days was observed for these mixtures. Meanwhile, highest Mg concentration was detected after one day and then decreased over time for 6 and 8 % Na_2O. It indicates that higher activator dosage supports the Mg dissolution process.

A closer look on the results obtained for concentration of analysed elements change due to the immersion of basalt fibres in WG/SH solutions should be done as well. These are given in Fig. 35. Despite the prediction the highest Si concentration was detected for 10 % Na_2O mixture instead of 12 % at some point of evaluated immersion period. On the other hand, this 25 % increase corresponding to concentration of Si increase about 21 g/l after 56 days or other results from 28 days significantly exceeds the theoretical possible amount of silicon produced by the dissolution of the fibres. Hence, this should be attributed to the local inhomogeneities of composition presence same as partial hardening of the mixtures due to the carbonatation. The concentration of Si increased about 12.4; 12.6; 15.1 and 19.8 % with dependence on activator dosage with following order 6; 8; 12 and 10 % Na_2O when comparing concentration at the beginning and after 84 days of immersion of the fibres. Still, this concentration increase did not match the amount of silicon in BFs beside the 6 % Na_2O WG/SH. The local jumps for 6 and 8 % Na_2O should be taken with reserve.

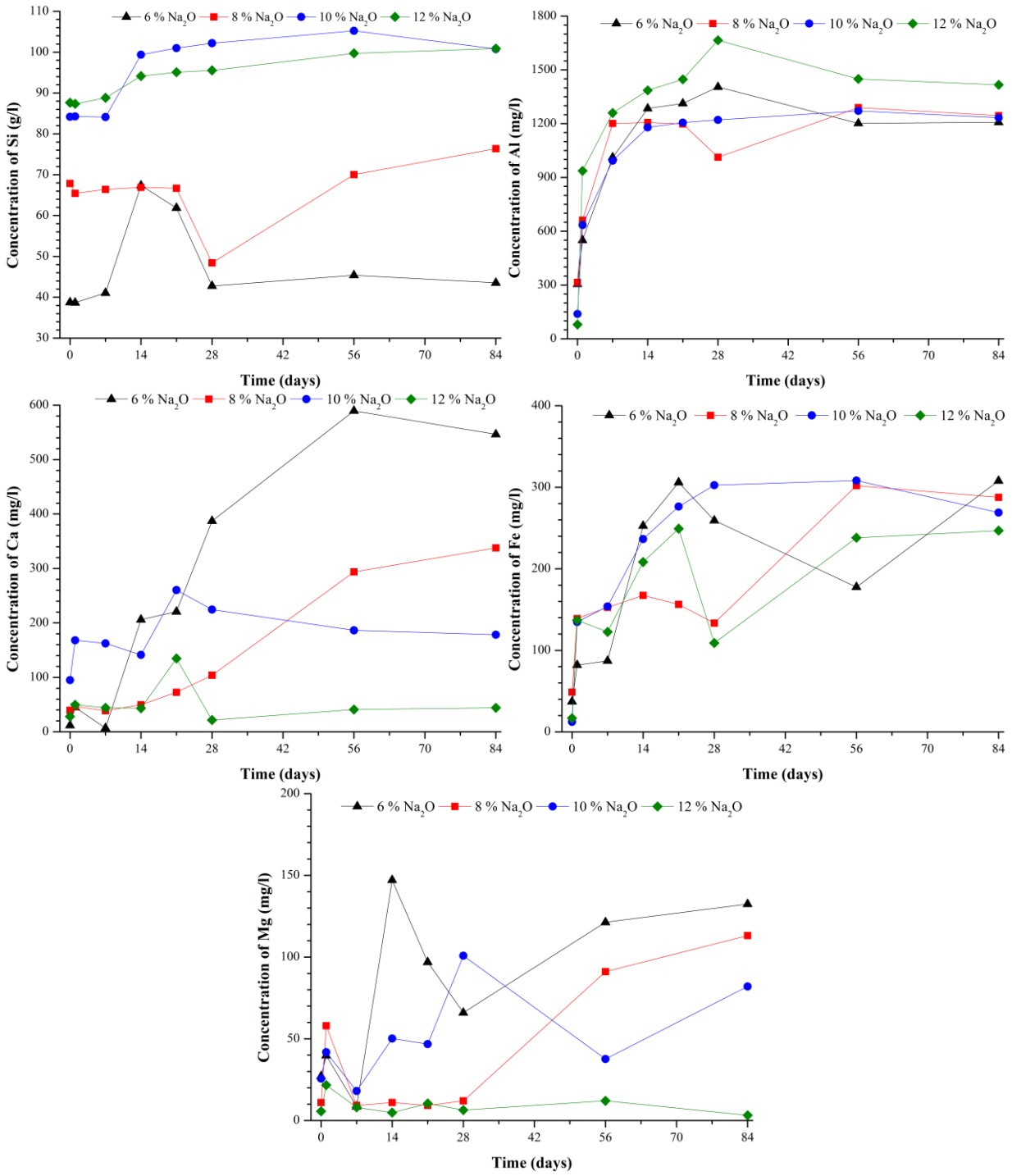

Fig. 35: Concentration development of chosen elements as a function of activator dosage due to the immersion of basalt fibres in WG/SH solutions.

More clear results were obtained regarding the ICP-OES analysis possibilities for concentration of Al development due to the immersion of the fibres. The concentration of Al increase was more significant after one day for WG/SH when compared with WG/SC solutions. Unlike the WG/SC solutions, concentration stabilization without other further development was observed after 14 days. It is different against the WG/SC solutions where concentration drop to the values like the ones after 1 day of leaching was found after 84 days. Still, the amount of Al concentration increase was noticeably higher for WG/SH than WG/SC solutions. It indicates that dissolution of fibres is more significant at the beginning of the immersion and lead to

complete leaching of Al from the fibres. Moreover, it seems that no further recrystallization or precipitation of Al from the solution is realized due to the oversaturated solution formation as can be seen in WG/SC mixtures. These results are in a good agreement with the ones for the loss of mass tests where weight stabilization was also found after 14 days. A dissolution rate increased with increasing activator dosage from 6 to 12 % Na_2O at the initial period of immersion. However, no significant concentration of Al difference was observed for dosages from 6 to 10 % Na_2O after 84 days. The amount of Al leached was the highest for 12 % Na_2O WG/SH solution.

The reversed trend of concentration change dependence of analysed element on the activator dosage was found out for iron. Thus, the amount of its concentration gain decreased with increasing activator dosage from 6 to 12 % Na_2O after 84 days. On the other hand, trend development was quite non-uniform during the whole-time interval. The most significant concentration of Fe increase was observed after one day and continued up to 14 days. Results obtained for all activator dosages except 8 % Na_2O did not show other increase after 21 days and beyond this age. Meanwhile, 8 % Na_2O showed significant concentration of Fe increase between 28 and 56 days. The amount of Fe leached from the fibres is slightly higher for all WG/SH than for WG/SC mixtures. It may be related with higher pH of WG/SH solutions. The ICP-OES results for Fe as well as Al indicate higher dissolution efficiency of WG/SH mixtures, however loss of mass test results cannot confirm this conclusively. A lower effect of WG/SH activator dosage on the dissolution of the BFs compared to WG/SC can be confirmed. The weight loss of fibres immersed in WG/SH was not such rapid as would be predicted based on ICP-OES results. The rapid decrease in compactness of the fibres was observed due to the immersion in WG/SH solutions despite the fibres weight loss in these solutions was not such rapid. This differs WG/SH immersion solutions greatly from the WG/SC where even at higher weight losses the compactness of the fibres was preserved. This was also confirmed by tensile strength development described in 5.3.2.

The dependence of Ca concentration on activator dosage was not persuasive until 28 days. Nevertheless, some dependence was found beyond this age. Amount of Ca leached into the solution increased with decreasing activator dosage from 12 to 6 % Na_2O. No significant change (0.02 g/l) of calcium contained in solution was found for 12 % Na_2O WG/SH solution considering the entire immersion interval. Meanwhile, the lowest activator dosage (6 % Na_2O) solution showed the most rapid increase (about 0.54 g/l) during the evaluated immersion interval. The rest of dosages lie between those two. The dosage of 8 % Na_2O showed gradual concentration increase during the entire period. Meanwhile concentration of Ca increases up to 21 days, but slight simultaneous decrease was observed beyond this age for the 10 % Na_2O mixture. The amount of Ca released from basalt fibres seems to be similar for WG/SC and WG/SH solutions but with different dependence on activator dosage.

Concentration development dependence on the activator dosage was quite similar for Mg. The most stable concentration level of Mg was found for 12 % Na_2O. Unlike the 6 and 10 % Na_2O solutions where a rapid increase of Mg was observed (0.12 and 0.17 g/l) after 14, respectively 21 days. Some concentration of Mg decrease was observed after those immersion times, but it was followed by another simultaneous concentration increase which resulted into 0.11, respectively 0.06 g/l of Mg gain after 84 days. The last activator dosage solution (8 % Na_2O) showed rapid increase after one day (0.05 g/l) which was followed by drop and concentration stable zone from 7 to 28 days. Further increase of Mg concentration was observed beyond 28 days and resulted into total 0.1 g/l gain after 84 days. The amount of Mg leached from the fibres was similar for both WG/SC and WG/SH solution types.

The brief summary of results obtained for WG/SC mixtures will be done in this paragraph. It can be assumed that increase of concentration of analysed elements relates to the dissolution of the fibres. The process of dissolution of the fibres is more intense with increasing activator dosage (6–12 % Na_2O). The concentration of elements gradually increases with prolonging time of treatment until it reaches maximum but beyond this concentration simultaneous decrease was observed in most cases. It is related with simultaneous dissolution of the fibres until the chemical equilibrium is reached, followed by formation of oversaturated solution, and finished with elimination of the least soluble component.

Immersion of basalt fibres in WG/SH based solutions resulted in less clear results. The development of Al concentrations had similar results almost independently on the activator dosage. The amount of Fe, Ca and Mg formed by dissolution of the fibres during immersion decreased with increasing activator dosage from 6 to 12 % Na_2O despite the assumptions and results for WG/SC mixtures. Time dependence of concentration of these elements in WG/SH solutions did not indicate formation of oversaturated solutions followed by the elimination of the least soluble component from the solution. Hence, once the dissolution of the fibres take place the released elements stays in solution in most cases. That is also different against WG/SC mixtures.

The ICP-OES outcomes complement and validate results obtained for the loss of mass testing for both mixture types. It was possible to observe the increase in the concentration of iron and magnesium in the solution in both cases which indicates that no stable insoluble layer retarding the dissolution process based on these elements was formed. These results and the ones for the loss of mass confirmed, that dissolution of the basalt fibres take place when immersed in mixtures simulating initial mixing composition for preparation of the AAMs without addition of slag for both $M_s = 0.5$; WG/SC and WG/SH. On the other hand, real AAMs would include slag as well which should be associated with higher concentration of Si, Ca, Al, Fe or Mg due the slag dissolution continued by hydration products formation. Thus, the dissolution rate of basalt fibres in these systems should be lower because of lower concentration gradient for these elements. Which along with the simultaneous pore solution pH lowering should results into their slower dissolution or some protective insoluble layer formation. This assumption can be confirmed by SEM-EDX analysis presented in 5.2.1 where no significant signs of rapid degradation or dissolution of the fibres were found.

The composition of residual solid phase in $M_s = 0.5$; 10 % Na_2O WG/SC and WG/SH solutions was determined using XRD analysis at the end of the testing period (84 days). Relevant diffractograms are given as Attachments 10 and 11.

Firstly let´s focus on the WG/SC solution. Sodium carbonate in two various modifications was the main component of the crystalline phase (93 %). Low-temperature modification formed about 91 % while 2 % of total crystalline phase content belonged to the high-temperature modification of sodium carbonate. An existence of two sodium carbonate modifications may be explained by the crystalline lattice planes movement due to the different ions (formed by dissolution of basalt fibres) incorporation into the crystalline structure. Hence, various cell dimensions were detected. The rest of crystalline phase was formed by Pirssonite (6 %) defined with formula $Na_2Ca(CO_3)_2 \cdot 2\,H_2O$; and some zeolitic compound (sodium aluminate silicate hydrate) with content about 1 %. The existence of these phases is in a good agreement with theoretical presumptions since the sodium carbonate was one of two main solution components beside the sodium water glass. XRD results for WG/SH residual solid phase composition is less divergent. Crystalline content was formed by sodium silicate (63 %)

and sodium carbonate (37 %) which was formed by carbonation of sodium water glass as one of the main constituents of the beginning solution.

5.3.3.2 Surface chemical composition of basalt fibres

The BFs surface chemical composition changes were determined using XPS technique after 28 days of treatment under alkaline conditions (WG/SC and WG/SH 10 % Na_2O; $M_s = 0.5$ solutions) at elevated temperatures. A special emphasis was put on determination of the oxidation state of present iron due to its significant influence on the dissolution resistance of basalt fibres under alkaline conditions. The monovalent and divalent cations are more extensively and rapidly exchanged from the surface of fibres than trivalent cations due to their lower bonding energy to the glass structure. Hence, a ferric ions dominance within the basaltic glass surface layer should be more inhibiting for the dissolution process than the ferrous ions since the entrapment of Fe^{3+} in the glass structure is higher. Moreover, ferric ions would act as intermediates and favour the formation of glassy structure due to their lower ionic radius and higher field intensity compared to Fe^{2+}as stated in paper [66].

It seems that immersion of basalt fibres in WG/SC solutions cause lower releasing of iron from the fibres into the solution than WG/SH solutions based on the ICP-OES. More specifically, concentration of Fe in the 10 % Na_2O WG/SC solution increased because of dissolution of the fibres only about 0.01 g/l after 28 days. Meanwhile, the concentration of Fe increased about 0.29 g/l in the WG/SH mixture with the same activator dosage. These results indicate that iron ions presented in previous glassy structure of the fibres were released into the solution and only small residue or none sustained on the surface of the fibres. This is where importance of XPS analysis arises. The XPS results (Fig. 36) confirmed that there was no presence of Fe $2p_{3/2}$ photoelectric peak between 710.6–711.2 eV as defined in publication [68]. Hence, immersion of the fibres led to the iron elimination from their surface in 10 % Na_2O WG/SH solution after 28 days. A presence of Si 2s and Si 2p peaks was detected in this sample using XPS as well but it is not surprising since the Si is main constituent of the BFs and is also contained in sodium water glass which together with sodium hydroxide forms the immersion solution. Na 1s and Na 2s photoelectric peaks were also detected along with Augers peaks of Na transition from L to K shell (Na KLL). The sodium presence can be explained by formation of some residual solid phase due to the reaction of fibres with leaching solution. The detection of Ca 2s, Ca 2p and Ca 3s photoelectric peaks same as Mg KLL Auger peak (can be observed even if Mg 1s is not visible due to the difference in electron kinetic energies) was unexpected since their concentration in the WG/SH solution increased about 0.13 g/l and 0.075 g/l and regarding their share in composition of the BFs. Whereas, the iron presence was not detected. It indicates that, protective layer on the surface of fibres causing the mass of loss retarding is not formed by Fe^{3+} but Mg^{2+} in this case. This possibility was outlined in paper [42]. The XRD measurements were performed for a closer determination of the compound formed on the the fibres. The fibres immersion in WG/SH led to the formation of some silicate compound probably containing Na, Al, Ca and Mg. However, exact stechiometry of this compound could not been determined due to the width of diffraction peaks.

Ferrous and ferric ions have different contribution to the dissolution resistance under the alkaline conditions as already outlined. Thus, content of Fe^{2+} and Fe^{3+} in the surface layer should be determined if they are present. Ferrous and ferric compounds can be calculated by multiplet peaks fit of high-resolution iron $2p_{3/2}$ spectra envelope. Multiplet splitting of photoelectron peak arises from different spin distributions of the electrons of the band structure. The Fe $2p_{3/2}$ envelope from Fe^{3+} and Fe^{2+} can be well fit using multiplet splitting calculated by

Gupta and Sen as described in paper [67]. The experimentally obtained and evaluated results for iron oxidation state on the surface of the fibres determination using high-resolution iron spectra are presented in Fig. 36. It has been found out that surface of the fibres after 28 days of immersion in 10 % Na_2O WG/SC solution contain iron in both oxidation states. More preciously, Fe^{3+} forms 60.5 at. % and the rest of total iron belongs to the Fe^{2+} (39.5 at. %). These results are not in the full agreement with theoretical assumptions described at the beginning of this chapter. Since the presence of Fe^{2+} on the surface of the fibres was detected even after 28 days of accelerated leaching. Thus, a difference between these two iron forms regarding the influence on the dissolution process of the fibres is not as significant as expected. However, it has been shown that WG/SC mixture is less aggressive in dissolving of the iron fraction but also other constituents in the basalt fibres than the WG/SH one as already predicted based on the ICP-OES results. This statement can also be supported by detection of Al 2s and Al 2p photoelectric peaks that were not detected in the fibres leached in the WG/SH solution. It indicates that dissolution of glassy structure of the fibres is less developed in WG/SC solutions since the second main constituent of the fibres can be detected beside the Si 2s and Si 2p photoelectric peaks. Photoelectric peaks for Na 1s Na 2s, same as Ca 2p and Ca 2s were detected along Augers peaks of Na KLL and Mg KLL in both solution types.

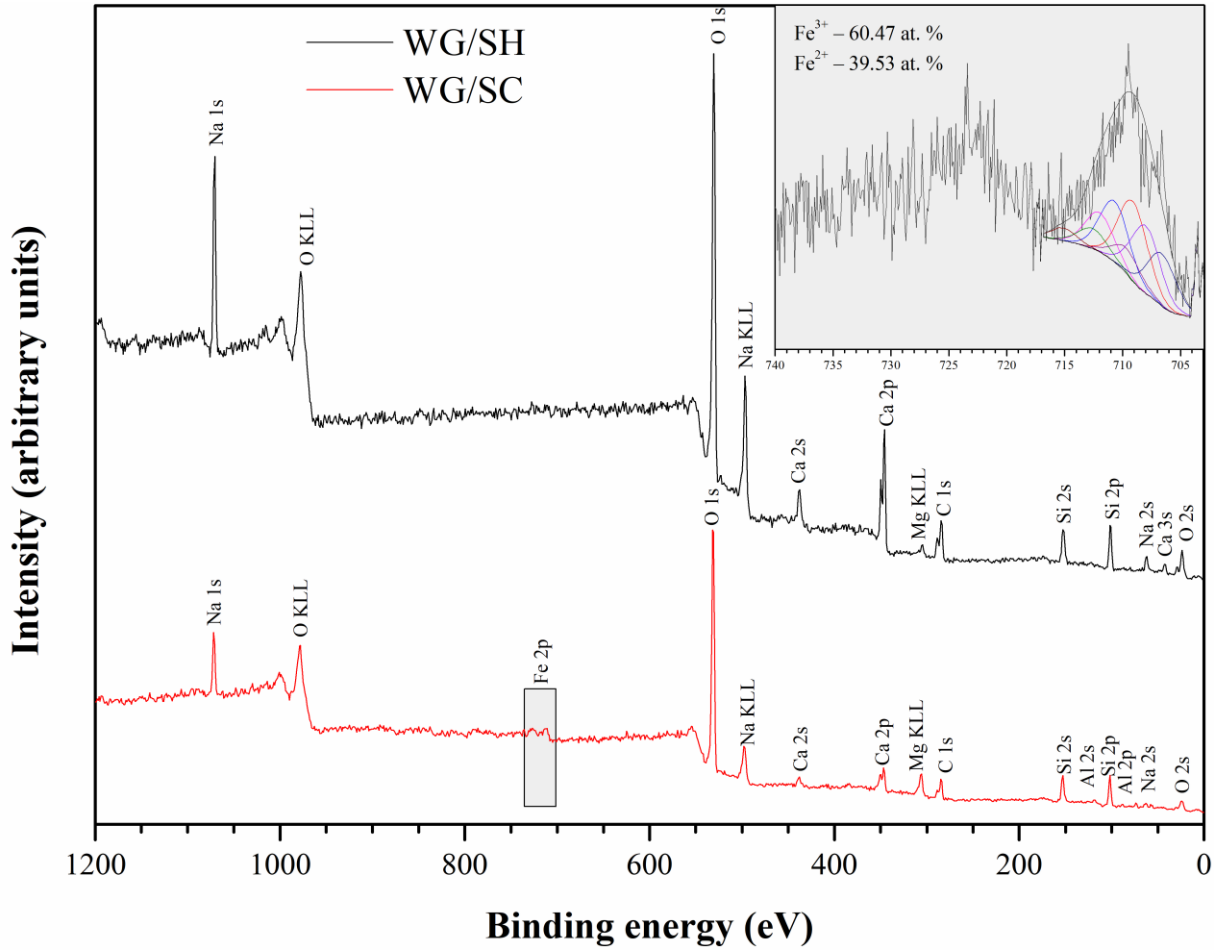

Fig. 36: Graph showing the results of XPS analysis of basalt fibres immersed in 10 % Na_2O WG/SC and WG/SH solutions up to 28 days.

The determination of reaction products on the fibres have been done using XRD for completion. Despite the assumptions the presence of sodium carbonate was not detected using

XRD analysis for WG/SC immersion solution, meanwhile formation of calcium carbonate has been found out next to the amorphous hump (Attachment 12). It may be related with a very low solubility of calcium carbonate, hence its precipitation from the solution take place before sodium carbonate with much higher solubility. Formation of carbonate compounds is realized due to the carbonatation process.

To sum up, the results of XPS analysis of fibres treated in 10 % Na_2O WG/SC and WG/SH solutions at elevated temperatures for 28 days confirmed that WG/SH creates more aggressive environment regarding the dissolution of the basalt fibres since the presence of Fe and Al was not detected in WG/SH solutions. Meanwhile, iron sustained present on the surface of the immersed basalt fibres in both oxidation states Fe^{2+} same as Fe^{3+} for WG/SC solutions. It indicates that protective layer containing iron is formed independently on the iron oxidation state. Hence, the influence of the iron oxidation state to the retarding of the fibres dissolution process is not such significant as was predicted in paper [66]. The layer formed on the surface of the fibres consisted of calcium carbonate according to the XRD results for WG/SC. The composition of the reaction product on the surface of the fibres for WG/SH was not clearly determined using XRD.

6 CONCLUSION

This paper was focused on the utilization of the basalt fibres in the AAMs based on the BFS activated using various alkaline activators.

Firstly, the influence of basalt fabric implementation in one or more layers as reinforcement of the AAMs on the mechanical properties was studied. There was not observed any significant improvement of compressive and flexural strengths when the various matrices were reinforced with one or more layers of basalt fabric. Nevertheless, an indication of considerable improvement of mechanical properties due to the implementation of basalt fabric in one layer was observed in case of BFS activated with M_s = 0.5; 10 % Na_2O; WG/SC mixture since it led to the compressive strength improvement for up to 84 days, but a strength decrease was observed beyond this age too. More preciously, increase of compressive strengths against the pure matrix about 24.7; 0.5; 17.5 and 14.5 % was noticed after 7; 28; 56 and 84 days of curing. However, no further mechanical properties development was realized when the number of basalt fabric layers was increased to two or three. An implementation of basalt fabric into the WG/SH, WG, SH but also WG/SC activated systems using activator dosages between 6 and 12 % Na_2O (beside the 10 % Na_2O WG/SC) did not show any beneficial effect. Moreover, it made the mechanical properties even worse in same cases. These results can be explained by a poor F/M interaction leading to low or none adhesion and ineffective stress transfer between F/M which is crucial for the reinforcement to be effective. The deterioration of the stress transfer capability of the fibres due to their degradation under alkaline conditions same as a contribution of stress concentration because of local disorientations or bending along with a poor constitution of the fabric should be considered as well.

The second part deals with the F/M interface characterization. The SEM images confirmed that no quality adhesion for 10 % Na_2O WG/SC activated system is formed after 7 or 28 days. An indication of better adhesion due to the presence of matrix fragments on the surface of the fibres was noticed for 10 % Na_2O WG/SH after 7 days. Nonetheless, this sign was refuted since these fragments were no longer visible after 28 days of hydration. It has been found out that the pure matrix is formed mainly by C-A-S-H gel with some possible minor phases (Ca/Si ratio about 0.9–1 and Al/Si ratio about 0.2) for both AAMs tested. A transition zone existence was observed for both activator types after seven days. The transition zone composition of WG/SC activated systems was quite the same when compared to the pure matrix but with higher Na content. Meanwhile, WG/SH activated systems showed differences in Na content but for Ca/Si ratio (0.8 vs. 1.0) as well. Still, rather than a place with different hydration products it is the place with a lower degree of hydration which can also be confirmed by the presence of higher amount of unreacted slag particles but the fact that this area is no longer recognizable after 28 days of hydration too. Minor changes of Ca/Si (WG/SC – 0.3; WG/SH – 0.4) ratios were observed when comparing zone near the fibres and pure matrix after 28 days which indicates that presence of basalt fibres slightly influence the nearby hydration products. The fibre pull-out tests were also used for the characterization of the interface properties. It was found out that the F/M resistance against the pull-out of the fibres is realized mainly due to the frictional bonds which corresponds to the development of mechanical properties. The indication of chemical interaction in WG/SH activated BFS systems predicted based on the SEM results did not seems to be sufficient enough for its clear show in the pull-out tests. However, the results of pull-out test for 12 % Na_2O WG/SH activated system make it impossible to completely disprove the possibility of a chemical forces contribution against the fibre pull-out from the surrounding matrix.

The last part was focused on the study of basalt fibres durability under alkaline conditions like the one in the AAMs using the accelerated leaching tests. It was found that the weight loss of the fibres increases with increasing activator dosage from 6 to 12 % Na_2O for WG/SC mixtures. Hence, it resulted in the weight losses about 16.1; 38.1; 41.7 and 96.5 % for 6; 8; 10 and 12 % Na_2O due to the immersion up to 28 days at 60 °C in WG/SC solutions. The results obtained for WG/SH mixtures showed lower differences between the activator dosages when compared with WG/SC mixtures. There was observed no such persuasive dependence of loss of mass on the activator dosage since the immersion of basalt fibres led to the loss of mass about 41.5; 45.8; 48.7 and 58.1 % for 8; 10; 6 and 12 % Na_2O WG/SH mixtures. The weight loss of the fibres was the most crucial during first 14 days of immersion and it slowed down over time in all tested mixtures with an exception of 12 % Na_2O WG/SC mixture. It can be explained by some stable layer formation on the surface of the fibres or formation of oversaturated solution on some of the dissolving elements which retard further dissolution. These results are not as unfavourable as they seem, because they were obtained from accelerated tests under the worst scenario conditions. The SEM images showed that such rapid degradation or rupture of the fibres embedded in the real AAMs (BFS activated with 10 % Na_2O WG/SC and WG/SH mixtures) was not observed after 28 days.

The loss of mass of the fibres is closely connected with the deterioration of tensile strength as has been found out. The most significant drop of tensile strength was observed after one day and led to the reduction of tensile strengths to 33.9; 45.1; 20.8 and 17.2 % when compared with the reference for 6; 8; 10 and 12 % Na_2O WG/SC. The tensile strengths of the fibres continued to fall gradually until non-strength could not been measured after that. These results are in a good agreement with the one obtained for the weight loss determination unlike the results of WG/SH immersion solutions where the maintenance of fibres tensile strengths does not respond significantly to the fibres weight loss. Since the maintenance of fibres tensile strengths was about 46.9; 28.2; 26.2 and 23.2 % for 6–12 % Na_2O dosages even after one day and it could not be measured no more due to high degree of fibres disintegration. It may be related to the formation of some compounds layer at the surface of the fibres which is ineffective for tensile strength behaviour.

The ICP-OES outcomes complement and validate the results obtained for the loss of mass testing for both WG/SC and WG/SH solution types. It can be assumed that increase of concentration of analysed elements in the immersion solutions relates to the dissolution of the fibres. The process of dissolution of the fibres is more intense with increasing activator dosage (6–12 % Na_2O). The concentration of elements gradually increases with prolonging time of treatment until it reaches maximum but beyond this concentration simultaneous decrease was observed in most cases. It is related with simultaneous dissolution of the fibres until the chemical equilibrium is reached, followed by formation of oversaturated solution, and finished with elimination of the least soluble component. This can be supported by the presence of calcium carbonate foundation determined using the XRD. All these statements were valid for WG/SC immersion solutions. The immersion of basalt fibres in WG/SH based solutions resulted in less clear results. The development of Al concentrations in immersion solutions had similar results almost independently on the activator dosage. The amount of Fe, Ca and Mg formed by dissolution of the fibres during immersion decreased with increasing activator dosage from 6 to 12 % Na_2O despite the assumptions and results for WG/SC mixtures. The time course of the concentration of the analysed elements development does not indicate the precipitation of the components from the solution.

The results of XPS analysis confirmed that WG/SH solutions create more aggressive environment than WG/SC regarding the dissolution of the basalt fibres since the presence of Fe and Al were not detected in WG/SH solutions. Meanwhile, iron sustained present on the surface of the immersed basalt fibres in both oxidation states Fe^{2+} same as Fe^{3+} for WG/SC solutions. It indicates that protective layer containing iron is formed independently on the iron oxidation state for WG/SC meanwhile this layer cannot be formed in WG/SH since the iron presence was not detected due to the iron releasement into the immersion solution. The protective layer formed on the surface of the fibres consisted of calcium carbonate according to the XRD results for WG/SC. The composition of the reaction product on the surface of the fibres for WG/SH was not clearly determined using XRD but existence of some zeolitic aluminosilicate compound containing Mg and Ca was predicted.

The conclusion that utilization of basalt fibres in form of basalt fabric did not bring any significant improvement of mechanical properties with an exception of 10 % Na_2O WG/SC activated system can be noted. Along with the statement that alkali activated systems based on WG/SC activators with $M_s = 0.5$ seem to be preferable for the implementation of basalt fibres since it forms less aggressive environment as have been found out from the weight and tensile strength maintenances or the XPS results after immersion of the fibres. Nevertheless, a low durability of basalt fibres under the alkaline conditions same as a noticeable deterioration of their mechanical properties were observed and confirmed the theoretical assumptions for both activator types.

There are many further experiments which would beneficially extent this thesis. The testing of basalt fabric reinforcement efficiency in matrices based on fly-ashes is noteworthy along with determination of other composite properties like fracture toughness, shrinkage, durability at elevated temperatures, etc. The utilization of basalt fabric in different form same as chopped basalt fibres as a reinforcement of the AAMs would be interesting as well. The study of the possibility of increasing the durability of basalt fibres in an alkaline environment represents a very large area of a potential research too.

7 BIBLIOGRAPHY

[1] PROVIS, John L. Alkali-activated materials. *Cement and Concrete Research* [online]. 2017 [cit. 2017-11-05]. DOI: 10.1016/j.cemconres.2017.02.009. Available at: http://linkinghub.elsevier.com/retrieve/pii/S0008884616307700.

[2] ŠKVÁRA, František. ALKALI ACTIVATED MATERIALS OR GEOPOLYMERS? In: *Ceramics – Silikáty* [online]. 2007, s. 173–177 [cit. 2017-11-05]. ISSN 1804-5847. Available at: http://www.ceramics-silikaty.cz/2007/pdf/2007_03_173.pdf.

[3] DUXSON, P., A. FERNÁNDEZ-JIMÉNEZ, J. L. PROVIS, G. C. LUKEY, A. PALOMO and J. S. J. VAN DEVENTER. Geopolymer technology: the current state of the art. *Journal of Materials Science* [online]. 2007, 42(9), 2917–2933 [cit. 2017-11-05]. DOI: 10.1007/s10853-006-0637-z.

Available at: http://link.springer.com/10.1007/s10853-006-0637-z.

[4] KÜHL, Hans. *Cement and process of making the same*. 1926. US1594178 A US PATENT.

[5] PROVIS, John L. and Jannie S. J. VAN DEVENTER. *Alkali Activated Materials: State-of-the-Art Report, RILEM TC 224-AAM*. 2014. ISBN 978-940-0776-722.

[6] SHI, Caijun, Pavel V. KRIVENKO and Della ROY. *Alkali-Activated Cements and Concretes*. New York: Taylor & Francis, 2006. ISBN 978–0–415–70004–7.

[7] PACHECO-TORGAL, Fernando, João CASTRO-GOMES and Said JALALI. Alkali-activated binders: A review. *Construction and Building Materials* [online]. 2008, **22**, 1305–1314 [cit. 2017-11-05]. DOI: 10.1016/j.conbuildmat.2007.10.015. Available at: http://linkinghub.elsevier.com/retrieve/pii/S0950061807002462.

[8] PACHECO-TORGAL, Fernando, João CASTRO-GOMES and Said JALALI. Alkali-activated binders: A review. Part 2. About materials and binders manufacture. *Construction and Building Materials* [online]. 2008, 1315-1322 [cit. 2017-11-05]. DOI: 10.1016/j.conbuildmat.2007.03.019. Available at: http://linkinghub.elsevier.com/retrieve/pii/S0950061807000918.

[9] PROVIS, John L., Angel PALOMO and Caijun SHI. Advances in understanding alkali-activated materials. *Cement and Concrete Research* [online]. 2015, 78, 110–125 [cit. 2017-11-05]. DOI: 10.1016/j.cemconres.2015.04.013. Available at: http://linkinghub.elsevier.com/retrieve/pii/S0008884615001192.

[10] FERNANDEZ-JIMENEZ, A. and F. PUERTAS. Effect of activator mix on the hydration and strength behaviour of alkali-activated slag cements [online]. 2003, 15(3), 129–136 [cit. 2017-11-05]. DOI: 10.1680/adcr.15.3.129.36623. Available at: http://www.extenza-eps.com/TELF/doi/abs/10.1680/adcr.15.3.129.36623.

[11] Základní informace o vodním skle. In: *Vodní sklo* [online]. [cit. 2017-11-15]. Available at: http://www.vodnisklo.cz/cz/clanky/zakladni-informace-o-vodnim-skle.

[12] KOTLÍK, P. *Stavební materiály historických objektů*. Praha: VŠCHT Praha, 1999. ISBN 80-7080-347-9.

[13] Blast Furnace Slag. In: *National slag association* [online]. [cit. 2017-11-15]. Available at: http://www.nationalslag.org/blast-furnace-slag.

[14] Properties and uses of iron and steel slags. In: *National Slag Association* [online]. [cit. 2017-11-15]. Available at: http://www.nationalslag.org/sites/nationalslag/files/documents/nsa_182-6_properties_and_uses_slag.pdf.

[15] PAL, S.C, A MUKHERJEE and S.R PATHAK. Investigation of hydraulic activity of ground granulated blast furnace slag in concrete. *Cement and Concrete research* [online]. 2003, 1481–1486 [cit. 2017-11-15]. DOI: 10.1016/S0008-8846(03)00062-0. Available at: http://linkinghub.elsevier.com/retrieve/pii/S0008884603000620.

[16] Processes: Air cooling, expanding, pelletizing. In: *LAFARGE: Building better cities* [online]. [cit. 2017-11-15]. Available at: http://www.lafarge-na.com/wps/portal/na/en/3_B_3_B_2_3-Processes.

[17] ABS/GBS: Euroslag. In: *EUROSLAG* [online]. [cit. 2017-11-15]. Available at: http://www.euroslag.com/products/absgbs/.

[18] WANG, Shao-Dong, Karen L. SCRIVENER and P.L. PRATT. Factors affecting the strength of alkali-activated slag. *Cement and Concrete Research* [online]. 1994, 24(6), 1033–1043 [cit. 2017-11-15]. DOI: 10.1016/0008-8846(94)90026-4. Available at: http://www.sciencedirect.com/science/article/pii/0008884694900264?via%3Dihub.

[19] PUERTAS, F. Cementos de escorias activadas alcalinamente: Situación actual y perspectivas de futuro. *Materiales de construccion* [online]. 1995, 45(239), 53–64 [cit. 2017-11-15]. Available at: http://materconstrucc.revistas.csic.es/index.php/materconstrucc/article/view/553/601.

[20] FERNANDEZ-JIMENEZ, A., F. PUERTAS and A. ARTEAGA. Determination of Kinetic Equations of Alkaline Activation of Blast Furnace Slag by Means of Calorimetric Data. *Journal of Thermal Analysis* [online]. 1998, **52**(3), 945–955 [cit. 2017-11-15]. Available at: https://link.springer.com/article/10.1023%2FA%3A1010172204297.

[21] FERNANDEZ-JIMENEZ, A. and F. PUERTAS. Effect of activator mix on the hydration and strength behaviour of alkali-activated slag cements. *Advances in Cement Research* [online]. 2003, 15(3), 129–136 [cit. 2017-11-15]. DOI: 10.1680/adcr.15.3.129.36623. Available at: https://www.researchgate.net/publication/250071918_Effect_of_Activator_Mix_on_the_Hydration_and_Strength_Behaviour_of_Alkali-Activated_Slag_Cements

[22] FERNÁNDEZ-JIMÉNEZ, A., J.G. PALOMO and F. PUERTAS. Alkali-activated slag mortars: Mechanical strength behaviours. *Cement and Concrete Research* [online]. 1999, 29(8), 1313–1321 [cit. 2017-11-15]. DOI: 10.1016/S0008-8846(99)00154-4. ISBN 10.1016/S0008-8846(99)00154-4. Available at: http://www.sciencedirect.com/science/article/pii/S0008884699001544?via%3Dihub.

[23] BEN HAHA, M., G. LE SAOUT, F. WINNEFELD and B. LOTHENBACH. Influence of activator type on hydration kinetics, hydrate assemblage and microstructural development of alkali activated blast-furnace slags. *Cement and Concrete Research*[online]. 2011, 41(3), 301–310 [cit. 2017-11-15]. DOI: 10.1016/j.cemconres.2010.11.016. Available at: http://www.sciencedirect.com/science/article/pii/S0008884610002590?via%3Dihub.

[24] GEBREGZIABIHER, Berhan Seium, Robert J. THOMAS and Sulapha PEETHAMPARAN. Temperature and activator effect on early-age reaction kinetics of alkali-activated slag binders. *Construction and Building Materials* [online]. 2016, 113(15), 783–793 [cit. 2017-11-15]. DOI: 10.1016/j.conbuildmat.2016.03.098. Available at: http://www.sciencedirect.com/science/article/pii/S0950061816303944.

[25] SHI, Caijun and Robert L. DAY. A calorimetric study of early hydration of alkali-slag cements. *Cement and Concrete Research*[online]. 1995, 25(6), 1333–1346 [cit. 2017-11-15]. DOI: 10.1016/0008-8846(95)00126-W.
Available at: http://www.sciencedirect.com/science/article/pii/000888469500126W.

[26] KRIZAN, Darko and Branislav ZIVANOVIC. Effects of dosage and modulus of water glass on early hydration of alkali–slag cements. *Cement and Concrete Research* [online]. 2002, 32(8), 1181–1188 [cit. 2017-11-15]. DOI: 10.1016/S0008-8846(01)00717-7.
Available at: http://www.sciencedirect.com/science/article/pii/S0008884601007177.

[27] CHEN, W. and H. J. H. BROUWERS. The hydration of slag, part 1: reaction models for alkali-activated slag. *Journal of Materials Science* [online]. 2007, 42(2), 428–443 [cit. 2017-11-15]. DOI: 10.1007/s10853-006-0873-2.
Available at: https://link.springer.com/article/10.1007%2Fs10853-006-0873-2.

[28] PROVIS, John L. Geopolymers and other alkali activated materials: why, how, and what? *Materials and Structures* [online]. 2014, 47(1–2), 11–25 [cit. 2017-11-15]. DOI: 10.1617/s11527-013-0211-5.
Available at: https://link.springer.com/article/10.1617%2Fs11527-013-0211-5.

[29] MYERS, Rupert J., Susan A. BERNAL, Rackel SAN NICOLAS and John L. PROVIS. Generalized Structural Description of Calcium–Sodium Aluminosilicate Hydrate Gels: The Cross-Linked Substituted Tobermorite Model. *Langmuir* [online]. 2013, **29**(17), 5294–5306 [cit. 2017-11-15]. DOI: 10.1021/la4000473.
Available at: http://pubs.acs.org/doi/abs/10.1021/la4000473.

[30] DHAND, Vivek, Garima MITTAL, Kyong Yop RHEE, Soo-Jin PARK and David HUI. A short review on basalt fiber reinforced polymer composites. *Composites Part B: Engineering* [online]. 2015, 166–180 [cit. 2017-11-15].
DOI: 10.1016/j.compositesb.2014.12.011.
Available at: http://linkinghub.elsevier.com/retrieve/pii/S1359836814005873.

[31] SINGHA, Kunal. A Short Review on Basalt Fiber. *International Journal of Textile Science* [online]. 2012, 19–28 [cit. 2017-11-15]. DOI: 10.5923/j.textile.20120104.02.
Available at: http://article.sapub.org/pdf/10.5923.j.textile.20120104.02.pdf.

[32] SIM, Jongsung, Cheolwoo PARK and Do Young MOON. Characteristics of basalt fiber as a strengthening material for concrete structures. *Composites Part B: Engineering* [online]. 2005, 36(6–7), 504–512 [cit. 2017-11-15]. DOI: 10.1016/j.compositesb.2005.02.002.
Available at: http://linkinghub.elsevier.com/retrieve/pii/S1359836805000454.

[33] Basalt Fiber Tech properties: Recyclable Resource. In: *Basalt Fiber Tech: Advanced Basalt Fiber and products* [online]. [cit. 2017-11-15].
Available at: http://www.basaltft.com/prop/rec.htm.

[34] Charakteristika čedičových vláken. In: *Basaltex a.s.* [online]. [cit. 2017-11-15].
Available at: http://www.basaltex.cz/cedic/cedic_charakteristika_cz.htm.

[35] Inorganic Fiber Technology. In: *US Basalt* [online]. [cit. 2017-11-15].
Available at: http://www.usbasalt.com/about-us/inorganic-fiber-technology.

[36] Basalt: Igneous rocks. In: *Sandatlas* [online]. [cit. 2017-11-15].
Available at: http://www.sandatlas.org/basalt/.

[37] Basalt. In: *Alexstrekeisen* [online]. [cit. 2017-11-15].
Available at: http://www.alexstrekeisen.it/english/vulc/basalt.php.

[38] WEI, Bin, Hailin CAO and Shenhua SONG. Tensile behavior contrast of basalt and glass fibers after chemical treatment. *Materials & Design* [online]. 2010, **31**(9), 4244–4250 [cit. 2017-11-15]. DOI: 10.1016/j.matdes.2010.04.009.
Available at: http://linkinghub.elsevier.com/retrieve/pii/S0261306910002207.

[39] YING, Shuni and Xiaodong ZHOU. Chemical and thermal resistance of basalt fiber in inclement environments. *Journal of Wuhan University of Technology-Mater. Sci. Ed* [online]. 2013, 28(3), 560–565 [cit. 2017-11-15]. DOI: 10.1007/s11595-013-0731-4.
Available at: https://link.springer.com/article/10.1007/s11595-013-0731-4.

[40] WELTER, Michael, Martin SCHMÜCKER and Kenneth J.D. MACKENZIE. Evolution of the Fibre-Matrix Interactions in Basalt-Fibre-Reinforced Geopolymer-Matrix Composites after Heating. *Journal of Ceramic Science and Technology* [online]. 2015, 6(1), 17–24 [cit. 2017-11-15]. DOI: 10.4416/JCST2014-00034. Available at: https://www.researchgate.net/publication/282953566_Evolution_of_the_Fibre-Matrix_Interactions_in_Basalt-Fibre-Reinforced_Geopolymer-Matrix_Composites_after_Heating.

[41] RYBIN, V.A., A.V. UTKIN and N.I. BAKLANOVA. Alkali resistance, microstructural and mechanical performance of zirconia-coated basalt fibers. *Cement and Concrete Research* [online]. 2013, 1–8 [cit. 2017-11-15]. DOI: 10.1016/j.cemconres.2013.06.002.
Available at: http://linkinghub.elsevier.com/retrieve/pii/S0008884613001373.

[42] LIPATOV, Ya.V., S.I. GUTNIKOV, M.S. MANYLOV, E.S. ZHUKOVSKAYA and B.I. LAZORYAK. High alkali-resistant basalt fiber for reinforcing concrete. *Materials & Design* [online]. 2015, 60–66 [cit. 2017-11-15]. DOI: 10.1016/j.matdes.2015.02.022.
Available at: http://linkinghub.elsevier.com/retrieve/pii/S0261306915000680.

[43] LEE, Jung Jin, Jiyeon SONG and Hodong KIM. Chemical stability of basalt fiber in alkaline solution. *Fibers and Polymers*[online]. 2014, 15(11), 2329–2334 [cit. 2017-11-15]. DOI: 10.1007/s12221-014-2329-7.
Available at: http://link.springer.com/10.1007/s12221-014-2329-7.

[44] FUNKE, Henrik, Sandra GELBRICH and Lothar KROLL. The Durability and Performance of Short Fibers for a Newly Developed Alkali-Activated Binder. *Fibers* [online]. 2016, 1–8 [cit. 2017-11-15]. DOI: 10.3390/fib4010011.
Available at: http://www.mdpi.com/2079-6439/4/1/11.

[45] DU, Yunxing, Mengmeng ZHANG, Fen ZHOU and Deju ZHU. Experimental study on basalt textile reinforced concrete under uniaxial tensile loading. *Construction and Building Materials* [online]. 2017, 88–100 [cit. 2017-11-15].
DOI: 10.1016/j.conbuildmat.2017.01.083.
Available at: http://linkinghub.elsevier.com/retrieve/pii/S0950061817301198.

[46] DIAS, Dylmar Penteado and Clelio THAUMATURGO. Fracture toughness of geopolymeric concretes reinforced with basalt fibers. *Cement and Concrete Composites* [online]. 2005, 27(1), 49–54 [cit. 2017-11-15]. DOI: 10.1016/j.cemconcomp.2004.02.044. Available at: http://linkinghub.elsevier.com/retrieve/pii/S0958946504000575.

[47] PORTAL, Natalie Williams, Nelson SILVA, Katarina MALAGA and Peter H. BILBERG. *Durability study of textile fibre reinforcement* [online]. 2015, 408–413 [cit. 2017-11-15]. Available at: https://www.researchgate.net/publication/283641274_Durability_study_of_textile_fibre_reinforcement.

[48] TIMAKUL, Patthamaporn, Weerada RATTANAPRASIT and Pavadee AUNGKAVATTANA. Improving compressive strength of fly ash-based geopolymer composites by basalt fibers addition. *Ceramics International* [online]. 2016, **42**(5), 6288–6295 [cit. 2017-11-15]. DOI: 10.1016/j.ceramint.2016.01.014. Available at: http://linkinghub.elsevier.com/retrieve/pii/S0272884216000420.

[49] RILL, E., D. R. LOWRY and W. M. KRIVEN. *Properties of basalt fiber reinforced geopolymer composites* [online]. 2010 [cit. 2017-11-15]. DOI: 10.13140/2.1.1763.3287. Available at: https://www.researchgate.net/publication/267394277_PROPERTIES_OF_BASALT_FIBER_REINFORCED_GEOPOLYMER_COMPOSITES.

[50] RIBERO, Daniel, Waltraud M. KRIVEN and P. COLOMBO. *Properties of Geopolymer Composites Reinforced with Basalt Chopped Strand Mat or Woven Fabric* [online]. 2016 [cit. 2017-11-15]. DOI: 10.1111/jace.14079. ISBN 10.1111/jace.14079. Available at: http://doi.wiley.com/10.1111/jace.14079.

[51] MASI, Giulia, William D.A. RICKARD, Maria Chiara BIGNOZZI and Arie VAN RIESSEN. The effect of organic and inorganic fibres on the mechanical and thermal properties of aluminate activated geopolymers. *Composites Part B: Engineering* [online]. 2015, (76), 218–228 [cit. 2017-11-15]. DOI: 10.1016/j.compositesb.2015.02.023. Available at: http://linkinghub.elsevier.com/retrieve/pii/S1359836815001092 .

[52] LI, Weimin and Jinyu XU. Impact characterization of basalt fiber reinforced geopolymeric concrete using a 100-mm-diameter split Hopkinson pressure bar. *Materials Science and Engineering: A* [online]. 2009, (513–514), 145–153 [cit. 2017-11-15]. DOI: 10.1016/j.msea.2009.02.033. Available at: http://linkinghub.elsevier.com/retrieve/pii/S0921509309001890.

[53] LI, Weimin and Jinyu XU. Mechanical properties of basalt fiber reinforced geopolymeric concrete under impact loading. *Materials Science and Engineering: A* [online]. 2009, (505), 178–186 [cit. 2017-11-15]. DOI: 10.1016/j.msea.2008.11.063. Available at: http://linkinghub.elsevier.com/retrieve/pii/S0921509308013567.

[54] Effect of Single Fiber Pull Out Test Result on Flexural Performance of ECC. Civil & Environmental Engineering [online]. 2014, 4(2) [cit. 2018-03-16]. DOI: 10.4172/2165-784X.1000140. ISBN 10.4172/2165-784X.1000140. Available at: https://www.omicsgroup.org/journals/effect-of-single-fiber-pull-out-test-result-on-flexural-performance-of-ecc-2165-784X.1000140.php?aid=25345.

[55] MAKWANA, J. J. and Dr. J. D. RATHOD. Interface Characterization of Different Types of Fibers in Engineered Cementitious Composites (ECC). *IOSR Journal of Mechanical and Civil Engineering* [online]. 2017, 14(1), 8–14 [cit. 2018-03-16]. DOI: 10.9790/1684-1401020814. ISBN 10.9790/1684-1401020814.
Available at: http://www.iosrjournals.org/iosr-jmce/papers/vol14-issue1/Version-2/B1401020814.pdf.

[56] CHOI, Won-Chang, Seok-Joon JANG and Hyun-Do YUN. Interface Bond Characterization between Fiber and Cementitious Matrix. International Journal of Polymer Science [online]. 2015 [cit. 2018-03-16]. DOI: 10.1155/2015/616949. ISBN 10.1155/2015/616949.
Available at: http://www.hindawi.com/journals/ijps/2015/616949/.

[57] ŠILER, Pavel, Iva KOLÁŘOVÁ and Halina SZKLORZOVÁ. Instrumentation in materials engineering. Brno University of Technology, 2015.

[58] MÁSÍLKO, Jiří. 2011. Rentgenová difrakční analýza na práškových vzorcích. *Chempoint* [online]. [cit. 2018-03-16].
Available at: http://www.chempoint.cz/rentgenova-difrakcni-analyza-na-praskovych-vzorcich.

[59] X-ray Diffraction Techniques. 2007. UNIVERSITY OF CAMBRIDGE. *DoITPoMS: TLP Library* [online]. [cit. 2018-03-16].
Available at: http://www.doitpoms.ac.uk/tlplib/xray-diffraction/index.php.

[60] XPS Equipment. European Action towards Leading Centre for Innovative Materials [online]. [cit. 2018-03-16].
Available at: http://www.eagle-regpot.eu/EAgLE-Equipment_XPS.html.

[61] WASSERBAUER, J.; TKACZ J. and M. BŘEZINA. Praktikum z kovových materiálů. Brno: Vysoké učení technické v Brně, Fakulta chemická, 2017. ISBN 978-80-214-5463-7.

[62] DURAN ATIŞ, Cengiz, Cahit BILIM, Özlem ÇELIK and Okan KARAHAN. Influence of activator on the strength and drying shrinkage of alkali-activated slag mortar. Construction and Building Materials [online]. 2009, 23(1), 548–555 [cit. 2018-03-29]. DOI: 10.1016/j.conbuildmat.2007.10.011. ISBN 10.1016/j.conbuildmat.2007.10.011. Available at: http://linkinghub.elsevier.com/retrieve/pii/S0950061807002486.

[63] JANČÁŘ, Josef. Úvod do materiálového inženýrství polymerních kompozitů. Brno: Vysoké učení technické v Brně, Fakulta chemická, 2003. ISBN 80-214-2443-5.

[64] ARNON, Bentur a Mindess SIDNEY. Fibre reinforced cementitious composites. Essex, England: Elsevie science publishers, 1990. ISBN 1-85166-393-2.

[65] BAKHAREV, Tatiana, Jay Gnananandan SANJAYAN and Yi-Bing CHENG. Alkali activation of Australian slag cements. Cement and Concrete Research. 1999, 29(1), 113-120. DOI: 10.1016/S0008-8846(98)00170-7. ISBN 10.1016/S0008-8846(98)00170-7.
Available at: http://linkinghub.elsevier.com/retrieve/pii/S0008884698001707.

[66] FÖRSTER, T., C. SCHEFFLER, E. MÄDER, G. HEINRICH, D.A. JESSON and J.F. WATTS. Dissolution behaviour of model basalt fibres studied by surface analysis methods. Applied Surface Science [online]. 2014, (322), 78–84 [cit. 2018-04-13]. DOI: 10.1016/j.apsusc.2014.10.058. ISBN 10.1016/j.apsusc.2014.10.058.
Available at: http://linkinghub.elsevier.com/retrieve/pii/S0169433214022971.

[67] GROSVENOR, A. P., B. A. KOBE, M. C. BIESINGER and N. S. MCINTYRE. Investigation of multiplet splitting of Fe 2p XPS spectra and bonding in iron compounds. Surface and Interface Analysis [online]. 2004, 36, 1564–1574 [cit. 2018-04-14]. DOI: 10.1002/sia.1984. ISBN 10.1002/sia.1984. Available at: http://doi.wiley.com/10.1002/sia.1984.

[68] YAMASHITA, Toru and Peter HAYES. Analysis of XPS spectra of Fe^{2+} and Fe^{3+} ions in oxide materials. Applied surface science [online]. 2008, (254), 2441–2449 [cit. 2018-04-14]. DOI: 10.1016/j.apsusc.2007.09.063. ISBN 10.1016/j.apsusc.2007.09.063. Available at: http://linkinghub.elsevier.com/retrieve/pii/S0169433207013748.

8 LIST OF ABBREVIATIONS

AA	alkali activation
AAM	alkali activated material
ABFS	air cooled BFS
AE	Augers electrons
BF	basalt fibre
BFS	blast furnace slag
BSE	backscattered electrons
C-A-H	calcium aluminium hydrate
C-A-S-H	calcium aluminium silicate hydrate
C-(N)-A-S-H	calcium sodium aluminium silicate hydrate
C-S-H	calcium silicate hydrate
CTOD	crack tip opening displacement
DP	degree of depolymerization
EDX	energy dispersive spectroscopy
F/M	fibre/matrix
FRC	fibre reinforced composite
GBFS	granulated BFS
GGBFS	ground granulated BFS
ICP-OES	inductively coupled plasma optical emission spectroscopy
M_s	silicate modulus
OPC	ordinary Portland cement
SC	sodium carbonate
SE	secondary electrons
SEM	scanning electron microscopy
SEM-EDX	scanning electron microscopy with energy dispersive spectroscopy
SH	sodium hydroxide
SRC	steel reinforced concrete
TRC	textile reinforced concrete
w/b	water to binder ratio
WDX	wavelength dispersive spectroscopy
WG	sodium water glass
XPS	X-ray photoelectron spectroscopy
XRD	X-ray diffraction
XRF	X-ray fluorescence

9 ATTACHMENTS

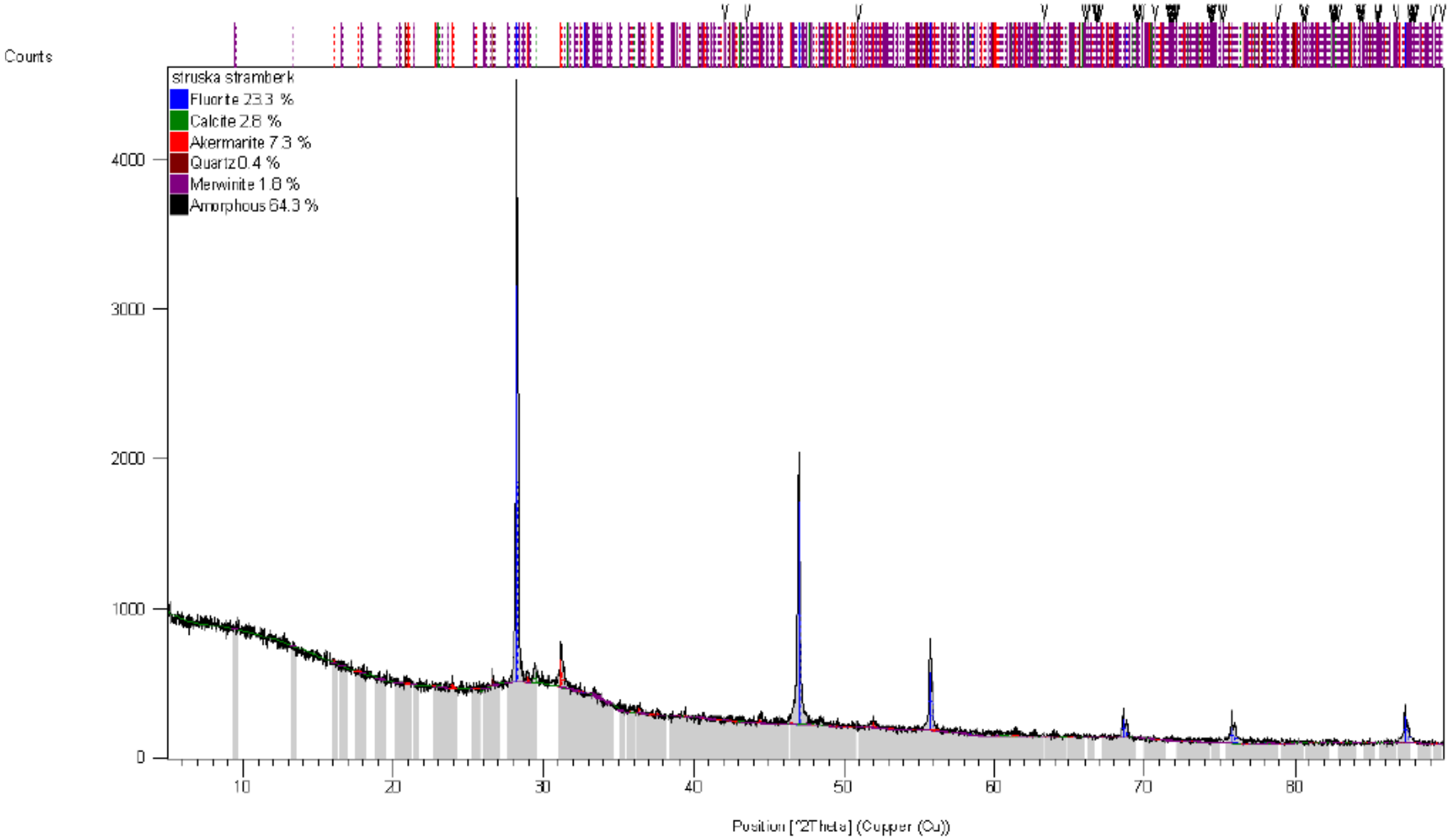

Attachment 1: XRD diffractogram of blast furnace slag (Štramberk).

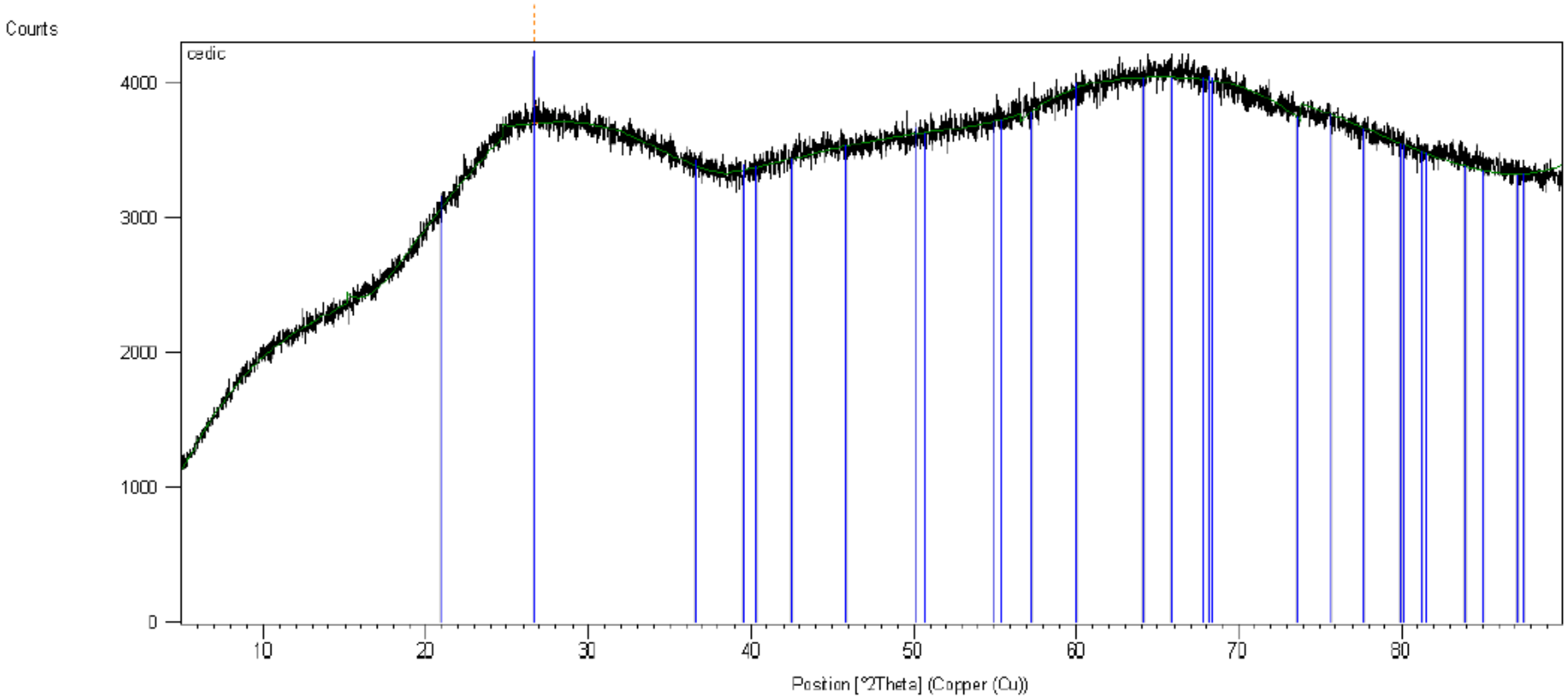

Attachment 2: XRD diffractogram of basalt fibre from Kammeney Vek.

Attachment 3: Photos of overall pull-out testing samples preparation process.

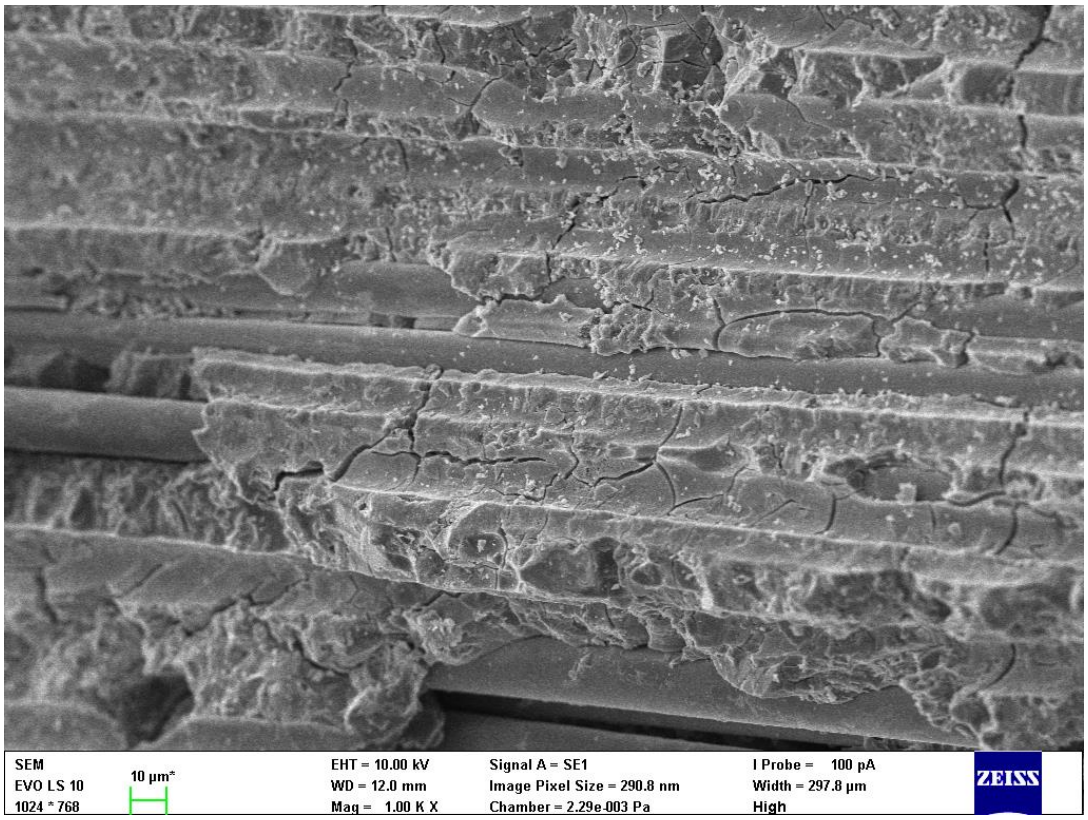

Attachment 4: SEM image showing detail of F/M interface for WG/SC activated system after 28 days of hydration.

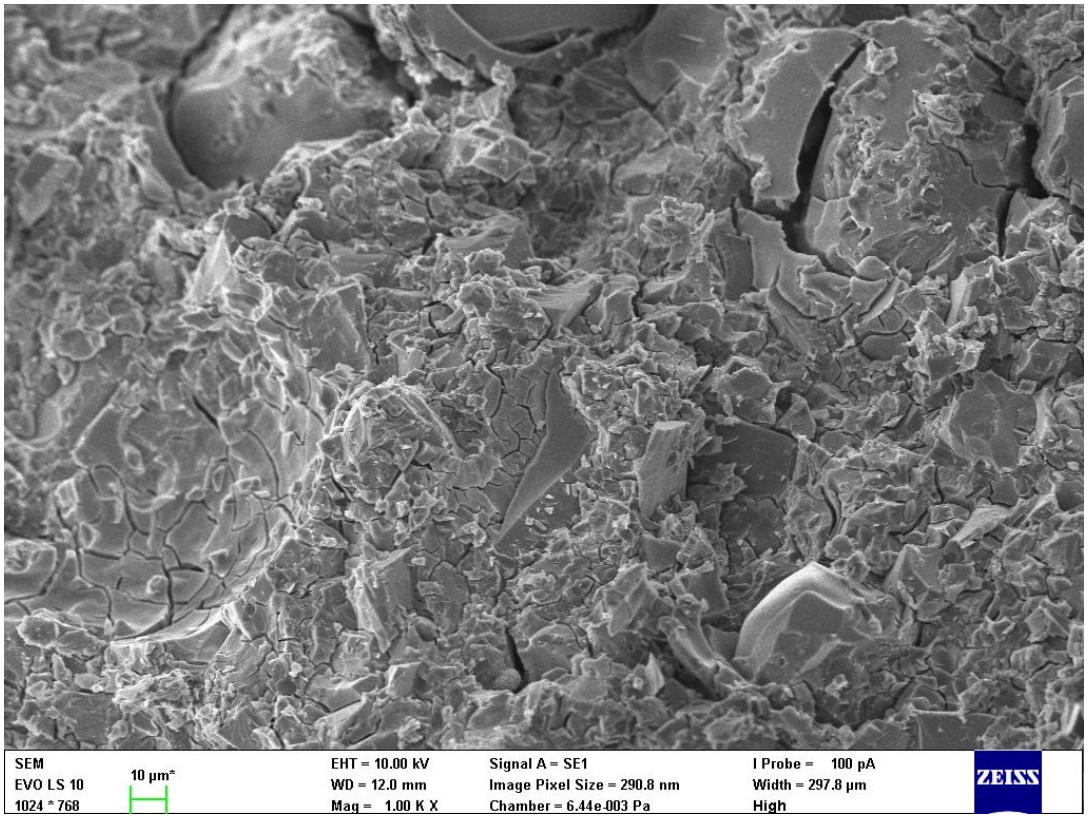

Attachment 5: SEM image showing transition zone of WG/SC activated system after 7 days of hydration.

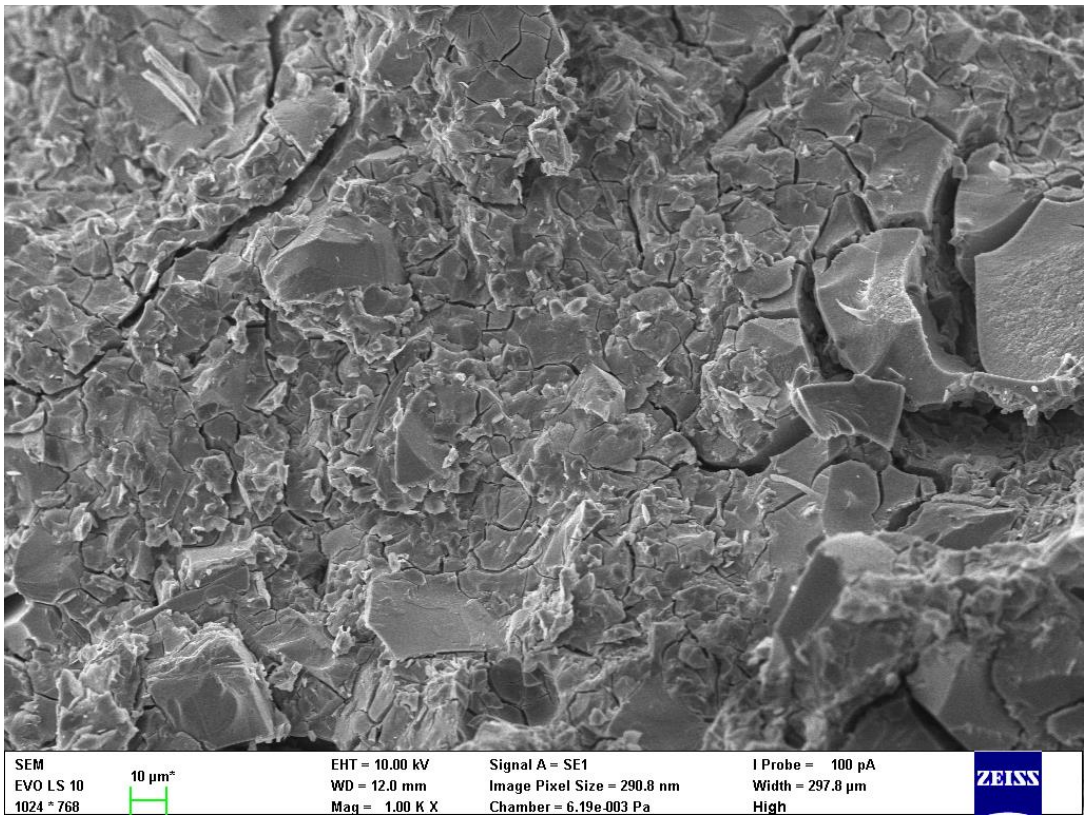

Attachment 6: SEM image showing pure matrix microstructure of WG/SC activated system after 7 days of hydration.

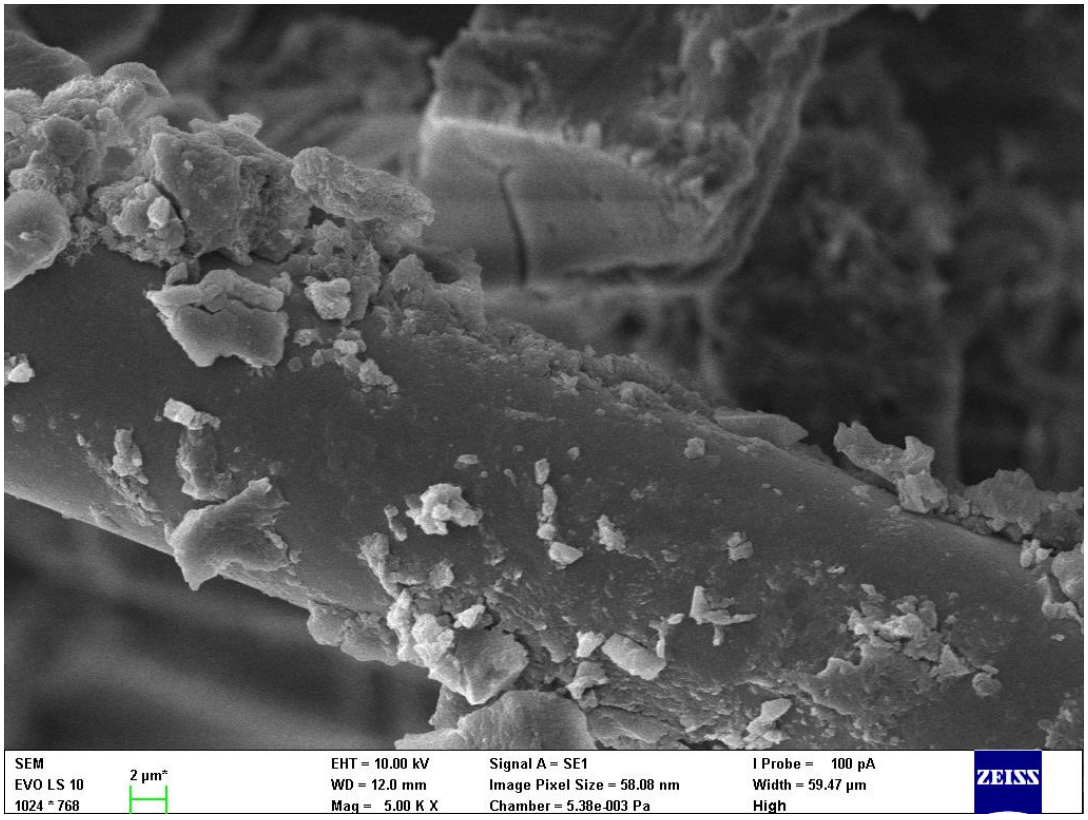

Attachment 7: SEM image showing detail of protrusion on the fibre surface of WG/SH activated system after 7 days of hydration.

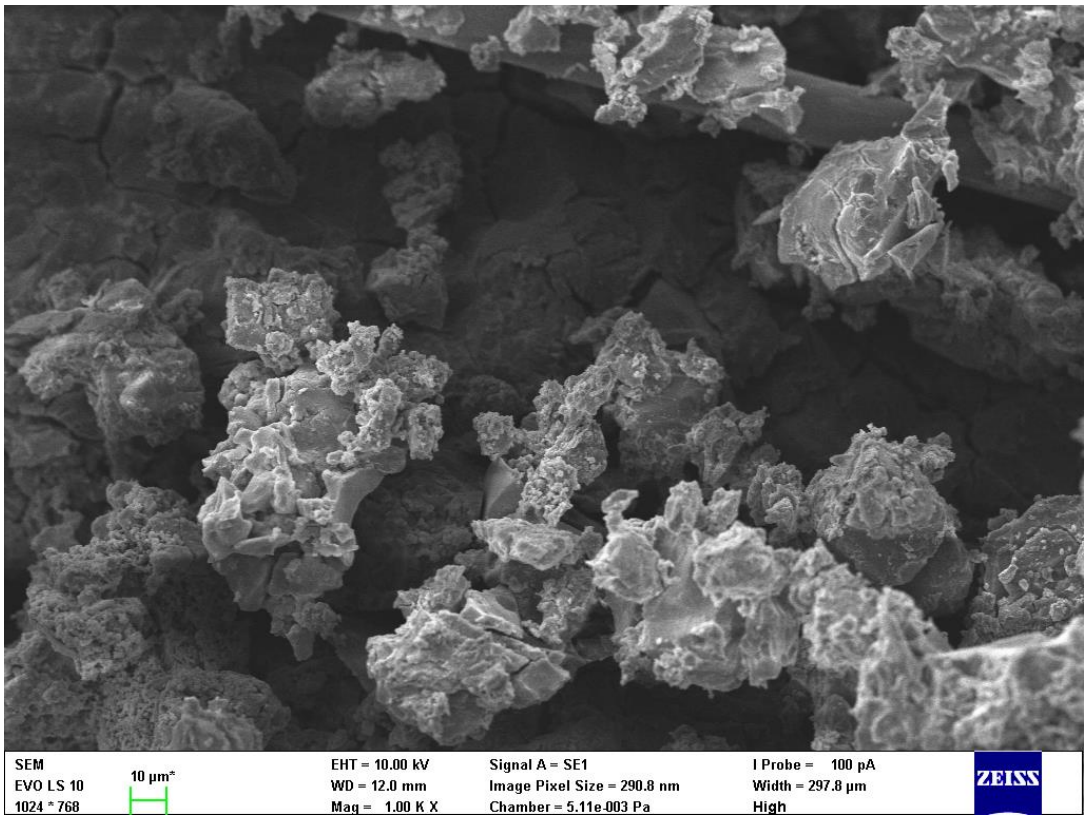

Attachment 8: SEM image showing transition zone of WG/SH activated system after 7 days of hydration.

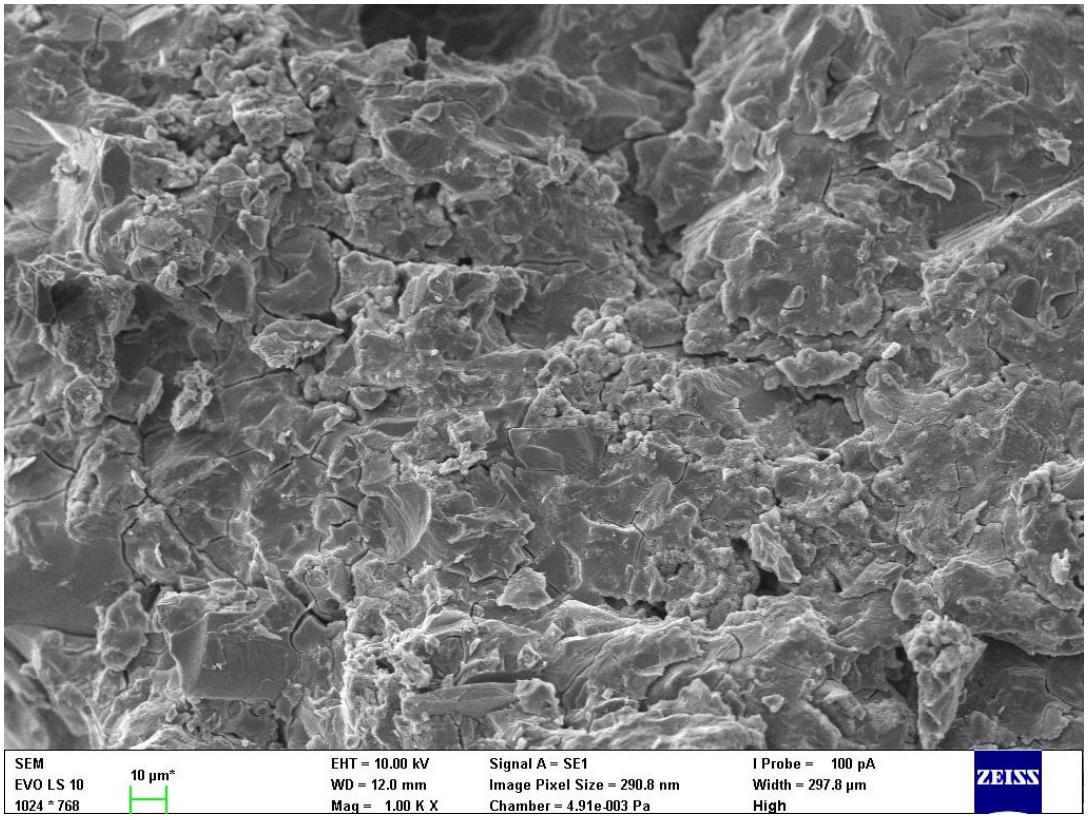

Attachment 9: SEM image showing pure matrix microstructure of WG/SH activated system after 7 days of hydration.

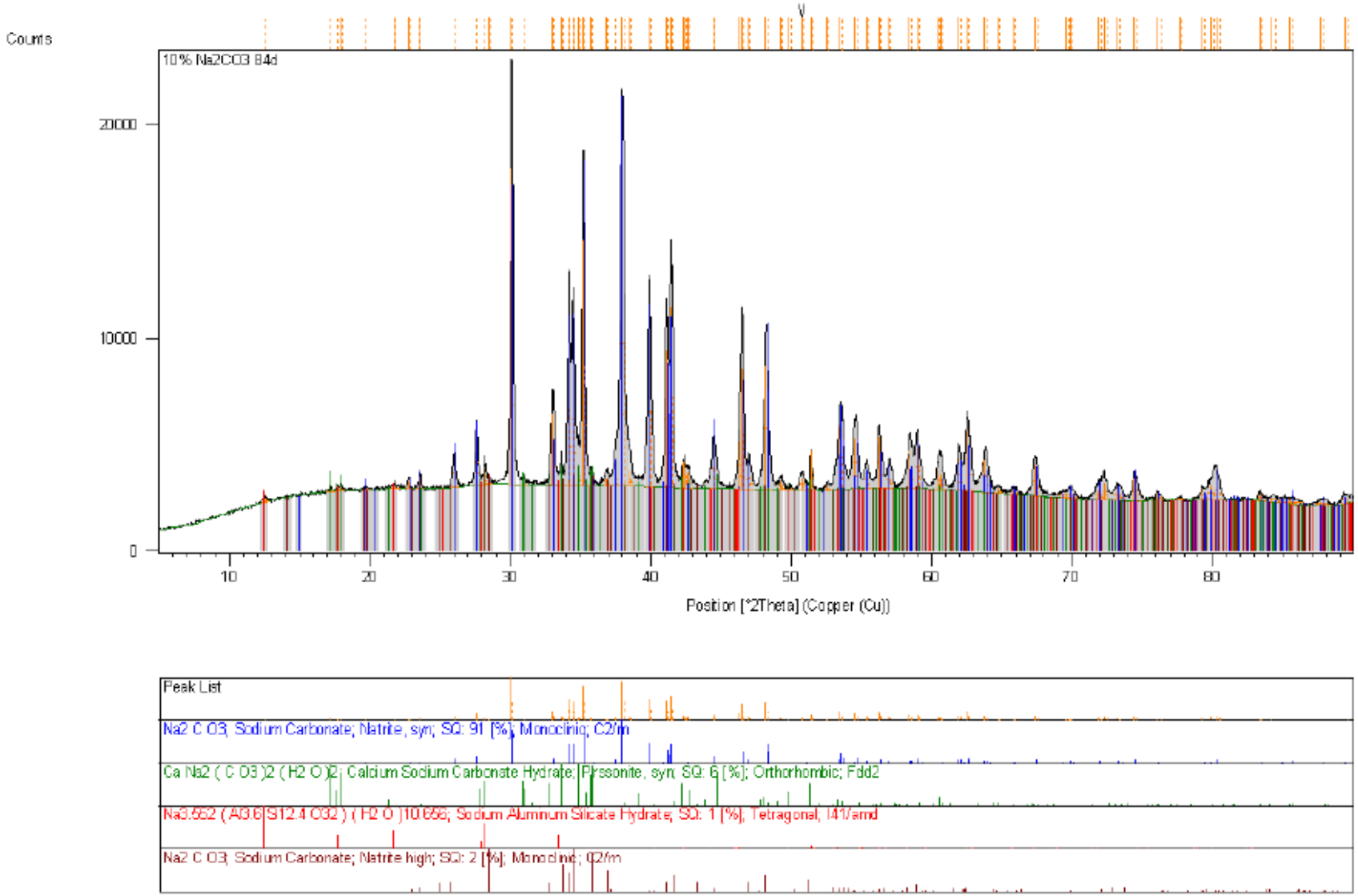

Attachment 10: XRD diffractogram of residual solid phase after leaching of basalt fibres in 10 % Na_2O; M_s = 0.5; WG/SC solution up to 84 days.

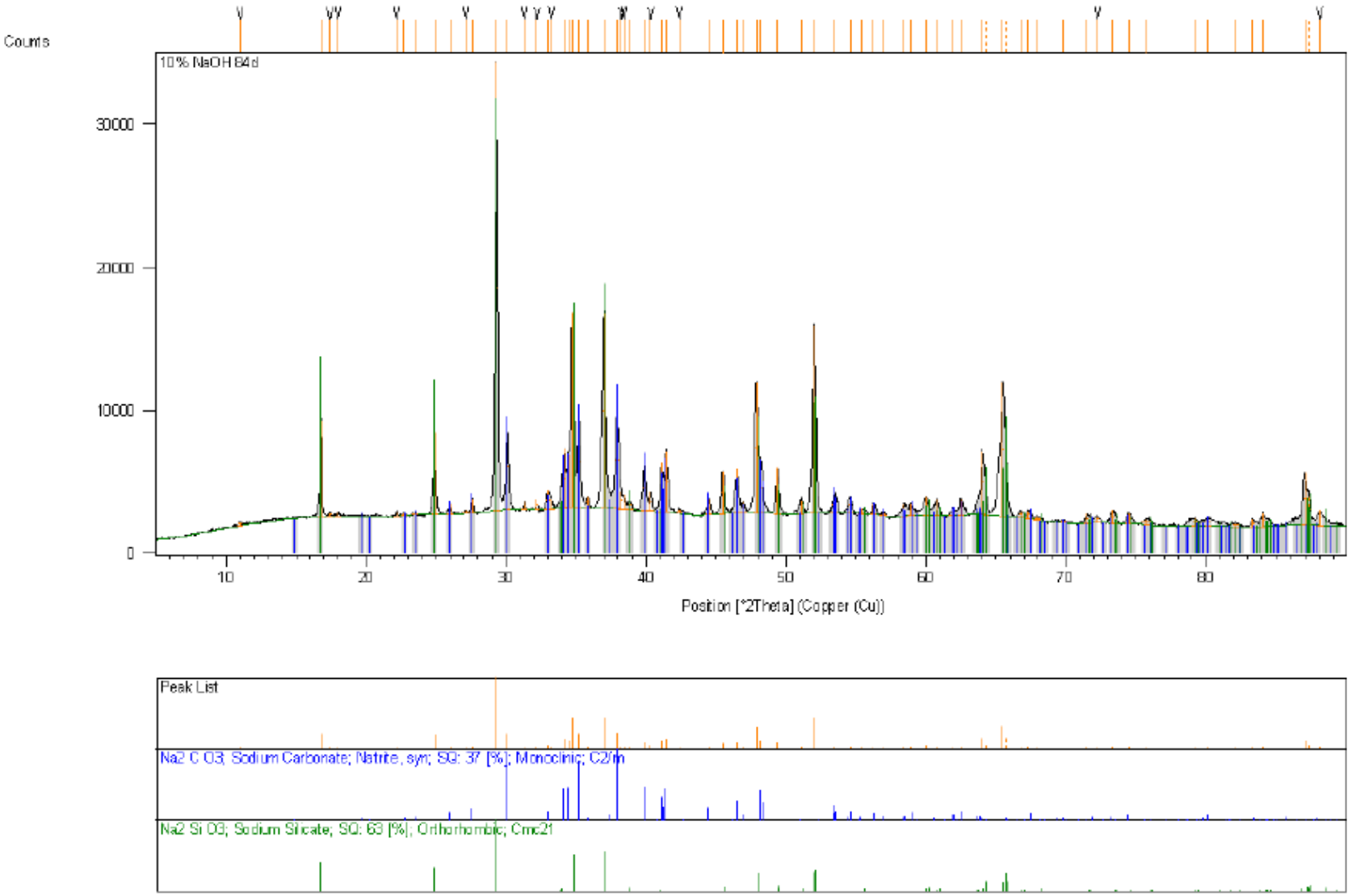

Attachment 11: XRD diffractogram of residual solid phase after leaching of basalt fibres in 10 % Na_2O; M_s = 0.5; WG/SH solution up to 84 days.

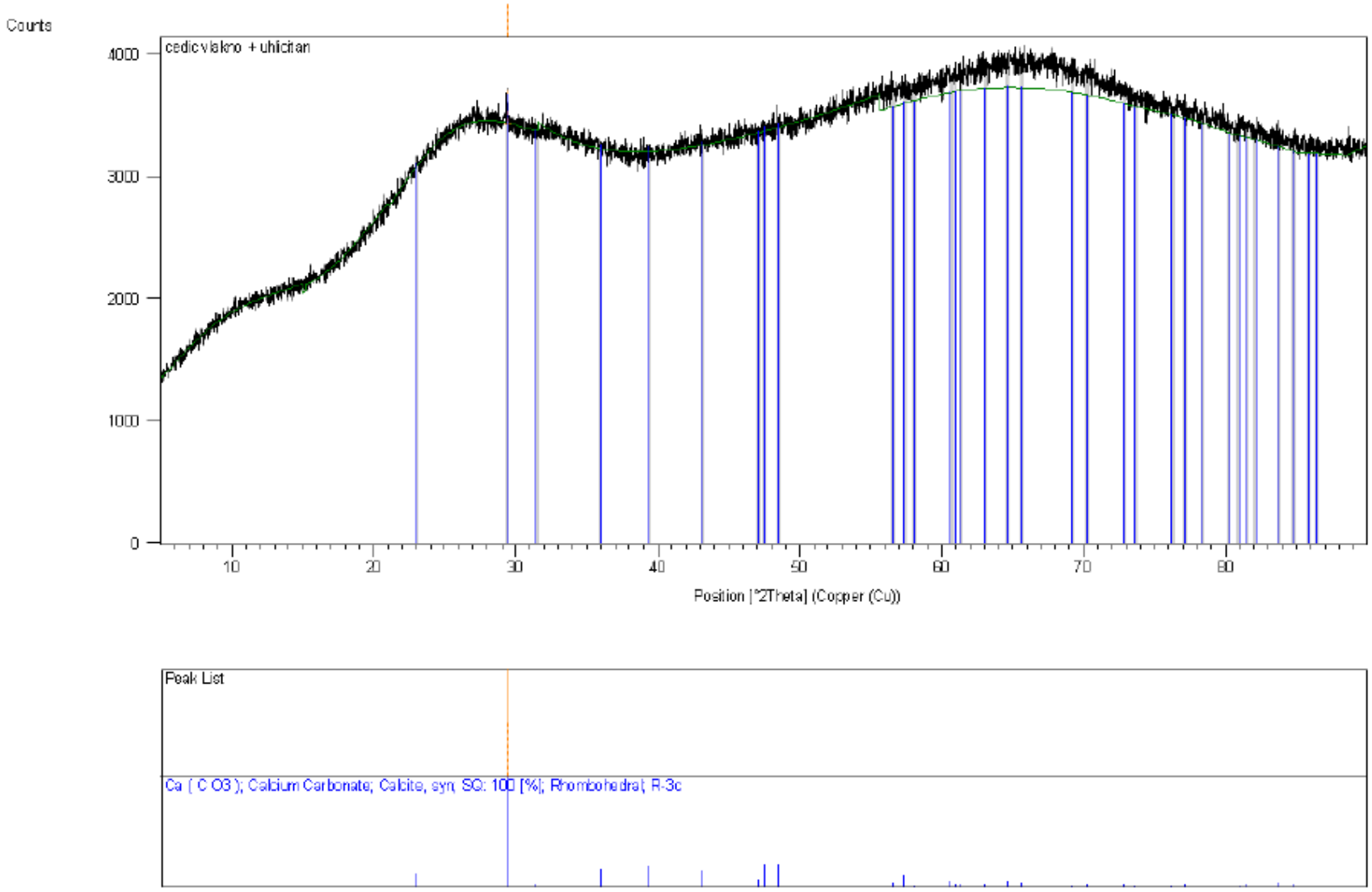

Attachment 12: XRD diffractogram of basalt fibres immersed in 10 % Na_2O WG/SC solution up to 28 days.